ΠΟΛΥΤΕΧΝΕΙΟ ΚΡΗΤΗΣ
Σχολή Μηχανικών Παραγωγής & Διοίκησης

Hybrid composites consisting of a thermosetting matrix, nano-particles and macro-fibres

Υβριδικά σύνθετα υλικά αποτελούμενα από θερμοσκληρυνόμενη μήτρα, νανοσωματίδια και μακριές ίνες

Γεώργιος Τσελίκος

Επιβλέπων: Γεώργιος Σταυρουλάκης

ΔΙΠΛΩΜΑΤΙΚΗ ΕΡΓΑΣΙΑ

ΠΟΛΥΤΕΧΝΕΙΟ ΚΡΗΤΗΣ
30 ΧΡΟΝΙΑ ΠΡΟΣΦΟΡΑΣ 1984 – 2014
Σχολή Μηχανικών Παραγωγής & Διοίκησης

ΠΟΛΥΤΕΧΝΕΙΟ ΚΡΗΤΗΣ
Μ.Π.Δ.

HYBRID COMPOSITES CONSISTING OF A THERMOSETTING MATRIX, NANO-PARTICLES AND MACRO-FIBRES

Υβριδικά σύνθετα υλικά αποτελούμενα από
θερμοσκληρυνόμενη μήτρα,
νανοσωματίδια και μακριές ίνες

Γεώργιος Τσελίκος

Διπλωματική εργασία υποβληθήσα στα πλαίσια των απαιτήσεων για
την απόκτηση του Διπλώματος της σχολής
Μηχανικών Παραγωγής & Διοίκησης

4 Ιουλίου, 2014

4 Ιουλίου, 2014
ΔΙΠΛΩΜΑΤΙΚΗ ΔΙΑΤΡΙΒΗ

Γεώργιος Τσελίκος,
αρ. μητρώου: 2008010026

e-mail: gtselikos@hotmail.com

Ημερομηνία παρουσίασης: 3 Ιουλίου, 2014

Τριμελής Συμβουλευτική Επιτροπή:

1. Γεώργιος Σταυρουλάκης, καθηγητής Πολυτεχνείου Κρήτης, επιβλέπων
2. Αλέξανδρος Δ. Γκότσης, αναπλ. καθηγητής Πολυτεχνείου Κρήτης
3. Αριστομένης Αντωνιάδης, καθηγητής Πολυτεχνείου Κρήτης.

*Ε*ικόνα εξωφύλλου:
The Boeing 787 makes greater use of composite materials in its airframe and primary structure than any other Boeing commercial airplane

ΔΙΕΥΘΥΝΣΗ ΕΡΓΑΣΤΗΡΙΟΥ:

ΠΟΛΥΤΕΧΝΕΙΟ ΚΡΗΤΗΣ
Εργαστήριο Υλικών

Κτήριο Επιστημών, Πανεπιστημιούπολη, Κουνουπιδιανά, 73100 Χανιά

τηλ. 2821037259
fax. 2821037672
e-mail: gotsis@science.tuc.gr

Contents

DECLARATION

I hereby declare that the work presented here has been my independent work and has been performed during the course of my Diploma of Engineering studies at the Department of Production and Management Engineering, Technical University of Crete, Chania.
All contributions drawn from external sources have been acknowledged with due reference to the literature.

ΔΗΛΩΣΗ

Δηλώνω υπεύθυνα ότι η παρούσα διατριβή είναι προϊόν ανεξάρτητης εργασίας μου που διεξήχθη κατά τις προπτυχιακές μου σπουδές στο τμήμα Μηχανικών Παραγωγής και Διοίκησης του Πολυτεχνείου Κρήτης, στα Χανιά.
Για ό,τι δεδομένα ή πληροφορίες χρησιμοποίησα που προέρχονται από εξωτερικές πηγές έχουν δοθεί οι αρμόζουσες αναγνωρίσεις και αναφορές.

Γεώργιος Τσελίκος

Acknowledgements

First and foremost I would like to thank Prof. A.D. Gotsis, for giving me the opportunity to carry out the present Diploma Thesis study. His guidance and motivation led to the successful completion of the present work.

I would also like to thank my supervisor Prof. G. Stavroulakis and Prof. A. Antoniadis for their participation and contribution as members of the advisory committee.

Special thanks to Prof. N. Kallithrakas-Kontos and Assoc. Prof. P. Maravelaki-Kalaitzaki and the group members of the Analytical and Environmental Chemistry Laboratory of Technical University of Crete for their help and their hospitality.

I wish to thank the all the members and staff of Technical University of Crete in Chania, as well as, the ones supporting the program " Incubator of Ideas", for allowing me to conduct the required experiments and for fuelling me with new and innovative ideas.

Also, I would like to thank my friends Panos, Meletis,Ilias, Dimitris, Michail, Elina, Penny and Marilena for being there for me whenever I needed them the most and for giving me guidance through our extensive conversations. Especially, I want to thank Chara, from the bottom of my heart, for believing in me and supporting and standing by whenever I needed her the most.

Last, but not least, I would like to express my gratitude to my parents, to whom I dedicate this Diploma Thesis, for supporting me with everything I needed throughout my studies.

European Union
European Social Fund

OPERATIONAL PROGRAMME
EDUCATION AND LIFELONG LEARNING
investing in knowledge society
MINISTRY OF EDUCATION & RELIGIOUS AFFAIRS
MANAGING AUTHORITY

NSRF 2007-2013
programme for development
EUROPEAN SOCIAL FUND

Co-financed by Greece and the European Union

Ελληνική Περίληψη

Εισαγωγή

Οι ολοένα αυξανόμενες απαιτήσεις για ανθεκτικότερες και ελαφρύτερες κατασκευές οδήγησαν στην ανάπτυξη νέων υλικών. Η αύξηση της αντοχής με την ταυτόχρονη μείωση του βάρους έχουν σαν αποτέλεσμα την εξοικονόμηση ενέργειας και πόρων. Για αυτό το λόγο, χαρακτηριστικό στοιχείο των νέων υλικών είναι οι υψηλές τιμές, σε σχέση με τα υπόλοιπα υλικά, του λόγου *αντοχή/βάρος*. Πλήθος βιομηχανικών κλάδων επενδύουν στη μελέτη, κατασκευή και βελτιστοποίηση νέων υλικών, όπως η αεροδιαστημική βιομηχανία, η αυτοκινητοβιομηχανία, η βιομηχανία αθλητικών ειδών και πολλές ακόμα στην παραγωγή προϊόντων καθημερινής χρήσης.

Στην κατηγορία των *νέων υλικών* συγκαταλέγονται τα **σύνθετα υλικά** (*composite materials*) που ήδη παρουσιάζουν ευρεία εφαρμογή στους παραπάνω κατασκευαστικούς τομείς, κυρίως σε αυτούς της αυτοκίνησης και της αεροναυπηγικής/αεροδιαστημικής. Η αυξανόμενη χρήση των σύνθετων υλικών βασίζεται σε ορισμένα ιδιαίτερα χαρακτηριστικά τους, εκτός της ελάφρυνσης της κατασκευής που έχει ήδη σημειωθεί, όπως είναι το σχετικά χαμηλό κόστος τους και η μεγαλύτερη ελευθερία στο σχεδιασμό προϊόντων και κατασκευών.

Σκοπός της παρούσας Διπλωματικής είναι η κατασκευή σύνθετων υβριδικών υλικών καθώς και η μελέτη και χαρακτηρισμός των ιδιοτήτων τους. Κύριος στόχος είναι η κατανόηση και μελέτη της φύσης των συστατικών που χρησιμοποιήθηκαν για τη τελική σύνθεση, ώστε να προκύψει μια λεπτομερής ανάλυση των μηχανικών ιδιοτήτων του σύνθετου υλικού υπό εφελκυστικό φορτίο.

Σύνθετα υλικά ορίζονται τα υλικά εκείνα που αποτελούνται από δύο ή περισσότερα συστατικά, ο συνδυασμός των οποίων παράγει ένα τελικό προϊόν με ειδικές ιδιότητες και χαρακτηριστικά, διαφορετικά από τα υπόλοιπα υλικά. Αποτελούνται από δύο κύρια μέρη, τη *μήτρα* και την *ενίσχυση*. Η πρώτη κατασκευάζεται από διάφορα υλικά, όπως πολυμερή, κεραμικά ή και μέταλλα. Η ενίσχυση ενός σύνθετου υλικού, πάντως, πρέπει να έχει μεγαλύτερη αντοχή από το υλικό της μήτρας, αφού αυτή παραλαμβάνει το σύνολο της φόρτισης. Έτσι, η πιο διαδεδομένη επιλογή υλικού ενίσχυσης είναι ο άνθρακας, μαζί με το γυαλί και το αραμίδιο (™Kevlar). Λόγω του πλήθους των συνδυασμών σε υλικά και μηχανισμούς κατασκευής, τα σύνθετα υλικά μπορούν κατηγοριοποιηθούν σε:

- Σύνθετα υλικά με ενίσχυση τεμαχιδίων
- Ινώδη σύνθετα υλικά (με κοντές και μακριές ίνες)
- Prepreg cloth
- Σύνθετα υλικά τύπου sandwich (αποτελούμενα από δομικό αφρό και κυψελωτό panel)
- Πολύστρωτα σύνθετα υλικά

Υλικά ενίσχυσης

Ο κύριος σκοπός χρήσης ινωδών σύνθετων υλικών, είναι η αύξηση της αντοχής και του μέτρου δυσκαμψίας του υλικού μήτρας, το οποία είναι συνήθως πιο μαλακό και με λιγότερη πυκνότητα, καθιστώντας την συνολική κατασκευή ελαφριά.

Η ενίσχυση σύνθετων υλικών με τεμαχίδια (σωματίδια) αποτελεί την πιο οικονομική λύση όσον αφορά το συνολικό κατασκευαστικό κόστος και μπορεί να κατηγοριοποιηθεί σύμφωνα με το μέγεθος των σωματιδίων. Η χρήση τέτοιου είδους ενίσχυσης έχει ως στόχο την αύξηση του μέτρου ελαστικότητας της μήτρας, ακόμα και κατά 2 ως 3 φορές. Παρόλα αυτά , η αντοχή του παραγόμενου προϊόντος δεν βελτιώνεται, αλλά παρουσιάζεται ελαφρώς μειωμένη με τη διεπιφάνεια ίνας-μήτρας να αποτελεί πρόδρομο εντοπισμένων τάσεων και ρηγματώσεων. Το βασικότερο πλεονέκτημα αυτού του τύπου ενίσχυσης, είναι ότι το υλικό καθίσταται ισότροπο. Εφαρμογές όπου γίνεται χρήση μεγάλου μεγέθους σωματιδίων αποτελούν το χαλίκι και η άμμος στο τσιμέντο και για μικρότερα μεγέθη, σωματίδια αιθάλης (20-50 nm) σε λάστιχα αυτοκινήτων.

Τα κοντά ινίδια (whiskers) δρουν ως σωματίδια ενισχυτικά στο μηχανισμό μεταφοράς φορτίου από τη μήτρα στην ίνα. Ο χαρακτηρισμός ως ”κοντές” προέρχεται από το μικρό μέγεθος του λόγου L/D, όπου L είναι το μήκος της ίνας και D η διάμετρος της και συνήθως βρίσκεται κοντά στο 100. Αυτού του είδους η ενίσχυση αυξάνει τη δυσκαμψία του παραγόμενου υλικού μόνο όταν οι δυνάμεις δρουν στη διεύθυνση της ίνας. Για αυτό το λόγο, υπάρχουν δυο διαφορετικές κατασκευαστικές τεχνικές, η μία έχει τις ίνες ευθυγραμμισμένες μεταξύ τους μέσα στη μήτρα, καθιστώντας το σύνθετο ανισότροπο, και η δεύτερη περιέχει ίνες τυχαίου προσανατολισμού, ενισχύοντας την ισοτροπικότητα του υλικού αλλά μειώνοντας τις υπόλοιπες μηχανικές ιδιότητες του.

Μεγιστοποιώντας το λόγο L/D, την κατεύθυνση των ινών και τις μηχανικές ιδιότητες της ενίσχυσης, είμαστε σε θέση να πραγματοποιήσουμε αύξηση του μέτρου ελαστικότητα, ακόμα και 400 %. Επιπροσθέτως, λαμβάνοντας ως κριτήριο ότι η διεπιφάνεια μήτρας-ίνας είναι δυνατή και ο μηχανισμός μεταφοράς φορτίου αποδίδει, μπορούμε να καταλήξουμε σε αύξηση της αντοχής σε θραύση του σύνθετου υλικού. Όμως, η ενίσχυση κοντών ινών αποδεικνύεται ως υπεύθυνη για την μείωση των ιδιοτήτων δυσθραυστότητας και παραμόρφωσης σε θραύση του υλικού.

Η χρήση συνεχών ινών για την ενίσχυση μήτρας σύνθετου υλικού οδηγεί στην ενδυνάμωση της δεύτερης, αφού οι ίνες λαμβάνουν το σύνολο των ασκούμενων φορ-

τίων στο σύνθετο υλικό. Με αυτό το τρόπο πραγματοποιείται η πλήρης αξιοποίηση του δυναμικού των ινών και ο ρόλος της μήτρας περιορίζεται στο να κρατάει τις ίνες στη θέση τους και να διατηρεί το μηχανισμό μεταφοράς φορτίου. Η πιο διαδεδομένη μορφή ινών ενίσχυσης αποτελούν οι μονοαξονικές ίνες, οι οποίες παρέχουν στο τελικό προϊόν μεγάλη αντοχή στη διεύθυνση των ινών και μεγάλη ανισοτροπία κάθετα αυτών. Η αντοχή αυτού του τύπου ενίσχυσης περιγράφεται από την Κλασσική Θεωρία Πλακόστρωτων υλικών και αναλύεται από τα μοντέλα του Reuss και Halpin-Tsai.

Η καλύτερη μέθοδος αξιοποίησης των δυνατοτήτων που προσφέρεται από την συνεχή ινώδη ενίσχυση, είναι από τη χρήση πλεγμένων ινών. Αυτή η μορφή ενίσχυσης αποτελείται από την αλληλεπίδραση υφαδιού και στημονιού, κατά 90°, για τη δημιουργία μοτίβων σε δισδιάστατη μορφή και κατηγοριοποιούνται ανάλογα με την περιοδικότητα της πλέξης σε plain, twill και satin πλέξη. Το παραπάνω υλικό ενίσχυσης είναι εύκολο στη χρήση και αποδίδει στο παραγόμενο σύνθετο υλικό ισοτροπικότητα στο επίπεδο.

Άλλα είδη ενίσχυσης, αποτελούν τα prepreg και sandwich σύνθετα υλικά τα οποία είναι ευρέως διαδεδομένα στο κλάδο της αεροναυπηγικής και της αυτοκινητοβιομηχανίας. Τα Prepreg αποτελούνται από ίνες προ εμποτισμένες με καθορισμένη ποσότητα εποξειδικής ρητίνης (θερμοσκληρυνόμενο υλικό). Συνήθης μορφή αυτής της ενίσχυσης είναι η μονοαξονική ταινία, η οποία επιτρέπει την εύκολη επικάθιση της σε καλούπια. Η μορφή sandwich των σύνθετων υλικών αποτελεί μία πολύ ελαφριά κατασκευή με υψηλή ειδικό μέτρο ελαστικότητας και ειδικής αντοχής. Αποτελούνται από δύο εξωτερικά φύλλα σύνθετου πολύστρωτου υλικού και στο εσωτερικό του είτε από δομικό αφρό είτε από κυψελοειδή πυρήνα.

Υβριδικά σύνθετα υλικά

Κλάδοι όπως αυτοί της αεροναυπηγικής και της αυτοκινητοβιομηχανίας, όπου τα κριτήρια στα υλικά σχεδίασης νέων προϊόντων είναι ιδιαίτερα υψηλά για λόγους ασφαλείας, αποτελούν τους κυριότερους παράγοντες έρευνας και ανάπτυξης σε νέα κατασκευαστικά υλικά. Κύρια, λοιπόν, τάση σήμερα, αποτελεί η χρήση των ήδη ανεπτυγμένων υλικών σε διαφορετικούς συνδυασμούς μεταξύ τους, για την εκμετάλλευση των ειδικών ιδιοτήτων τους χωρίς να υπάρχει οποιοσδήποτε συμβιβασμός ως προς τη δομική ακεραιότητα της τελικής κατασκευής. Ένα τέτοιο, ανεπτυγμένο υλικών σχεδίασης, αποτελούν οι νανοσωλήνες άνθρακα (CNTs). Η χρήση τέτοιου είδους υλικού μπορεί να πραγματοποιηθεί με του ακόλουθους τρόπους:

- Χρήση νανοϋλικών για την ενίσχυση της δομής μίας κοινής κατασκευής από σύνθετα υλικά
- Εκμετάλλευση των μοναδικών ιδιοτήτων των CNTs ως αισθητήρες παραμόρφωσης, σε πραγματικό χρόνο, καθώς και της δυνατότητας τους να δρουν ως ενεργοποιητές

Ελαττώματα σε δομικό επίπεδο ενός σύνθετου υλικού, όπως η ύπαρξη χαμηλών επιδόσεων σε διατμητικές τάσεις, στη διεπιφάνεια μεταξύ των στρώσεων, καθώς και

η χαμηλή δυσθραυστότητα, βελτιώνονται από την ενίσχυση κατά την διεύθυνση του πάχους του συνθέτου, με υλικά στη νάνο κλίμακα. Η μορφή αυτή ενίσχυσης ουσιαστικά ενεργοποιεί ένα μηχανισμό γεφύρωσης των μικρορωγμών, αυξάνοντας με αυτό το τρόπο την δυσθραυστότητα του τελικού προϊόντος.

Για την αξιοποίηση όλων των θετικών στοιχείων, από τη χρήση ένθετων υλικών ενίσχυσης σε νάνο κλίμακα, είναι απαραίτητη η καλή ποιότητας διασπορά αυτών στην μήτρα του σύνθετου υλικού. Για το σκοπό αυτό, υπάρχουν δύο κύριες κατηγορίες μεθόδων διασποράς νανοϋλικών σε μια σύνθετη μήτρα. Η πρώτη, περιλαμβάνει τη χημική διεργασία των νάνο υλικών πριν τοποθετηθούν και διασπαρούν στο υλικό της μήτρας, και η δεύτερη, τη μηχανική διασπορά τους κατευθείαν μέσα στο υλικό μήτρας. Η χημική διεργασία περιλαμβάνει την χημική μετατροπή της επιφάνειας του νανό υλικού με την επικόλληση διάφορων χημικών ενώσεων, όπως αυτή του καρβοξυλίου και της αμίνης. Στη συνέχεια απαιτείται, η χρήση μηχανικών μηχανισμών διασποράς, όπως αυτοί της ανάμιξης υψηλής διάτμησης (high shear) καθώς και της ανάμιξης με τη χρήση συσκευής υπερήχων (ultrasonication tip/or bath). Η εκμετάλλευση των τελευταίων αποτελεί μέρος της κατηγορίας μεθόδων μηχανικής διασποράς που μπορούν χρησιμοποιηθούν και αυτοτελώς για μια ποιοτική τελική μορφή διασποράς.

Σημαντικό ρόλο σε οποιαδήποτε σύνθετη μορφή υλικού, είτε αυτό πρόκειται για απλό σύνθετο, είτε για υβριδικό, έχει το υλικό μήτρας που χρησιμοποιείται. Η μήτρα είναι υπεύθυνη για τη μεταφορά των φορτίων στις πιο δυνατές ίνες του συνθέτου, να τις κρατάει στη θέση τους, καθώς επίσης να τις προστατεύει από τη μεταξύ τους τριβή και τον κίνδυνο διάβρωσης από χημικές ή άλλες ακραίες περιβαλλοντικές συνθήκες. Τα κύρια υλικά μήτρας είναι τα πολυμερή, με αυτά από κεραμικά και μεταλλικά υλικά να χρησιμοποιούνται σε μικρότερο βαθμό. Εστιάζοντας στα πολυμερικά υλικά, παρατηρούμε την κατηγοριοποίηση τους σε θερμοπλαστικά και θερμοσκληρυνόμενα. Ο όρος θερμοπλαστικά καλύπτει τα πολυμερή υλικά τα οποία υπό την επίδραση θερμό΄τητας και πίεσης καθίστανται εύπλαστα και ρέουν. Κατ' αυτόν τον τρόπο, τα περισσότερα θερμοπλαστικά μπορούν να μορφοποιηθούν πολλές φορές (ανακύκλωση), αν και η εμφάνιση φαινομένων αποπολυμερισμού μειώνει σε πολλές περιπτώσεις το δυνατό αριθμό των κύκλων μορφοποίησης. Ο όρος **θερμοσκληρυνόμενα** αποδίδεται στα πολυμερή τα οποία στην τελική φάση επεξεργασίας αποκτούν σταυροδεσμούς και σχηματίζουν ένα δικτύωμα με την επίδραση της θερμότητας. Τα μόρια δηλαδή στο τελικό προϊόν συνδέονται σταθερά με κύριους δεσμούς μεταξύ τους κι έτσι επιτυγχάνεται τέτοια συνοχή στο πλέγμα, ώστε δεν μπορεί πλέον το πολυμερές να μεταβεί στην πλαστική κατάσταση με θέρμανση. Τέτοιου είδους δικτυώματα συνιστούν εξαιρετικά κατασκευαστικά υλικά, λόγω της διαστατικής τους σταθερότητας σε υψηλές θερμοκρασίες και το υψηλό μέτρο ελαστικότητάς τους. Η παρουσία των σταυροδεσμών παρεμποδίζει τη πλαστική παραμόρφωση και τον ερπυσμό του υλικού, καθώς αναστέλλει την ελευθερίας κινήσεως των μακρομοριακών αλυσίδων. Με αυτόν τον τρόπο η πλαστική παραμόρφωση του υλικού γίνεται αδύνατη χωρίς τη θραύση των σταυροδεσμών. Τα συνηθέστερα χρησιμοποιούμενα θερμοσκληρυνόμενα πολυμερή ως μήτρες είναι οι φαινολικές ρητίνες, οι ρητίνες μελαμίνης και ουρίας, οι σιλικόνες, οι ακόρεστοι πολυεστέρες κλπ. Στη παρούσα εργασία, θα χρησιμοποιηθεί ένα ευρέως χρήσης θερμοσκληρυνόμενο υλικό, αυτό της εποξειδικής ρητίνης.

Στόχος της διπλωματικής εργασίας

Το βασικό αντικείμενο της εργασίας αυτής είναι η καθιέρωση νέων μεθόδων για τη βελτίωση των μηχανικών ιδιοτήτων της πολυμερικής μήτρας, με την προσθήκη νανοσωματιδίων και τη δημιουργία υβριδικών νανο-μακρο-συνθέτων. Τα συνήθη πολυστρωματικά σύνθετα υλικά επιδεικνύουν πολύ χαμηλή αντοχή σε φορτία θλίψεως παράλληλα με την διεύθυνση των ινών. Έχοντας παρόμοια μορφή με ένα απλό σχοινί, οι ίνες, όταν συμπιέζονται αξονικά, λυγίζουν σε σχετικά χαμηλές δυνάμεις μέχρι να επέλθει η αστοχία του υλικού. Εκείνο, όμως, που θα τις αποτρέψει από το να λυγίσουν, είναι η ακαμψία της μήτρας. Σε περίπτωση που αυξηθεί η ακαμψία του υλικού, θα ενισχυθεί και η αντίσταση του στο λυγισμό και μαζί της και η αντοχή σε θλίψη. Σε αυτή την εργασία στοχεύουμε ουσιαστικά στη βελτίωση της αντοχής σε θλίψη του σύνθετου υλικού με συνεχείς ίνες, ενισχύοντας τις ελαστικές ιδιότητες της μήτρας. Αυτό μπορεί να πραγματοποιηθεί με την προσθήκη ενισχυτικών νανοσωματιδίων στη μήτρα.

Παρόμοια τεχνική με την παραπάνω, πραγματοποιήθηκε από τον Vlasveld [2005] στο Technical University του Delft, όπου χρησιμοποιήθηκαν νανοσωματίδια πυριτικού αργιλίου για την ενίσχυση του μέτρου ελαστικότητας μιας πολυμερικής μήτρας από πολυαμίδιο-6, για τη δημιουργία ενός υβριδικού σύνθετου υλικού με ενίσχυση συνεχών ινών γυαλιού. Στην παρούσα διπλωματική εργασία επιλέγουμε να κάνουμε χρήση νανοσωλήνων άνθρακα, CNTs, για καλύτερη συμβατότητα με την εποξειδική μήτρα και τις μακροσκοπικές ίνες άνθρακα, με γνώμονα την βελτίωση των μηχανικών ιδιοτήτων του τελικού προϊόντος σε δυσθραυστότητα και εφελκυστική αντοχή. Με αυτό το τρόπο, εστιάζουμε στην εισαγωγή και την επίτευξη μιας υψηλής, από άποψη ποιότητας, διασπορά των CNTs στην εποξειδική ρητίνη, χρησιμοποιώντας διάφορες τεχνικές διασποράς, είτε χημικής φύσεως, είτε μηχανικής. Οι χημικές μέθοδοι διασποράς νανοσωματιδίων περιλαμβάνουν είτε την χημική τροποποίηση της επιφάνειας των νανοσωλήνων άνθρακα και τη μετέπειτα μηχανική διασπορά τους στη ρητίνη, είτε τη χρήση οργανικού διαλύτη, όπως είναι η ακετόνη, με άμεσο επακόλουθο τη μηχανική επεξεργασία. Ακόμα, γίνεται χρήση μόνο μηχανικών μεθόδων, όπως η συνεχής ανάδευση και η χρήση υπερήχων (ultrasonication).

Επιπροσθέτως, στόχος μας αποτελεί η μελέτη και ανάλυση της εφελκυστικής αντοχής του υβριδικού σύνθετου υλικού , καθώς επίσης και η σχέση τάσης/παραμόρφωσης υπό εφελκυστικό φορτίο. Πειράματα θλίψης και λυγισμού τριών σημείων (three-point bending) δεν ήταν δυνατό να πραγματοποιηθούν, λόγω έλλειψης αντίστοιχων μηχανημάτων μέτρησης. Έτσι, προσπαθήσαμε να προσδιορίσουμε οποιαδήποτε βελτίωση της θλιπτικής αντοχής του υβριδικού υλικού, μέσα από εφελκυστικές μετρήσεις του μέτρου ελαστικότητας και αντοχής. Η περαιτέρω συνέχιση της έρευνας με επιπλέον μετρήσεις κρίνεται απαραίτητη για τον πλήρη προσδιορισμό των μηχανικών ιδιοτήτων του τελικού υβριδικού σύνθετου μοντέλου.

Αποτελέσματα και συμπεράσματα

Αποτελέσματα

Για την ανάλυση και μελέτη των πειραματικών αποτελεσμάτων χρησιμοποιήθηκαν διαφορετικά όργανα μέτρησης. Για τον προσδιορισμό της ποιότητας διασποράς των νανοσωλήνων άνθρακα στην ρητίνη, λάβαμε εικόνες σε τυχαίες περιοχές των δειγμάτων μας με τη βοήθεια ηλεκτρονικού μικροσκοπίου σάρωσης (SEM). Ακόμα, κάναμε χρήση φασματοσκοπίας υπερύθρου (FTIR) για τον προσδιορισμό όλων των στοιχείων που υπάρχουν μέσα στο νανοσύνθετο υλικό μήτρας, καθώς και την ανίχνευση κορυφών απορρόφησης που να δηλώνουν την ύπαρξη χημικών δεσμών καρβοξυλίου και αμίνης, στα δείγματα όπου η επιφάνεια των CNTs τροποποιήθηκε με τη χρήση νιτρικού οξέως και δεκαεξιλαμίνης (HDA), αντίστοιχα. Παράλληλα με τα παραπάνω πραγματοποιήθηκαν και μηχανικές μετρήσεις για τον προσδιορισμό της εφελκυστικής αντοχής και παραμόρφωσης στα υβριδικά σύνθετα δείγματα μας, τα οποία είχαν κοπεί σύμφωνα με τις οδηγίες του ASTM D 639 - 99.

Η ανάλυση σύστασης των δειγμάτων με τη μέθοδο της υπέρυθρης φασματοσκοπίας (FTIR) πραγματοποιήθηκε στο εργαστήριο του Καθηγητή Ν. Πασαδάκη με τη βοήθεια της Επικ. Καθ. Π. Μαραβελάκη και της συνεργάτιδας της Α. Βεργανελάκη. Όσον αφορά τα αποτελέσματα μας 3.1 , (σελ. 68) , οι κορυφές που χαρακτηρίζουν τους δεσμούς καρβοξυλικής ρίζας και βρίσκονται στην περιοχή των 1700 cm^{-1}, δεν ταυτοποιήθηκαν με αποτέλεσμα να συμπεράνουμε την μη επικόλληση της ρίζας καρβοξυλίου στην επιφάνεια των CNTs. Για τα δείγματα που τροποποιήθηκαν με συνταγές ενός και δύο βημάτων, παρατηρήθηκε η ύπαρξη αμίνης στη περιοχή των 1500 cm^{-1}. Για την καλύτερη ποιότητα της ανάλυσης μας ταυτοποιήσαμε όλες τις κορυφές που εμφανίστηκαν στα δείγμα της καθαρά εποξειδικής ρητίνης. Χρησιμοποιώντας τα αποτελέσματα από αυτό το δείγμα ήμασταν σε θέση να ξεχωρίσουμε αν υπάρχουν οι παραπάνω ζητούμενες κορυφές. Σχετικά, τώρα, με το δείγμα της ακετόνης ταυτοποιήθηκε η ύπαρξη της μέσα στο νανοσύνθετο, γεγονός που εμφανίζεται και στα αποτελέσματα των μηχανικών μετρήσεων.

Η λήψη φωτογραφιών υψηλής ευκρίνειας με τη μέθοδο του ηλεκτρονικού μικροσκοπίου σάρωσης πραγματοποιήθηκε στο τμήμα Μηχανικών Ορυκτών Πόρων με τη καθοδήγηση της Δρ. Ε. Ρεπούσκου. Λάβαμε φωτογραφίες από ένα δείγμα καθαρής ρητίνης και το συγκρίναμε με αυτές από δείγματα με CNTs στο εσωτερικό τους. Στις φωτογραφίες που περιείχαν νανοσωματίδια επεξεργασμένα χρησιμοποιώντας από τις μεθόδους “ενός σταδίου” και “δύο σταδίων” 3.4, (σελ. 70) και 3.5, (σελ. **??**) αντίστοιχα, διαπιστώσαμε την ύπαρξη αμίνης γύρω από την επιφάνεια του των νανοσωλήνων άνθρακα καθώς και το πολύ μεγάλο ποσοστό διασποράς τους στη ρητίνη. Αντίθετα, στα δείγματα με CNTs, όπου χρησιμοποιήθηκε νιτρικό οξύ και ακετόνη, παρατηρούμε την ύπαρξη συσσωματωμάτων 3.2, (σελ. 69) και 3.3, (σελ. 69) αντίστοιχα.

Όσον αφορά της μηχανικές μετρήσεις σε εφελκυστική αντοχή και παραμόρφωση, αρχικά προσδιορίστηκε το κλάσμα όγκου για κάθε δείγμα σύμφωνα με τον παρακάτω τύπο:

$$f = \frac{nc}{\rho t} \ ,$$

όπου η παράμετρος n αντιστοιχεί στα στρώματα ανθρακονήματος που χρησιμοποιήθηκαν, το $\rho = 1.97$ g/cm^3 αποτελεί τη πυκνότητα των ινών άνθρακα, το πάχος των δειγμάτων συμβολίζεται με t και το $c = 0.02$ αποτελεί μια σταθερά.

Τα δείγματα κατηγοριοποιήθηκαν βάση του αριθμού των στρωμάτων ανθρακονήματος που διαθέτουν, σε **δείγματα με μονό ανθρακοϋφασμα** και **δείγματα με 3 ανθρακοϋφάσματα**. Όλα τα υβριδικά σύνθετα αποτελούνται από εποξειδική ρητίνη και $0.445\ g$ CNTs ως μήτρα και φύλλα ανθρακονήματος ως μακροσκοπική ενίσχυση.

Σχετικά με την πρώτη κατηγορία δειγμάτων, κατασκευάστηκαν ένα δείγμα χωρίς νανοσωματίδια και άλλα δύο που είχαν. Στα δύο τελευταία χρησιμοποιήθηκε οργανικός διαλύτης για τη διασπορά των CNTs στην ρητίνη, όμως με διαφορετικό τρόπο κατασκευής. Το δείγμα #3 δημιουργήθηκε με τη μέθοδο σακούλας κενού ενώ το #4 με τη μέθοδο hand lay-up. Λόγω της μεγάλης διαφοράς σε κλάσμα όγκου των ινών άνθρακα μεταξύ του πρώτου δείγματος αναφοράς και των άλλων δύο δεν μπορούμε να βγάλουμε ασφαλή συμπεράσματα σχετικά με τα ποσοτικά αποτελέσματα που προέκυψαν για την εφελκυστική αντοχή, το μέτρο ελαστικότητας και τη παραμόρφωση. Μπορούμε όμως να πούμε ότι παρατηρούμε μια μείωση στις τιμές των παραπάνω μηχανικών ιδιοτήτων για τα δείγματα με CNTs και ακετόνη. Ο λόγος είναι, ο εγκλωβισμός της ακετόνης στο εσωτερικό της σύνθετης μήτρας κάτι που οδηγεί στην πλαστικοποίηση του υλικού και τη μείωση των τιμών των μηχανικών χαρακτηριστικών του. Ακόμα, γίνεται εμφανής η διαφορά μεταξύ των δειγμάτων #3 και #4, με ακετόνη και CNTs στο εσωτερικό τους. Μπορεί η χρήση της τεχνικής vacuum-bag να δημιουργεί δείγματα με πολύ καλύτερη εξωτερική επιφάνεια σε σχέση με τη μέθοδο hand lay-up, παρόλα αυτά, αποδεικνύεται αναποτελεσματική για τη δημιουργία υβριδικών σύνθετων υλικών 3.9, (σελ. 74) και 3.10, (σελ. 74).

Για την ενίσχυση του πάχους των δειγμάτων συνεχίσαμε τη πειραματική διαδικασία με τη κατασκευή δειγμάτων με τρία φύλλα άνθρακα στη σύνθεση τους. Συγκεκριμένα δημιουργήσαμε έξι σειρές δειγμάτων, με τις #1 και #10 να μην διαθέτουν CNTs στο εσωτερικό τους και με μόνη διαφορά το διαφορετικό τρόπο κατασκευής τους. Το #1 δημιουργήθηκε με τη μέθοδο vacuum-bag, έχοντας πολύ καλύτερη εξωτερική επιφάνεια και μεγαλύτερο ποσοστό όγκου ινών, ενώ το #10 με τη μέθοδο hand lay-up και χρησιμοποιήθηκε σαν δείγμα αναφοράς με τα υβριδικά δείγματα 3.17, (σελ. 78) και 3.18, (σελ. 78).

Συμπεράσματα

Έχοντας δει τα διαγράμματα τάσης-παραμόρφωσης, παρατηρούμε τις χαμηλές τιμές σε μέτρο ελαστικότητας που προκύπτουν. Η ονομαστική τιμή δυσκαμψίας των ινών άνθρακα είναι της τάξεως των 235 GPa, ενώ αυτή της εποξειδικής ρητίνης κοντά στα 3 GPa. Στη περίπτωση που είχαμε δείγματα με 40% κλάσμα όγκου ινών, με προσανατολισμό κατά μήκος της κατεύθυνσης του φορτίου, τότε θα ανέμενε κανείς ότι το σύνθετο θα μπορούσε να έχει μέτρο ελαστικότητας περίπου 95 GPa, πολύ υψηλότερο από το 15 - 18 GPa που μετρήθηκαν. Τα σύνθετα αυτά έχουν κατασκευασθεί χρησιμοποιώντας ως ενίσχυση ίνες άνθρακα σε μορφή υφάσματος, όπου το εν δεύτερο των ινών είναι προσανατολισμένες κάθετα προς την κατεύθυνση φόρτισης. Επιπροσθέτως, καθώς οι ίνες είναι υφασμένες σε plain μορφή, δεν είναι ευθεία τεντωμένες αλλά

ακολουθούν μια κυματοειδή πορεία, όπου το στημόνι και το υφάδι εναλλάσσονται το ένα πάνω στο άλλο. Όταν βρίσκεται υπό φορτίο η κυματοειδής μορφή θα αρχίσει να τεντώνεται προς μια ευθεία γραμμή μαζί με την επιμήκυνση των ινών. Θεωρώντας ότι το στημόνι βρίσκεται παράλληλα στη κατεύθυνση που εφαρμόζεται το φορτίο, η αντίσταση που δέχεται προέρχεται από το τέντωμα του υφαδιού. Για να τεντώσουν τα νήματα του στημονιού, αυτά που είναι κάθετα στην κατεύθυνση φόρτισης πρέπει να λυγίσουν περισσότερο. Τα συγκεκριμένα όμως νήματα στα δοκίμια μας, δεν έχουν μεγάλο μήκος και δεν συγκρατούνται πουθενά στα άκρα του δοκίμιο, αντίθετα, κρατιούνται μαζί από τις διατμητικές δυνάμεις που ασκούνται από τη μήτρα και από τη τριβή μεταξύ των ινών τους. Κατά τα παραπάνω η αντίσταση σε παραμόρφωση κάτω από ένα εφελκυστικό φορτίο, είναι μικρότερη για τις ίνες κάθετα στη διεύθυνση του φορτίου. Έτσι, η απλή ευθυγράμμιση των ινών είναι ευκολότερη από το τέντωμα τους και η συνολική αντίσταση του σύνθετου υλικού στην συνολική παραμόρφωση είναι μικρότερη από αυτή που μετράται σε απλή περίπτωση, όπου υπάρχει μόνο τέντωμα των ινών. Συνεπώς, το μετρούμενο μέτρο ελαστικότητας είναι και το αποτελεσματικό.

Σύμφωνα με τη θεωρία, που αναπτύχθηκε από τον Α. Αντωνογιαννάκη [2013], μας δίνεται η ικανότητα να υπολογίσουμε το μακροσκοπικό μέτρο ελαστικότητας ινωδών σύνθετων υλικών. Η θεωρία αυτή χρειάζεται γνώση πολλών γεωμετρικών λεπτομερειών, το τύπο ύφανσης και τα χαρακτηριστικά του υφάσματος, καθώς και το στοίβαγμα των φύλλων ενίσχυσης. Για παρόμοια συστήματα με 30 - 50% ποσοστό ινών, το αποτελεσματικό μέτρο ελαστικότητας του υφάσματος σε ένα σύνθετο υλικό, μοιάζει να είναι κοντά στο 1/4 του μέτρου ελαστικότητας της ίνας.

Ακολουθώντας μια απλή προσέγγιση της παραπάνω θεωρίας, θεωρούμε ότι το σύνθετο υλικό φορτίζεται κατά τη διεύθυνση του στημονιού. Το μισό ποσοστό των ινών στο σύνθετο που αντιστοιχούν στα νήματα του υφαδιού έχουν μικρό αντίκτυπο στη δυσκαμψία των ινών του στημονιού και δίνονται από το παρακάτω τύπο:

$$\frac{1}{E_{weft}} = \frac{V_f}{E_f} + \frac{1-V_f}{E_m} \approx \frac{1-V_f}{E_m} \ .$$

Η παραπάνω τιμή προστίθεται στο υπόλοιπο μισό του ποσοστού των ινών του συνθέτου, οι οποίες είναι παράλληλες στον άξονα φόρτισης και δίνεται από το παρακάτω τύπο:

$$E_{warp} = E_{fabric}V_f + E_m(1-V_f) \ ,$$

όπου το E_{fabric} αποτελεί το αποτελεσματικό μέτρο ελαστικότητας των ινών και περιλαμβάνει την αντίσταση στην επιμήκυνση και την παρεμπόδιση από το περιβάλλον τους κατά το τέντωμα. Έτσι, το μέτρο ελαστικότητας του συνθέτου υπολογίζεται από τον παρακάτω τύπο:

$$E_1 = \frac{E_{warp}}{2} + \frac{E_{weft}}{2} = \frac{1}{2}\left(E_{fabric}V_f + E_m(1-V_f)\right) + \frac{1}{2}\frac{E_m}{1-V_f} \ . \qquad (1)$$

Για τα δείγματα της σειράς # 1 ($E_1 \approx 15.5$ GPa, $V_f = 0.4$ και $E_m = 2.7$ GPa) μπορούμε να λύσουμε ως προς το E_{fabric} είτε για τη διεύθυνση του στημονιού, είτε για αυτή του υφαδιού, και καταλήγουμε σε μια τιμή στα 65 GPa. Αυτό καταδεικνύει ότι η εφελκυστική τάση δρα ταυτόχρονα και για την ευθυγράμμιση των ινών αλλά και για

την επιμήκυνση τους σταδιακά. Κοντά στο 40 - 50% της μέγιστης παραμόρφωσης του συνθέτου αφορά την ευθυγράμμιση των ινών στο ύφασμα. Η τιμή του E_{fabric}, που υπολογίστηκε προηγουμένως, επιβεβαιώνεται και από τα δεδομένα που συλλέξαμε από τη σειρά δειγμάτων με τον αριθμό #10, το οποίο δεν περιέχει και αυτό CNTs στη μήτρα.

Ό,τι είδαμε παραπάνω για τα απλά σύνθετα υλικά, δηλαδή αυτά χωρίς νανοσωματίδια, θα πρέπει να ισχύουν με κάποιες μικροδιαφορές και στα σύνθετα υβριδικά υλικά. Η συνεισφορά των CNTs στις ελαστικές ιδιότητες του συνθέτου προέρχονται από την ενδυνάμωση της μέτρου δυσκαμψίας της μήτρας. Παρόλαυτά, λόγω της μεγάλης διαφοράς μέτρου ελαστικότητας μεταξύ ινών και μήτρας, ακόμα και να τριπλασιαστεί η τιμή της τελευταίας, από την εισαγωγή νανοσωματιδίων, μπορούμε να υποθέσουμε ασφαλώς ότι η συνεισφορά του ινώδους υφάσματος E_{fabric} στο μέτρο ελαστικότητας του συνθέτου, E_1, από την παραπάνω εξίσωση, δεν θα αλλάξει σημαντικά. Κρατώντας, λοιπόν, σταθερή τη τιμή για το E_{fabric} του υφάσματος, μπορούμε να λύσουμε τη τελευταία εξίσωση ως προς το μέτρο ελαστικότητας της νανοσύνθετης μήτρας E_m για κάθε σύνθετο υβριδικό δείγμα, μιας και γνωρίζουμε από τις πειραματικές μετρήσεις τις τιμές του μέτρου ελαστικότητας για το συνολικό σύνθετο υλικό, E_1. Τα αποτελέσματα παρουσιάζονται στο Πίνακα 4.1, σελ. 82

Τα αποτελέσματα του μέτρου ελαστικότητας της μήτρας για τα υβριδικά σύνθετα υλικά είναι σε αρμονία με τα αποτελέσματα της θεωρίας για σύνθετα με κοντές ίνες μέτρου ελαστικότητας 1 TPa και $L/D < 100$ τυχαία κατανεμημένες μέσα σε μαλακή μήτρα μέτρου ελαστικότητας 2.7 GPa. Αξίζει να σημειωθεί ότι το υψηλότερο μέτρο ελαστικότητας παρατηρήθηκε στη σειρά δειγμάτων στα οποία τα νανοσωματίδια δεν είχαν υποστεί καμία χημική τροποποιήση της επιφάνειας τους (Unmodified -Series 9) και το μικρότερο στα δείγματα που έγινε χρήση νιτρικού οξέως.

Απ΄ότι φαίνεται η αμίνη που επικάθεται επάνω στην επιφάνεια των CNTs δημιουργεί μία μαλακή κρούστα γύρω τους γεγονός που έχει αρνητικές επιπτώσεις στην συνολική ελαστική συμπεριφορά τους. Έτσι, το τελικό αποτελεσματικό μέτρο ελαστικότητας της νανοσύνθετης μήτρας να παρουσιάζεται μικρότερο από αυτό με τα μη τροποποιημένα CNTs. Ουσιαστικά μπορούμε να υποθέσουμε ότι αυτή η κρούστα, με χαμηλότερο δικό της μέτρο ελαστικότητας, δρα αρνητικά στη συνολική δυσκαμψία της μήτρας.

Όσον αφορά τη χαμηλή τιμή δυσκαμψίας της νανοσύνθετης μήτρας με CNTs, όπου χρησιμοποιήθηκε πολύ δυνατό οξύ για την τροποποίηση της επιφάνειας τους, ίσως οφείλεται είτε σε πιθανή καταστροφή του τοιχώματος στην επιφάνεια των CNTs από το οξύ, είτε σε χαμηλή τιμή της αναλογίας L/D από τη δημιουργία συσσωματωμάτων. Παρόλα αυτά, οι εικόνες που πήραμε με το ηλεκτρονικό μικροσκόπιο σάρωσης (SEM) για τα συγκεκριμένα δείγματα, δείχνουν μια κατακερματισμένη μορφολογία, όπου η συνεκτικότητα της μήτρας είναι απούσα σε πολλά σημεία μακριά από το σημείο θραύσης. Το παραπάνω σε συνδυασμό με την απουσία καρβοξυλικής ρίζας, από την ανάλυση με το FTIR, αποτελούν ένδειξη για περαιτέρω μελέτη.

Όπως είναι εμφανές και από το ιστόγραμμα 3.17, (σελ. 78), όταν συγκρίνουμε τα βασικά δείγματα #1 και #10 παρατηρούμε μεγαλύτερες τιμές αντοχής για αυτά που κατασκευάστηκαν με τη τεχνική vacuum-bag από αυτά με τη hand lay-up. Αυτό συμ-

βαίνει ακόμα και αν έχουμε παρόμοιο ποσοστό όγκου ινών στο σύνθετο. Αυτό μας οδηγεί στο συμπέρασμα ότι η πρώτη τεχνική οδηγεί σε μια πιο δυνατή διεπιφανειακή σχέση μήτρας-ίνας.

Ένα ακόμα συμπέρασμα που καταλήγουμε είναι ότι η εισαγωγή CNTs σε μήτρα σύνθετου υλικού, ενισχύει την αντοχή του δεύτερου. Η σύγκριση γίνεται μεταξύ των υβριδικών δειγμάτων και του βασικού #10, το οποίο έχει παρόμοιο κλάσμα όγκου με τα πρώτα και έχει κατασκευασθεί με την ίδια τεχνική. Επίσης, το αν είναι αναγκαία η οποιαδήποτε χημική τροποποίηση της επιφάνειας των CNTs, για να οδηγηθούμε σε καλύτερα μηχανικά αποτελέσματα αντοχής, είναι ακόμα υπό διερεύνηση.

Τα καλύτερα αποτελέσματα ενίσχυσης της αντοχής προήλθε από τα δείγματα που φτιάχτηκαν σύμφωνα με την 2-steps μέθοδο. Η διαφορά, στην αντοχή, μεταξύ αυτών και των δειγμάτων με τα μη τροποποιημένα CNTs είναι πολύ μικρή. Παρόλο που η διαφορά δεν είναι πολύ μεγάλη, είναι φανερό ότι η εισαγωγή σωματιδίων με υψηλό μέτρο δυσκαμψίας σε μια μήτρα (ο λόγος του μέτρου ελαστικότητας των CNTs σε σχέση με την ρητίνη είναι $>$ 300!) δεν είναι επιζήμια για την αντοχή και τη δυσθραυστότητα του συνόλου. Κάτι που φαίνεται και στην ιδιότητα παραμόρφωσης θραύσης του υλικού.

Σχετικά, λοιπόν, με την ιδιότητα της παραμόρφωσης θραύσης μπορούμε να τονίσουμε την μεγάλη διαφορά των περισσότερων συνθέτων από την ονομαστική τιμή των ινών άνθρακα 3.18, (σελ. 78). Αυτό είναι αποτέλεσμα του μηχανισμού ευθυγράμμισης των ινών στο ύφασμα, όπως περιγράφτηκε παραπάνω. Το τελικό μήκος των ινών πριν να επέλθει η θραύση, είναι το άθροισμα των επιμηκύνσεων (ως τη θραύση) του γραφιτικού υλικού, αυξημένο κατά ένα συντελεστή της τάξεως:

$$1.14\alpha_{weft}/2 \ ,$$

όπου α_{weft} είναι το σχετικό πλάτος των νημάτων του υφαδιού (αδιάστατο μέγεθος), πάνω και κάτω από εκεί που περνάει το κάθετο σε αυτή νήμα του υφάσματος, το στημόνι. Αυτό στην περίπτωσή μας, θα μπορούσε να προσθέσει ένα επιπλέον 20% επιμήκυνσης σε σχέση με το εκτιμώμενο 1,9% παραμόρφωση θραύσης των ινών άνθρακα που χρησιμοποιείται. Η προσθήκη των CNTs στη μήτρα μειώνεται σε κάποιο βαθμό την επιμήκυνση θραύσης. Αυτό μπορεί να αποδοθεί στην αύξηση της δυσκαμψίας της μήτρας, η οποία μπορεί να μειώσει την προστιθέμενη παραμόρφωση λόγω της ευθυγράμμισης των ινών. Επειδή είναι τόσο πολύ πιο δύσκαμπτο σαν υλικό, τα CNTs από τη μήτρα μπορούν επίσης να δημιουργήσουν σημεία συγκέντρωσης τάσεων στο υλικό που να επιταχύνει την ανάπτυξη των πιθανών ρωγμών. Ευτυχώς, η μείωση της παραμόρφωσης θραύσης λόγω CNTs δεν είναι σημαντική και η δυσθραυστότητα του σύνθετου δεν θυσιάζεται.

Στο ιστόγραμμα 4.1, (σελ. 83) παρουσιάζεται η επιφάνεια κάτω από τα τα διαγράμματα τάσης-παραμόρφωσης για διάφορα δείγματα σύνθετων υλικών με τρία φύλλα ανθρακοϋφάσματος. Αντιστοιχεί στην ενέργεια που απαιτείται για να επέλθει θραύση του συνθέτου μας και μας δείχνει με αυτό το τρόπο τη δυσθραυστότητα των δειγμάτων μας. Συγκρίνοντας τα δείγματα των υβριδικών σύνθετων υλικών μεταξύ τους αλλά και με αυτό που δεν έχει νανοσωματίδια άνθρακα στο εσωτερικό του #10, τότε δεν παρατηρείτε βελτίωση της δυσθραστότητας. Αντίθετα, η σειρά #1, που δεν

διαθέτει νανοσωλήνες άνθρακα και έχει κατασκευαστεί με τη μέθοδο vacuum-bag, παρουσιάζει εξαιρετικά ψηλές τιμές δυσθραυστότητας στα δείγματα της.

Από την παραπάνω ανάλυση προκύπτει ότι η προσθήκη νανοσωλήνων και η δημιουργία υβριδικών συνθέτων έχει περισσότερα πλεονεκτήματα απ' ότι μειονεκτήματα για τις μηχανικές ιδιότητες του υλικού. Ενώ οι ιδιότητες εφελκυσμού του συνθέτου δεν βελτιώνονται πολύ, η δυσκαμψία της μήτρας αυξήθηκε. Όπως αναφέρεται και στην εισαγωγή, συνήθως, τα σύνθετα υλικά συνεχών ινών, παρουσιάζουν πολύ χαμηλή αντοχή σε φορτία θλίψης, παράλληλα προς την κατεύθυνση των ινών. Όταν, λοιπόν, συμπιέζονται αξονικά, οι ίνες θα λυγίσουν σε σχετικά χαμηλές δυνάμεις και το σύνθετο θα αστοχήσει Εκείνο που θα αποτρέψει τις ίνες από το να λυγίσουν είναι η δυσκαμψία της μήτρας. Δεδομένου ότι αυτή η δυσκαμψία αυξάνεται στα υβριδικά σύνθετα δείγματα μας, από την προσθήκη CNTs, θα έχουμε τόσο αυξημένη αντίσταση στο λυγισμό από τη μεριά του σύνθετου υλικού, όσο και ενίσχυση της αντοχής του σε θλίψη. Δυστυχώς, δεν διαθέταμε τον κατάλληλο εξοπλισμό στο εργαστήριο μας για να μετρήσουμε την αντοχή σε θλίψη και αρκούμαστε να παρουσιάσουμε κάποια σχετικά αποτελέσματα από τη βιβλιογραφία. Το σχήμα 4.2 (σελ. (σελ. 85) δείχνει την αύξηση της αντοχής σε θλίψη, διάφορων σύνθετων υλικών, συναρτήσει της δυσκαμψίας της εκάστοτε μήτρας.

Chapter 1

GENERAL INTRODUCTION

1.1 Types of composite materials

The increased demand for stronger and lighter structures across many major sectors of industry, such as the aeronautical, the automotive and the construction, has led to the development of novel materials. Part of this innovative breakthrough of the material science and engineering are the composites.

Composites are materials consisting of two or more components, which are combined to produce a final product with special properties and characteristics, different from the individual constituents [Antonogiannakis, 2013]. They are composed of a **matrix** material, such as polymer, ceramic or metal and **reinforcing** materials, such as carbon, glass, aramid (Kevlar™), silicon carbide etc.

The advantages of high performance composites are numerous, including lower weight, the ability to tailor lay-ups for optimum strength and stiffness, improved fatigue life, corrosion resistance and, with good design practise, reduced assembly costs due to fewer parts and fasteners. The specific strength and specific modulus of high strength fibre composites, especially those based on of carbon fibres, are greater than other comparable materials used in aerospace/aeronautical and automotive industry. This specific feature, translates to great weight savings, particularly in the transportation sector, resulting in increased performance, greater payloads, longer range and fuel savings. [Campbell, 2008]

The selection of the initial materials and the suitable mixing technique can lead to a composite that satisfies the needed properties set by the designers. Due to a large number of combinations in materials and mixing techniques, the composites can be categorised as follows:

- Composites with particulate fillers
- Fibre reinforced composites (including short and continuous fibres)
- Composites with laminar fillers

- Prepreg cloth
- Sandwich composites (including structural foam or honeycomb panels)

1.2 Reinforcement

The main purpose of the reinforcing material is to increase the strength and stiffness of the matrix. Thus, the reinforcement has higher mechanical properties than the matrix. The modulus of elasticity of the reinforcement may sometimes be lower than the one of the matrix. In this case the aim is the improvement of toughness rather than stiffness.

Isometric particle reinforced composites are the most economical regarding the manufacturing cost and can be characterised by the size of their particle filler. The purpose of using this type of reinforcement, is to increase the matrix modulus by 2 to 3 times. On the contrary, the strength of the produced composite is not improved. Sometimes it may decrease somewhat. This phenomenon occurs because the reinforcement-matrix interface creates stress concentration spots and may initiate cracks. The most important advantage of using particle reinforcement is the isotropic performance of the product [Gotsis, 2008]. If well bound to the matrix, large particles, such as gravel and sand in concrete or tungsten, titanium carbide in cermets or in abrasives, enhance its tribological properties. Similarly, smaller sized fillers, like carbon black (20-50 nm) used in auto tires as reinforced rubber, hinder the motion of dislocations in the matrix limiting in that manner plastic deformation. These powder particles are cost efficient and offer ease of handling and processing [Hull and Clyne, 1996].

Short fibres, when used as reinforcements in composite material, are more efficient than isometric particles in enhancing the load transfer mechanism between matrix and fibre. The characterisation as ”short” comes from their relative small L/D ratio, where L stands for length and D for diameter. Short fibres usually present L/D ratio of less than 100. This type of reinforcement increases the stiffness of the final product efficiently only when the forces act in the fibre’s direction. For that reason, two different manufacturing methods have been created. The first, keeps the fibres aligned inside the matrix, giving anisotropic properties to the composite. The second, has the fibres randomly distributed inside the matrix, giving on one hand isotropy and, on the other, lower mechanical properties.

By increasing the L/D ratio, the fibre’s direction and the properties of the reinforcement the Young’s modulus of the composite can be increased by up to 400%. Moreover, when the interface of reinforcement-matrix is strong and the load transfer mechanism performs well the fracture strength of the composite increases. Nevertheless, the use of short fibres decreases the strain at break and the toughness of the material [Antonogiannakis, 2013].

Continuous fibres reinforcement can bring the mechanical properties of the composite to reach the ones of the fibres. In this manner, we exploit the full potential of the fibres and the matrix undertakes the role of load transferring agent and keeping

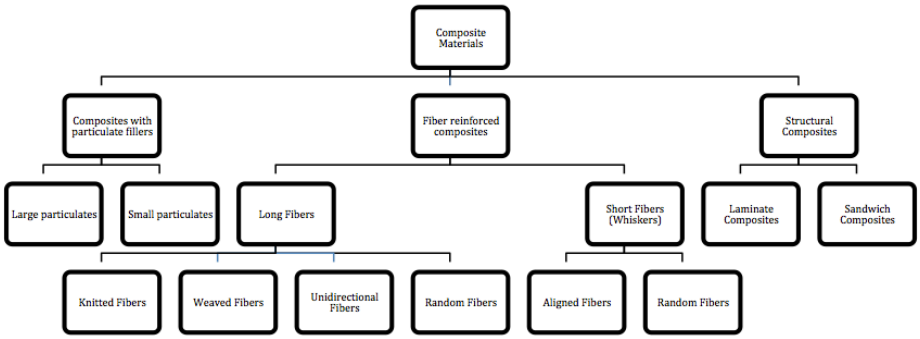

[Antonogiannakis, 2013]

Figure 1.1: Categories of composite materials

the fibres aligned. The most commonly used type of continuous fibre reinforcement is the unidirectional fibres, which provides the final product with great stiffness in the fibre's direction and great anisotropy perpendicular to them. The elasticity of the continuous fibres composites is described by the Classical Laminate Theory and is covered by the Reuss model and the Halpin-Tsai model for parallel and transverse loading respectively.

The best way to utilise the advantages given by the use of continuous fibre reinforcement in the composite is by using **woven fabrics** as reinforcement. Woven fabrics present usually a 2-D structure, where the wrap and the weft interact with each other in a 90°angle for the creation of patterns. These are categorised according to the periodicity of the weaving and the number of yarns per period to *plain*, *twill* and *satin* weave. Each type of weave inserts extra design parameters in addition to the material of the fibre, such as the density of the weaving, the number of fibres per yarn and the ratio of yarns per direction. All of these variations are easily found by customers, due to the increased availability in the composite market. Another form of fibre distribution, particularly for low-cost applications, is chopped strand mat, where bundles of relatively long fibres are assembled together with random in-plane orientations. The material is easy to handle as a preform and the composite produced has isotropic in-plane properties. However, the fibre volume fraction is limited to relatively low values.

Laminated reinforced composites have the form of a panel, in which the combination of a matrix and reinforcement enrich the final product properties such as stiffness, strength, corrosion resistance etc. This type of composites, usually characterised as anisotropic materials, is attributed with plane isotropy due to the use of several laminates in the construction structure. The most commonly produced fibre reinforcement is made from carbon, glass or other silicon compounds and several other organic materials, as aramid (™Kevlar), natural fibres etc. [Hull and Clyne, 1996].

Prepreg is a fibre form that has a predetermined amount of uncured thermosetting

polymer impregnated in the fibre strand by the material supplier. This form is available in many fibre and matrix combinations. Prepreg rovings and tapes are usually used in automated processes, such as filament winding and automated tape laying, while unidirectional tape and prepreg fabrics are used for hand-lay up [Campbell, 2008]. Specifically, the unidirectional prepreg tapes offer greater structural performance than woven prepregs, due to absence of fibre crimp and the ability to tailor more easily a variety of designs. Moreover, it is essential to use more than one unidirectional prepreg tape ply during laying up, in the form of 0 / 90°stacking, in order for the structure to achieve better plain isotropic behaviour. Prepreg reinforcement is very common in the construction of structures with complicated form, both in aerospace and in the automotive industry.

Sandwich structures is an extremely lightweight structural approach that exhibits high specific stiffness and strength. It is used extensively in aerospace and other commercial applications. The basic concept behind a sandwich panel is that the face sheets carry the bending loads, both tensional and compressional, while the core carries the shear loads [Campbell, 2008]. Sandwich construction, especially honeycomb core construction, is extremely structural efficient [Campbell, 2008] particularly in stiffness-critical applications. It has been shown that by doubling the thickness of the core, the overall stiffness increases by 7 times and, in that manner, by quadrupling it the stiffness of the composite increases 37 times [Campbell, 2008].

Face sheet materials that are normally used include glass, aluminium, carbon or aramid. These are extremely thin, leaving the rest of the structure thickness to the core. Between the face sheets, the core is made out of metallic or not metallic honeycomb, open and closed cell foams and syntactics. Sandwich panels are typically used for their structural, electrical, insulation and energy absorption characteristics.

1.2.1 Carbon Fibres

Carbon fibres are typically between 7 to 8 μm in diameter. They consist of small crystallites of "turbostatic" graphite, one of the allotropic forms of carbon [Hull and Clyne, 1996]. Turbostatic graphite resembles graphite single crystals, except that the layer planes are not regularly packed in the c-axis direction. A schematic representation of the carbon fibre structure is shown in the figure below.

The structure of a graphite single crystal has its carbon atoms arranged in hexagonal arrays in the form of sheets, stacked in a regular manner. In every sheet the carbon atoms are held together by strong covalent bonds. Weak van der Waals forces hold the sheets together. Therefore, the basic crystal unit of this structure is highly anisotropic, both mechanically and thermally. Thus, the in-plane Young's modulus, which is normal to the c-axis, is about 1000 GPa, close to that of diamond, while the perpendicular to the basal planes direction, is only 35 GPa [Hull and Clyne, 1996]. In order to achieve high values in terms of strength and modulus, the graphitic basal planes must be arranged in the main fibre's direction. The arrangement of these planes, parallel to the c-axis direction, is of great importance, due to its impact to the transverse and shear properties [Hull and Clyne, 1996].

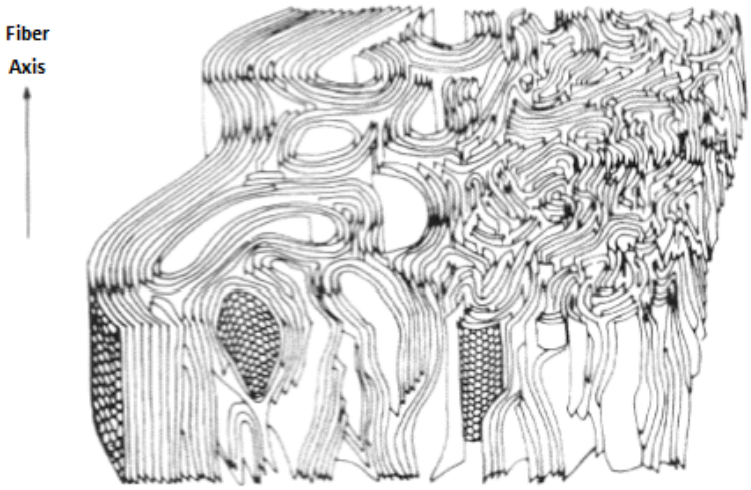

[Hull and Clyne, 1996]

Figure 1.2: Schematic representation of the structure of carbon fibres

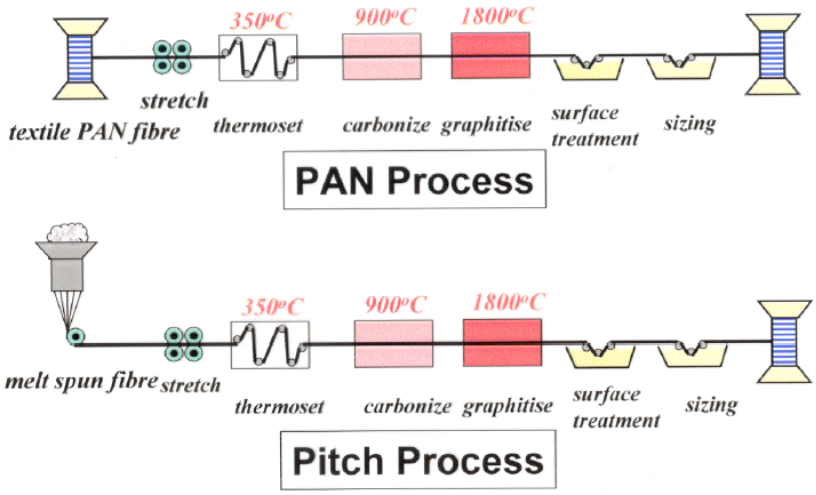

[Gotsis, 2008]

Figure 1.3: Schematic representation of the production process of carbon fibres

There are three main methods for the production of carbon fibres in industrial scale:

- From polyacrylonitrile fibres (PAN)
- From mesophase pitch
- From pyrolytic deposition

In one production process short length fibres (whiskers) are produced by pyrolytic deposition of hydrocarbons, such as methane, benzene and naphthalene in their gas phase.The other manufacturing procedures basically differ in the raw material they use. Polyacrylonitrile (PAN) or tar pitch (see figure 1.3) are used as a precursor. In both cases, the mechanical and thermal properties of the fibres depend on the final temperature treatment. Using high temperature, during the graphitisation phase, carbon fibres with high or even ultra high modulus are produced, but lower strength. On the contrary, the use of lower temperature values, during this final stage of production, creates high strength fibres. Table 1.1 presents the properties of different fibre materials. It is obvious that carbon fibres with higher strength are lighter but have lower stiffness.

Choosing the type of fibre needed for a specific application is a very important task, where various parameters should be considered during the design stage. Accordingly, the selection of the matrix material for the production of a carbon fibre composite

Table 1.1: Comparison of the mechanical properties of various types of fibres, [Hull and Clyne, 1996]

Material	E **Modulus** (GPa)	**Strength** (GPa)	**Density** (g cm^{-3})	**Sp. Modulus** (Mm)	**Sp. Strength** (Mm)
Aramid	124	3.6	1.45	8.5	.250
Boron	400	3.5	2.58	15.5	.136
Carbon/UHM	690	3.3	2.17	31.8	.152
Carbon/HM	400	380	1.95	21.5	.188
Carbon/IM	295	5.6	1.75	16.9	.320
Carbon/VHS	-	4.3	1.81	13.1	.237
Carbon/HS	235	3.5	1.75	13.3	.200
Glass E	71	2.4	2.54	2.7	.095
Glass R	86	4.4	2.55	3.4	.170
Steel wire	210	3.1	7.80	2.7	.040

must be taken into account. For applications employed in extreme conditions, such as hypersonic vehicles, low temperature carbon ($T = 500^{\circ}\mathrm{C}$) can react with oxygen, stating the entire structure subject to possible oxidative degradation [Bacos, 1993]. For that reason, usage of carbon/carbon composites, where the fibres are protected not only by ceramic matrix but have been cured with protective surfactants or additives, is essential for those types of extreme conditions. In case of simpler structures, polymer matrices, such as epoxy, are being preferred due to their lower cost of manufacture. Finally, the utilisation of metallic matrices with carbon reinforcement is not often, due to chemical reactions occurring with carbon atoms during the production phase, making the material too expensive for full scale production [Antonogiannakis, 2013].

1.2.2 Glass Fibres

Glass fibres are based on silica (SiO_2), with additions of certain oxides of boron, sodium, calcium, iron and aluminium. The content of these oxides, in the glass structure, affects both its physical and chemical properties, as we can see from the Table below 1.2.

The glass fibres are produced by melting the raw materials and letting the melt flow through platinum bushings, each having hundred of holes (spinneret). The glass, flowing under the force of gravity, forms fine filaments, which are drawn mechanically downwards. Then, the fibres are winded onto a drum at a very high speed. The diameter of these fibres vary according to several parameters, such as the viscosity of the molten glass, the diameter of the holes, the wrapping speed and by adjusting the head of the glass in the tank [Hull and Clyne, 1996]. Generally, in contrast with carbon, all types of glass fibres are isotropic.

There are three major types of commercially produced glass fibres. Those are the E-class, the C-class and the S-class. Each, has its unique properties and characteristics.

Table 1.2: Glass fibre composition and properties [Hull and Clyne, 1996].

Composition (%)	**E-Glass**	**C-Glass**	**S-Glass**
SiO_2	52.4	64.4	64.4
$Al_2O_3 + Fe_2O_3$	14.4	4.1	25.0
CaO	17.2	13.4	
MgO	4.6	3.3	10.3
$Na_2O + K_2O$	0.8	9.6	0.3
B_2O_3	10.6	4.7	
BaO		0.9	
Properties			
$\rho(Mgm^{-3})$	2.60	2.49	2.48
$K(Wm^{-1}K^{-1})$	13	13	13
$\alpha(10^{-6}K^{-1})$	4.9	7.2	5.6
$\sigma(GPa)$	3.45	3.30	4.60
$E(GPa)$	76.0	69.0	85.5
$T_{max}(^{\circ}C)$	550	600	650

The most common type of these three classes of glass fibre, is the E-class (Electrical) fibre with diameter between 8 to 15 μm and strength up to 3.5 GPa [Hull and Clyne, 1996]. This glass type has both fine electrical (isolator) and mechanical properties and it is more cost efficient than the other two. C-class (Corrosion), even though it has lower mechanical properties than E-class, has great corrosion resistance in extreme environments. Finally, the S-class (Strength) has higher strength and modulus than E-class glass, but is more expensive than the latter.

The strength depends on the environment of the test and the processing conditions. In humid environment, moisture is absorbed on the fibre's surface, degrading its mechanical properties. Apart of this, the presence of metallic oxides and at temperatures above $250^{\circ}C$ affect the fibre structural integrity [Antonogiannakis, 2013]. Regarding the production phase, damage dealt to the fibre's surface during wrapping on stools is a major factor of determining the strength of the final product, due to extensive friction.

1.2.3 Organic Fibres

Aramid is the most common organic polymer utilised in the creation of fibre reinforced composite structures. It was first developed by DuPont with the trade name ™Kevlar and is made also in Europe by Taijin-Twaron. According to the original patent of 1968, aramid fibres are derived from highly aromatic rigid chain polymer molecules (containing benzene rings on the backbone). These molecules form lyotropic liquid crystalline solutions and can oriented easily during processing to a very high degree. The produced fibres, thus, present very high Young's modulus and fracture strength. They are very anisotropic and because of the weak inter-chain bonding, they readily split into much finer fibrils and microfibrils [Hull and Clyne, 1996].

Applications that are based on aramid, span from racing sails and bicycle tires to bulletproof vests, due to the ability of the fibres to withstand extremely high impact forces in regard to its weight.

1.3 Matrices

The role of the matrix is to hold the fibres in their proper position, to transfer the load between fibres, to protect the fibres from abrasion and corrosion caused by chemical or extreme environmental conditions, to provide inter-laminar shear strength, to have high strain-to-failure, to be non-toxic and to cure at as low a temperature as possible. The most common materials used for matrix purpose in a composite structure are the polymers. Ceramic and metallic matrices are less often used and request high manufacturing cost.

1.3.1 Polymer Matrices

Polymeric matrices are the most common choice in composite manufacturing, due to the simplicity that they bring in the production of the composite structure. Moreover, several other attributes, as the low viscosity in room temperature, which provide easier fibre wetting, the compatibility with most of the reinforcement materials, the low weight, the elastoplastic behaviour etc., make the polymer based composites attractive and in high demand. They are categorised according to their chemical synthesis. The most common types of polymer composites use either thermosetting resins or thermoplastic polymers and their use is strongly depended on the operational temperature of the application, especially in the case of thermoplastics [Hull and Clyne, 1996].

Thermosetting Resins

Thermosetting resins usually consist of a resin, for example epoxy resin or unsaturated polyester, and a compatible curing agent (hardener). When the two are mixed, a low viscosity liquid is formed that undergoes a cross-linking reaction (curing) either exothermically or by externally applied heat. The chemical cross-linking reaction leads to the formation of a tightly bound three-dimensional molecular network [Hull and Clyne, 1996] and the liquid is converted into a hard, rigid solid. The formation of this network is responsible for the mechanical properties of the final product. Curing can be take place at room temperature, but it is usual to cure at higher temperatures to achieve optimum cross-linking and, hence, optimum properties. Thermosets are brittle with high variation in their properties and the most prevalent used in composite production are vinyl esters, polyesters, epoxies, polyimides, bismaleimides and phenolics [Campbell, 2008].

Thermoplastics

The thermoplastics, on the other hand are already fully polymerised. When molten they form high viscosity melts. Because of this particular feature they can be easily reused a number of times. Their stiffness and strength derives from the properties of their monomers and their high molecular weight. In the solid state they can be amorphous or semicrystalline materials. Even in the amorphous state the molecular entanglement is high, keeping the rigidity and stiffness of the structure. Comparing to the thermosetting resins, thermoplastics show higher failure strains and resistance to chemicals [Hull and Clyne, 1996]. Most known polymer of this category are Nylon, polyethylene, polypropylene, polystyrene, polyether ether ketone (PEEK) etc. [Hull and Clyne, 1996]. Their major disadvantage is the high viscosity of their melts that makes the impregnation of the fibres difficult. This limits their usefulness as matrices for continuous fibre composites.

1.3.2 Ceramic Matrices

Ceramic materials present many desirable properties, such as high compression strengths and moduli, very high temperature capability, high hardness and wear resistance, chemical inertness and low thermal conductivity. Especially, their high temperature capability makes them attractive for applications in very high temperature environments. For example, in the aerospace industry where such composites are used as heat shields, leading edges and thermal protection for space shuttles [Campbell, 2008]. However, due to their very low fracture toughness, ceramics are limited in structural applications. Contrary to metals, which deform plastically, ceramics do not show plastic deformation at room temperature and are prone to catastrophic failure under mechanical loading. Their very little tolerance in crack defects, which can easily result during production or in-service, can lead to sudden failure even from a small crack that grow quickly to critical size. For that reason reinforcements, such as fibres, whiskers or particles are required to increase toughness via dissipating mechanisms, such as fibre-to-matrix debunking, crack deflection, fibre bridging and fibre pull-out [Campbell, 2008]. Coatings are often applied on these reinforcements, to protect the fibre during the processing stage and provide a weak fibre-to-matrix bond. Examples of ceramic composite matrices are carbon, glass, glass-ceramic and crystalline ceramic matrices. As reinforcements, the most known is carbon for C-C composites, oxide fibres as alumina, non-oxide fibres as silicon carbide [Campbell, 2008].

1.3.3 Metallic Matrices

Metal matrix composites present many advantages compared to base metals, such as higher elevated temperature resistance, higher specific strength and modulus, lower coefficients of thermal expansion, good wear resistance and good creep performance. On the other hand, they are very expensive and show lower toughness than base metals and due to this high cost fabrication processes, the number of commercial applications is sparse [Campbell, 2008].Currently the development of metal matrix compos-

ites is concentrated mostly on three metals, aluminium, magnesium and titanium. The type of reinforcement used with metal matrix is either short fibres (whiskers), particulates and continuous monofilament fibres. A common example is an aluminium matrix with silicon carbide or alumina ceramic particles.[Campbell, 2008].

1.4 Elastic deformation of long fibre composites

In order to begin describing the theories regarding the mechanical properties of the long (continuous) fibre composites, we should, first, state some fundamental assumptions:

- Homogeneity of the matrix
- The interface of the fibre-matrix is significantly thin
- Strain compatibility between fibre and matrix
- Fibre alignment
- Both the fibre and the matrix follow ideal elastic behaviour

1.4.1 Axial Stiffness

Consider a unidirectional composite material, which is subject to a loading in the direction of the fibres. The overall load P, applied to the material, is the sum of of the loadings apply on the fibre and the matrix. The stress of the fibre is $\sigma_f = E_f * \epsilon_f$ and for the matrix $\sigma_m = E_m * \epsilon_m$. Assuming that the fibres are stiffer than matrix ($E_f >> E_m$), then the reinforcement is subject to much higher stresses than the matrix ($\sigma_1 f >> \sigma_1 m$). If *A* is the cross sectional area of the specimen then:

$$P = \sigma_1 A \qquad P_f = \sigma_f A_f \qquad P_m = \sigma_m A_m$$

$$P = P_f + P_m = \sigma_f A_f + \sigma_m A_m = \sigma_1 A$$

For excellent fibre-matrix contact: $\epsilon_= \epsilon_m = \epsilon_1$

$$\sigma_1 = E_1 \epsilon_1 \qquad \sigma_f = E_f \epsilon_1 \qquad \sigma_m = E_m \epsilon_1 \qquad P = P_f + P_m$$

$$E_1 \epsilon_1 A = E_m \epsilon_m A_m + E_f \epsilon_f A_f \Rightarrow E_1 = E_f \frac{A_f}{A} + E_m \frac{A_m}{A} \Rightarrow$$

$$E_1 = E_m(1 - \phi) + \phi E_f$$

where ϕ is the volume fraction of the fibres

According to the above equation, which is called *"Rule of Mixtures"*, it is clear that composite's stiffness is simply a weighted mean between the modulus of the two components, depending only to the volume fraction of the fibres. This equation is expected

to be of high degree of precision, providing the fibres are long enough for equal assumption to apply (often described as *"Voigt Model"*) [Hull and Clyne, 1996] , as it is stated earlier.

1.4.2 Transverse Stiffness

Prediction of the transverse stiffness of a composite from elastic properties of the constituents is far more difficult than in the axial direction. Measurements of transverse stiffness can lead to errors, partly as a result of higher stresses in the matrix [Hull and Clyne, 1996]. Trying to describe the phenomena we can use a simplified model, called *"Equal Stress Model"* (often described as *"Reuss Model"*.

The stress, applied perpendicularly to the cross sectional area of the composite, is equally distributed both the fibre and the matrix.

$$\sigma_f = \sigma_m \qquad \epsilon_2 \neq \epsilon_m \neq \epsilon_f \ ,$$

where

$$\epsilon_f = \frac{\sigma_2}{E_f} \qquad \epsilon_m = \frac{\sigma_2}{E_m} \ .$$

The overall strain is the weighted mean value of the strains of the fibre and the matrix, depending on the volume fraction of the fibre ϕ.

$$\epsilon_2 = \frac{\sigma_2}{E_2} = \frac{\sigma_2 \phi}{E_f} + \frac{\sigma_2 (1-\phi)}{E_m} \quad \Rightarrow \quad E_2 = \left[\frac{\phi}{E_f} + \frac{1-\phi}{E_m} \right]^{-1}$$

1.4.3 Poisson Ratio

The Poisson ratio, ν_{ij}, is defined by $\nu_{ij} = -\epsilon_j / \epsilon$ and describes the contraction in the j-direction on applying a stress in the i-direction. For an aligned fibre composite, there are three different Poisson's ratios, as illustrated in the figure below 1.4:

Because of the orthotropic nature of composites the following equations are describing the relation of the Poisson's ratios with the Young's modulus and the shear modulus.

$$\frac{\nu_{12}}{E_1} = \frac{\nu_{21}}{E_2} \ , \qquad G_{23} = \frac{E-2}{2(1+\nu_{23})}$$

For ν_{12}, as described above by the *"Rule of Mixtures"*, we have equal strains:

$$\epsilon_{1f} = \epsilon_{1m} = \epsilon_1 \qquad \text{and}$$

$$\epsilon_{2f} = \nu_f \epsilon_{1f} = -\nu_f \frac{\sigma_{1f}}{E_f} \qquad \epsilon_{2m} = \nu_f \epsilon_{1m} = -\nu_f \frac{\sigma_{1m}}{E_m}$$

This leads to:

$$\epsilon_2 = -\left[\frac{\phi \nu_f \sigma_{1f}}{E_f} + \frac{(1-\phi)\nu_m \sigma_{1m}}{E_m} \right] = -\phi \nu_f \epsilon_1 - (1-\phi)\nu_m \epsilon_1$$

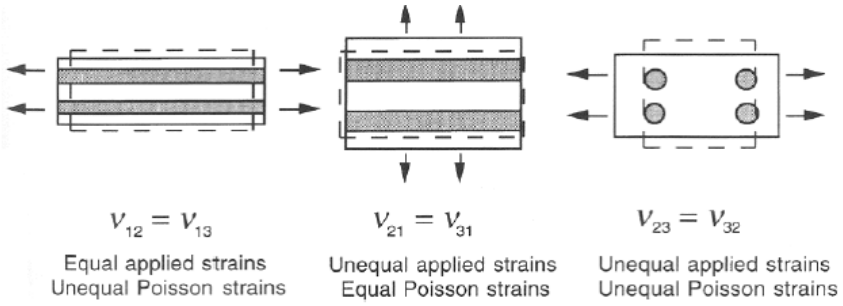

[Hull and Clyne, 1996]

Figure 1.4: Schematic representation of the three Poisson's ratios are defined for a fibre composite

$$\nu_{12} = -\frac{\epsilon_2}{\epsilon_1} \Rightarrow \nu_{12} = \phi\nu_f + (1-\phi)\nu_m$$

Additionally the Poisson ratio for ν_{23} is given from the *"Equal Stress Model"*:

$$\frac{1}{\nu_{23}} = \frac{\phi}{\nu_{23f}} + \frac{1-\phi}{\nu_m}$$

1.4.4 Shear Stiffness

A shear stress defined as τ_{ij} ($i \neq j$), refers to a stress acting in the i-direction on the plane with a normal in the j-direction. In the same manner, a shear strain γ_{ij} is a rotation towards the i-direction of the j-axis. Following the above, shear modulus G_{ij} is defined as the ratio of τ_{ij} to γ_{ij} and can be predicted in similar way to the axial and transverse stiffnesses. This is done by evaluating the net shear strain induced when a shear stress is applied to the composite, in terms of the individual displacement contributions from the two constituents.

As the composite structure does not perform rotation, the condition $\tau_{ij} = \tau_{ji}$ must hold. Similarly, $G_{ij} = G_{ji}$ and $\gamma_{ij} = \gamma_{ji}$. So we conclude that:

$$G_{12} = G_{21} = G_{13} = G_{31} \qquad \text{and} \qquad G_{23} = G_{32}$$

In order to calculate the values of the first group, we assume that shear stresses applied to the fibres and the matrix, are equal to the perpendicular to the direction of the fibres:

$$\tau_{12} = \tau_{12f} = \gamma_{12f}G_f = \gamma_{12m}G_m$$

And for $G_{23} = G_{32}$ we have equal strain values

$$\gamma_{23} = \gamma_{23f} = \frac{\tau_{23f}}{G_f} = \frac{\tau_{23m}}{G_m}$$

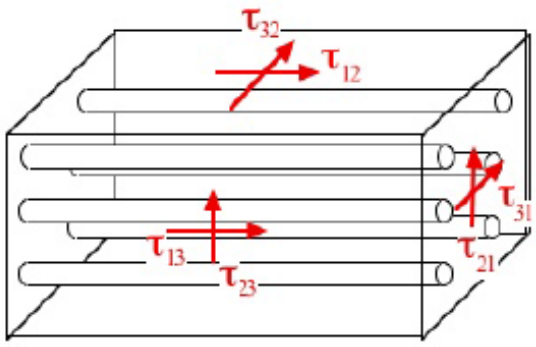

[Gotsis, 2008]

Figure 1.5: Shear tension in unidirectional composite material

So, the overall shear strain is the weight mean value of the strains of the fibre and the matrix, depending on the volume fraction of the fibre.

$$\gamma_{12} = \phi\gamma_{12f} + (1-\phi)\gamma_{12m}$$

Concluding, the shear modulus for G_{12} and G_{23} are:

$$G_{12} = \left[\frac{\phi}{G_f} + \frac{1-\phi}{G_m}\right]$$

$$G_{23} = \phi G_f + (1-\phi)G_m$$

1.4.5 Elastic deformation of anisotropic materials

Basic principles

Before we begin our analysis on the mechanical laws and properties of the fibre composites, which is described by the *Laminate Theory*, we should, first, review some basic points about stress and strain [Hull and Clyne, 1996],[Nye, 1985].

The state of stress at a point is defined by the nine components of the ***stress tensor***, σ_{ij}, in which the stress acts in the i-direction on the plane with normal to the j-direction. In case of, $i = j$, then σ_{ij} is a normal stress and if $i \neq j$, it represents a shear stress. defined as τ_{ij}.

Regarding the mechanical property of strain, care must be taken, distinguishing the ***strain tensor*** ϵ_{ij} from the ***relative displacement tensor*** e_{ij}. Application of shear stress τ_{ij} and τ_{ji}, produces angular rotations of the i- and j- directions in the body by ϵ_{ij} and

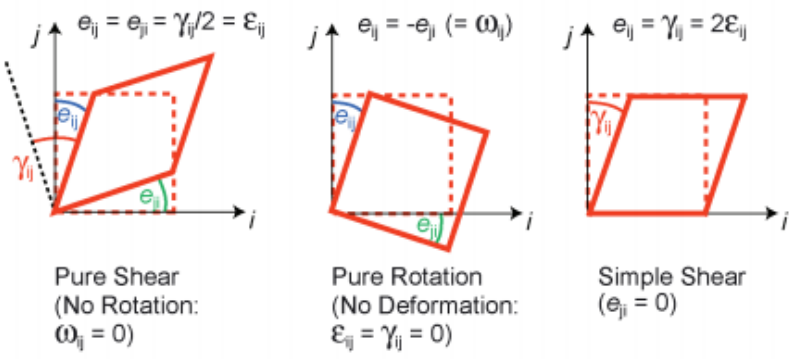

[Hull and Clyne, 1996]

Figure 1.6: 2-D relative displacement components displaying different combinations of shear and rigid body rotation

ϵ_{ji} respectively. These displacements represent a combination of distortion (strain) and rigid body rotation.

$$\epsilon_{ij} = \frac{1}{2}(e_{ij} + e_{ji}) + \frac{1}{2}(e_{ij} + e_{ji}) = \epsilon_{ij} + \omega_{ij}$$

where ϵ_{ij} is the strain tensor and ω_{ij} is the rotation tensor.

In exclusive cases, e.g. for *no rotation*, we have $\epsilon_{ij} = \epsilon_{ji}$ and $\tau_{ij} = \tau_{ji}$. Accordingly, when *no distortion* occurs, we have $\epsilon_{ij} = -\epsilon_{ji}$. Regarding the normal strains, there is no confusion, as $e_{ii} = \epsilon_{ii}$. However, the engineering shear strain, γ_{ij}, is defined as:

$$\gamma_{ij} = 2\epsilon_{ij} = e_{ij} + e_{ji}$$

The relationship between σ_{ij} and ϵ_{ij} can be expressed as

$$\sigma_{ij} = C_{ijkl}\epsilon_{kl} \ ,$$

where C_{ijkl} is the ***stiffness tensor***. For each equation (pair of i and j values), the terms which arise are dictated by ***Einstein summation convention***. This states that when a suffix appears twice in a product then the terms are summed with respect to that suffix. Therefore, the first equation will be

$$\begin{aligned}\sigma_{11} = {} & C_{1111}\epsilon_{11} + C_{1112}\epsilon_{12} + C_{1113}\epsilon_{13} \\ & + C_{1121}\epsilon_{21} + C_{1122}\epsilon_{22} + C_{1123}\epsilon_{23} \\ & + C_{1131}\epsilon_{31} + C_{132}\epsilon_{32} + C_{1133}\epsilon_{33}\end{aligned}$$

In practise, though, the equations are much more simpler, especially in the case of static equilibrium state of the body, which implies symmetry of the stress and strain

tensors.

$$C_{ijkl} = C_{ijlk} = C_{jikl} = C_{jilk}$$

In regard to this symmetry, we can employ a different notation, like the ***matrix notation***

$$\sigma_p = C_{pq}\epsilon_q$$

where p and q run from 1 to 6. So we conclude to the following form

$$\begin{bmatrix} \sigma_1 \\ \sigma_2 \\ \sigma_3 \\ \tau_{23} \\ \tau_{31} \\ \tau_{12} \end{bmatrix} = \begin{bmatrix} C_{11} & C_{12} & C_{13} & C_{14} & C_{15} & C_{16} \\ C_{21} & C_{22} & C_{23} & C_{24} & C_{25} & C_{26} \\ C_{31} & C_{32} & C_{33} & C_{34} & C_{35} & C_{36} \\ C_{41} & C_{42} & C_{43} & C_{44} & C_{45} & C_{46} \\ C_{51} & C_{52} & C_{53} & C_{54} & C_{55} & C_{56} \\ C_{61} & C_{62} & C_{63} & C_{64} & C_{65} & C_{66} \end{bmatrix} \begin{bmatrix} \epsilon_1 \\ \epsilon_2 \\ \epsilon_3 \\ \gamma_{23} \\ \gamma_{31} \\ \gamma_{12} \end{bmatrix}$$

Additionally with the above, it more useful to be able to express strains in terms of stresses, using the the ***compliance tensor***, S_{ijkl}.

$$\epsilon_{ij} = S_{ijkl}\sigma_{kl}$$

Following the matrix notation we have:

$$\epsilon_p = S_{pq}\sigma_q$$

Lamina analysis

Assuming that each thin unidirectional lamina in a composite material, is in a plane stress state, with can say that $\sigma_3 = \tau_{23} = \tau_{31} = 0$. Applying the compliance tensor, of matrix notation, S_{pq}.

$$\begin{bmatrix} \epsilon_1 \\ \epsilon_2 \\ \gamma_{12} \end{bmatrix} = [S] \begin{bmatrix} \sigma_1 \\ \sigma_2 \\ \tau_{12} \end{bmatrix} = \begin{bmatrix} S_{11} & S_{12} & 0 \\ S_{12} & S_{22} & 0 \\ 0 & 0 & S_{66} \end{bmatrix} \begin{bmatrix} \sigma_1 \\ \sigma_2 \\ \tau_{12} \end{bmatrix}$$

It can be, also, shown as

$$S_{11} = \frac{1}{E_1}$$

$$S_{12} = -\frac{\nu_{12}}{E_1} = -\frac{\nu_{21}}{E_2}$$

$$S_{22} = \frac{1}{E_2}$$

$$S_{66} = \frac{1}{G_1 2}$$

And by applying the stiffness tensor, C_{pq}

$$\begin{bmatrix} \sigma_1 \\ \sigma_2 \\ \tau_{12} \end{bmatrix} = [C] \begin{bmatrix} \epsilon_1 \\ \epsilon_2 \\ \gamma_{12} \end{bmatrix} = \begin{bmatrix} C_{11} & C_{12} & 0 \\ C_{12} & C_{22} & 0 \\ 0 & 0 & C_{66} \end{bmatrix} \begin{bmatrix} \epsilon_1 \\ \epsilon_2 \\ \gamma_{12} \end{bmatrix}$$

$$C_{11} = \frac{E_1}{1 - \nu_{12}\nu_{21}}$$
$$C_{12} = \frac{\nu_{12}E_2}{1 - \nu_{12}\nu_{21}} = \frac{\nu_{21}E_1}{1 - \nu_{12}\nu_{21}}$$
$$C_{22} = \frac{E_2}{1 - \nu_{12}\nu_{21}}$$
$$C_{66} = G_{12}$$

Because of the lamina's symmetry, we have as a result *four* independent elastic constants and no interaction between normal and shear behaviour [Hull and Clyne, 1996].

However, by changing, arbitrarily, the direction of loading to the lamina, as shown in the figure above 1.7, certain steps must be followed. Firstly, we have to establish the relation between the stresses, referred to the fibre's axis and the externally applied stress system. This can be achieved by using the classical conversion of coordinates, where $c = \cos\phi$ and $s = \sin\phi$.

$$[\sigma] = [\alpha]\,[\sigma']\,[\alpha]^T \qquad \text{or} \qquad \sigma_{ij} = \alpha_{ik}\sigma'_{kl}\alpha_{jl}$$

where the α array is consisted entirely by cosines of the angles between the two axis of the old and the new coordinate system. By that, we conclude to this

$$\begin{bmatrix} \sigma_1 \\ \sigma_2 \\ \tau_{12} \end{bmatrix} = [T] \begin{bmatrix} \sigma_x \\ \sigma_y \\ \tau_{xy} \end{bmatrix} \quad \text{with} \quad [T] = \begin{bmatrix} c^2 & s^2 & 2cs \\ s^2 & c^2 & -2cs \\ -cs & cs & c^2 - s^2 \end{bmatrix}$$

In the same manner, we have for the strain

$$\begin{bmatrix} \epsilon_1 \\ \epsilon_2 \\ \gamma_{12} \end{bmatrix} = [T'] \begin{bmatrix} \epsilon_x \\ \epsilon_y \\ \gamma_{xy} \end{bmatrix}$$

$$[T'] = \begin{bmatrix} c^2 & s^2 & cs \\ s^2 & c^2 & -cs \\ -2cs & 2cs & c^2 - s^2 \end{bmatrix}$$

There is a straightforward procedure, linking the stress-strain properties of the randomly loaded lamina. This is done by involving a ***transformed compliance tensor***, $\overline{S}$, which will depend on ϕ. So we begin by

$$\begin{bmatrix} \epsilon_x \\ \epsilon_y \\ \gamma_{xy} \end{bmatrix} = [T']^{-1} \begin{bmatrix} \epsilon_1 \\ \epsilon_2 \\ \gamma_{12} \end{bmatrix}$$

in which

$$[T']^{-1} = \begin{bmatrix} c^2 & s^2 & -cs \\ s^2 & c^2 & cs \\ 2cs & -2cs & c^2 - s^2 \end{bmatrix}$$

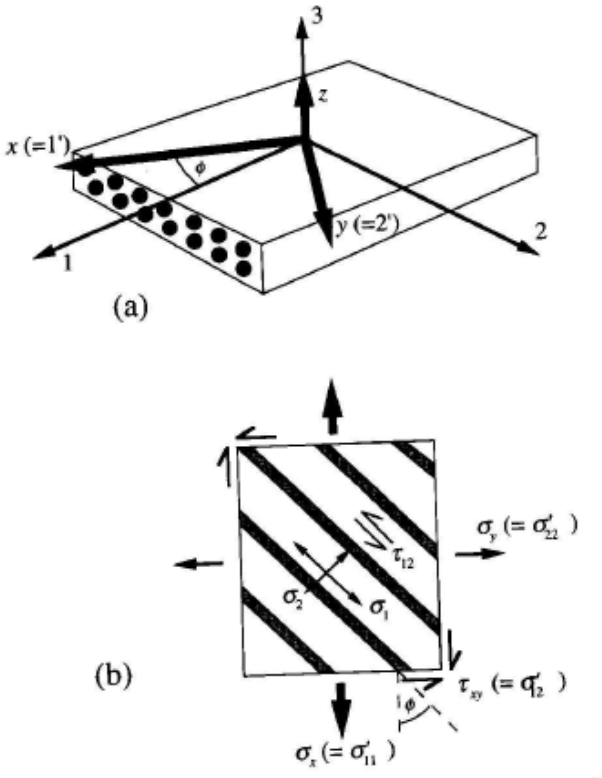

[Hull and Clyne, 1996]

Figure 1.7: (a) Relationship between the principal axis of a lamina (1,2,3) and the coordinate system (x,y,z) for an arbitrary in-plain applied stress. (b) Applied stress system σ_{ij} (σ_x, σ_y, τ_{xy}) produces stresses in the lamina σ_{ij} (σ_1 , σ_2, τ_{xy}).

Now by implementing the stresses in the direction of the fibres in the equation we end up with the following

$$\begin{bmatrix} \epsilon_x \\ \epsilon_y \\ \gamma_{xy} \end{bmatrix} = [T']^{-1}[S] \begin{bmatrix} \sigma_1 \\ \sigma_2 \\ \tau_{12} \end{bmatrix}$$

In addition to the above, we switch the stresses in the fibres direction to the ones implemented in the random direction:

$$\begin{bmatrix} \epsilon_x \\ \epsilon_y \\ \gamma_{xy} \end{bmatrix} = [T']^{-1}[S][T] \begin{bmatrix} \sigma_x \\ \sigma_y \\ \tau_{xy} \end{bmatrix} = \begin{bmatrix} \overline{S} \end{bmatrix} \begin{bmatrix} \sigma_x \\ \sigma_y \\ \tau_{xy} \end{bmatrix}$$

where $\begin{bmatrix} \overline{S} \end{bmatrix} = [T']^{-1}[S][T]$ is defined as ***concatenation matrix***

$$\begin{bmatrix} \epsilon_x \\ \epsilon_y \\ \gamma_{xy} \end{bmatrix} = \begin{bmatrix} \overline{S}_{11} & \overline{S}_{12} & \overline{S}_{16} \\ \overline{S}_{12} & \overline{S}_{22} & \overline{S}_{26} \\ \overline{S}_{16} & \overline{S}_{26} & \overline{S}_{66} \end{bmatrix} \begin{bmatrix} \sigma_x \\ \sigma_y \\ \tau_{xy} \end{bmatrix}$$

Particularly

$$\begin{aligned}
\overline{S}_{11} &= S_{11}c^4 + S_{22}s^4 + (2S_{12} + S_{66})c^2s^2 \\
\overline{S}_{12} &= S_{12}(c^4 + s^4) + (S_{11} + S_{22} - S_{66})c^2s^2 \\
\overline{S}_{22} &= S_{11}s^4 + S_{22}c^4 + (2S_{12} + S_{66})c^2s^2 \\
\overline{S}_{16} &= (2S_{11} - 2S_{12} - S_{66})c^3s - (2S_{22} - 2S_{12} - S_{66})cs^3 \\
\overline{S}_{26} &= (2S_{11} - 2S_{12} - S_{66})cs^3 - (2S_{22} - 2S_{12} - S_{66})c^3s \\
\overline{S}_{66} &= (4S_{11} + 4S_{22} - 8S_{12} - S_{66})c^2s^2 + S_{66}(c^4 + s^4)
\end{aligned}$$

The Young's and shear moduli and the Poisson ratios are:

$$E_x = \frac{1}{\overline{S}_{11}} \qquad E_y = \frac{1}{\overline{S}_{22}} \qquad G_{xy} = \frac{1}{\overline{S}_{66}}$$

$$\nu_{xy} = -E_x\overline{S}_{11} \qquad \nu_{yx} = -E_y\overline{S}_{11}$$

Similarly, we have the ***transformed stiffness tensor***, linking the stresses and strains in the created by the applied loading in the random direction

$$\begin{bmatrix} \sigma_x \\ \sigma_y \\ \tau_{xy} \end{bmatrix} = \begin{bmatrix} \overline{C}_{11} & \overline{C}_{12} & \overline{C}_{16} \\ \overline{C}_{12} & \overline{C}_{22} & \overline{C}_{26} \\ \overline{C}_{16} & \overline{C}_{26} & \overline{C}_{66} \end{bmatrix} \begin{bmatrix} \epsilon_x \\ \epsilon_y \\ \gamma_{xy} \end{bmatrix}$$

$$\begin{aligned}
\overline{C}_{11} &= C_{11}c^4 + S_{22}s^4 + (2C_{12} + 4S_{66})c^2s^2 \\
\overline{C}_{12} &= C_{12}(c^4 + s^4) + (C_{11} + C_{22} - 4C_{66})c^2s^2 \\
\overline{C}_{22} &= C_{11}s^4 + C_{22}c^4 + (2C_{12} + 4C_{66})c^2s^2 \\
\overline{C}_{16} &= (C_{11} - C_{12} - 2C_{66})c^3s - (C_{22} - C_{12} - 2C_{66})cs^3 \\
\overline{C}_{26} &= (C_{11} - C_{12} - 2C_{66})cs^3 - (C_{22} - C_{12} - 2C_{66})c^3s \\
\overline{C}_{66} &= (C_{11} + C_{22} - 2C_{12} - 2C_{66})c^2s^2 + C_{66}(c^4 + s^4)
\end{aligned}$$

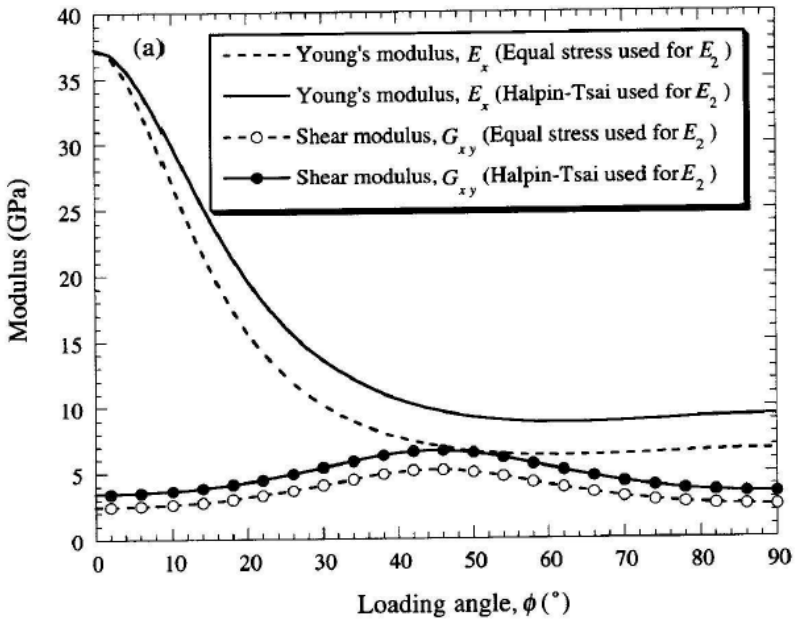

[Hull and Clyne, 1996]

Figure 1.8: Variation with loading angle ϕ of Young's modulus E_x and shear modulus G_{xy} for a lamina of glass/epoxy.

1.4.6 Elastic deformation of laminates

It is evident in Fig. 1.8 that the individual unidirectional laminae containing aligned fibres tend to exhibit highly anisotropic behaviour. This anisotropy can be reduced by stacking *n* laminae (plies) with different fibre orientations and bonding them together to form a laminate [Hull and Clyne, 1996].

The elastic properties of such laminate can be predicted from the constituent plies, providing that certain assumptions have been taken into account. Those assumptions, known as ***Kirchhoff assumptions***, are:

- The assembly is taken to be flat and thin
- No through-thickness stresses
- Edge effects are neglected
- We assume $\epsilon_x, \epsilon_y, \gamma_{xy} \ll 1$

Following the scheme in the above figure 1.9, we have the loading angle between the stress axis (x-axis) and the reference direction for the orientation of the plies $(\phi = 0^\circ)$, expressed as Φ. Therefore, the fibre direction of the k_{th} ply, lies at an angle $(\phi - \Phi)$ to the stress axis. The overall average stress in the direction of x-axis, is defined as

$$\sigma_{xg} = \frac{\sum_{k=1}^{n} \sigma_{xk} t_k}{\sum_{k=1}^{n} t_k} = \overline{C}_{11g}\epsilon_{xg} + \overline{C}_{12g}\epsilon_{yg} + \overline{C}_{16g}\gamma_{xyg}$$

in which t_k is the thickness of the k_{th} ply and the subscript *g* refers to a global value for the whole laminate. The stress in any lamina is the same and can be written as

$$\sigma_{xk} = \overline{C}_{11k}\epsilon_{xg} + \overline{C}_{12k}\epsilon_{yg} + \overline{C}_{16k}\gamma_{xyg}$$

$$\overline{C}_{11g} = \frac{\sum_{k=1}^{n} (\overline{C}_{11k} t_k)}{\sum_{k=1}^{n} t_k}$$

After several operations we conclude to the components of the compliance matrix

$$\overline{S}_{11} = \frac{(\overline{C}_{22}\overline{C}_{66} - \overline{C}_{26}^2)}{\Delta}$$

$$\overline{S}_{22} = \frac{(\overline{C}_{11}\overline{C}_{66} - \overline{C}_{16}^2)}{\Delta}$$

$$\overline{S}_{12} = \frac{(\overline{C}_{16}\overline{C}_{26} - \overline{C}_{12}\overline{C}_{66})}{\Delta}$$

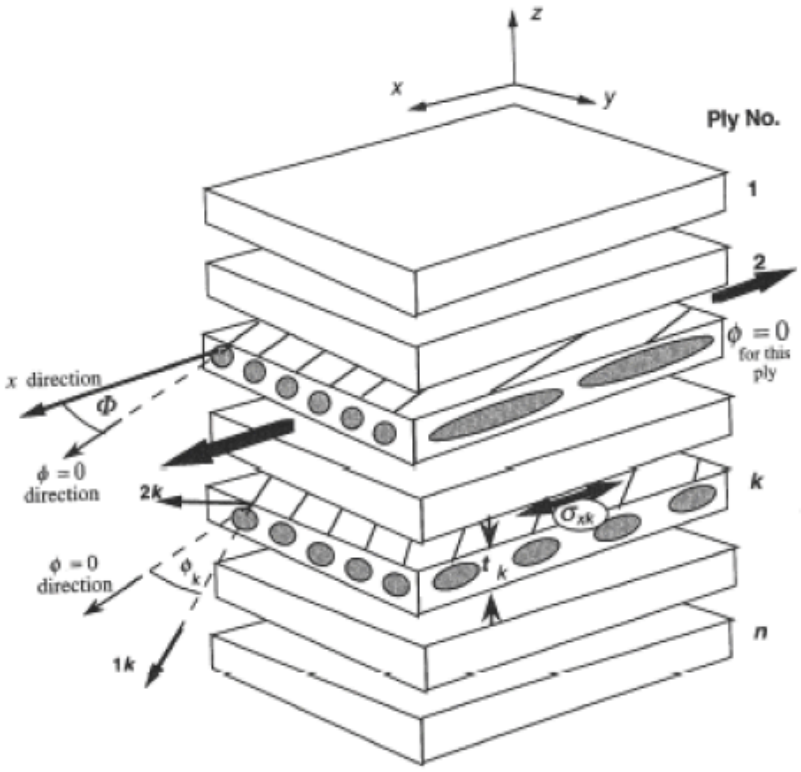

[Hull and Clyne, 1996]

Figure 1.9: Schematic presenting the loading angle of Φ for a laminate composed of *n* plies

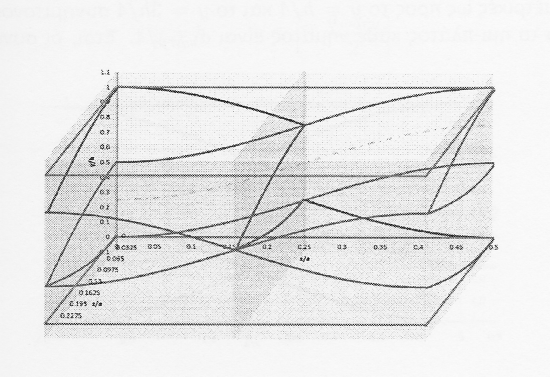

[Antonogiannakis, 2013]

Figure 1.10: Schematic structure of the unit cell

$$\overline{S}_{66} = \frac{(\overline{C}_{11}\overline{C}_{22} - \overline{C}_{12}^2)}{\Delta}$$

$$\overline{S}_{16} = \frac{(\overline{C}_{12}\overline{C}_{26} - \overline{C}_{22}\overline{C}_{16})}{\Delta}$$

$$\overline{S}_{26} = \frac{(\overline{C}_{12}\overline{C}_{16} - \overline{C}_{11}\overline{C}26)}{\Delta}$$

$$\Delta = \overline{C}_{11}\overline{C}_{22}\overline{C}_{66} + 2\overline{C}_{12}\overline{C}_{16}\overline{C}_{26} - \overline{C}_{22}\overline{C}_{16}^2 - \overline{C}_{66}\overline{C}_{12}^2 - \overline{C}_{11}\overline{C}_{26}^2$$

1.4.7 Elastic deformation of textile reinforced composites

In order to analyse and study the elastic behaviour of a textile reinforced composite material, we will focus on a unit cell structure of a single plain lamina composite material, as seen in Fig. 1.12. This cell is described by the structural form of a yarn. Specifically, h represents its thickness, a_{warp} is the periodicity of the yarn in the x-direction and a_{weft} the periodicity of the yarn in the z-direction. Because of the symmetrical behaviour of the cell, we will assume that it is limited inside known boundaries. So, regarding the x-axis the cell dimensions will have values between 0 and $a_{warp}/2$, in the y-axis between 0 and h, and for the z-axis between 0 and $a_{weft}/2$ [Antonogiannakis, 2013].

We assume that each yarn in the unit cell can be characterised as a composite material with a fibre volume fraction ϕ. As with the composite materials, this unit cell is receiving loads in the transverse, off-axis, and parallel to the fibres directions, and can be analysed by the Classical Laminate Theory we discussed above.

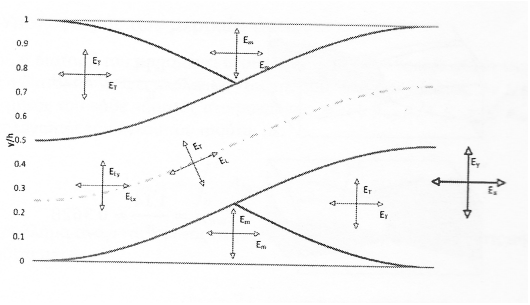

[Antonogiannakis, 2013]

Figure 1.11: Schematic representation of the coordinate system of a unit cell

The formula that provides the stiffness, E_x, of the overall composite is:

$$E_x = \frac{\frac{2.28}{\pi}\left(\frac{1-c+cb}{\overline{E}_x^L(b)+E_T(1-b)(1-c)}+\frac{(1-b)c}{E_T}\right)^{-1}+E_m\left(1-\frac{2.28}{\pi}\right)(1-n_0)}{1-n_0(1-2.28/\pi)},$$

where $\overline{E}_x^L$ corresponds to the average value of all the individual E_x^L inside the boundaries of $[0, a_{wrap}]$, and gives the stiffness parallel to the length of the yarn, along the direction of the x-axis:

$$\overline{E}_x^L = \left(\frac{2S_{11}}{a_{wrap}}\int_0^{a_{wrap}/2} c^4 dx + \frac{2S_{22}}{a_{wrap}}\int_0^{a_{wrap}/2} s^4 dx + \frac{4S_{12}+2S_{66}}{a_{wrap}}\int_0^{a_{wrap}/2} c^2 s^2 dx\right)^{-1}$$

where c is the "quota coefficient", taking values between 0 and 1 depending on the geometry of the fabric complexity; b is the anisotropy coefficient, taking values between 0 and 1 and depends on the ratio of the volume fraction of the wrap over the weft; n_0 corresponds to the overlapping coefficient, taking values between 0 and 1 and depends on the arrangement of the unit cells: 0 for zero overlapping between the unit cells and 1 for full overlap.

The parameters h and α influence the model bringing its predictions towards the parallel model (low h and high α) or the series model (high h and low α). The parameter n_0 depends on the characteristics of the fabric and the stacking. The modulus increases when n_0 increases.

1.5 Nanomaterials

Nanomaterials are defined as materials with at least one external dimension (size, diameter, edge) in the scale of *nanometre*, i.e. in the size range of 1 to 100 nm. Several examples of nanomaterials exist such as nanoparticles, nanoporous or nanostructured macroscopic materials [Vajtai, 2013].

Nanoparticles, which have all three dimensions at nanoscale, are usually physically and chemically heterogeneous and often cited as ultra fine particles. Engineered nanoparticles are designed and produced with very specific properties related to the size, the shape, the surface properties and chemistry. These, properties are reflected to aerosols, colloids, or powders. It is common, for the nano material behaviour, to depend more on the surface of area than particle composition itself.

Formation of nanosized materials is achieved by two basic routes, namely the so-called top-down and bottom-up methods [Vajtai, 2013]. In the former, macroscopic materials are used to fabricate nanomaterials and nanostructures using various sophisticated methods [Vajtai, 2013]. In the latter, nanoparticles and other forms of nanomaterials are constructed from their ultimate building blocks, such as atoms and molecules, via self-assembly processes [Vajtai, 2013].

Today, nanomaterials have already found applications in a wide range of engineering fields. From mechanical engineering to computer science and sport engineering, we use nanomaterials in our computers, in strain-resistant clothes for high performance sports, in aircraft components to reduce fatigue, in catalysts as eliminators of pollutants etc. . An other aspect of applications that nanocomposites are utilised, is medicine. Although, it is still in experimental stage, but the future of modern biomedicine and of course that of humanity's is in the full usage of the nano medicine applications. Examples of such forms, are the functionalised magnetic nanoparticles for the delivery of drugs to a specific target area inside the human body, nanomaterials that can recognise cancer tissue, enabling tumour visualisation, and anti-cancer drugs for the destruction of tumour cells [Barreto et al., 2011].

1.5.1 Carbon nanotubes

A significant nanoparticle discovery by Iijima [1991] was the carbon nanotubes (CNTs). Structurally, carbon nanotubes are made up of sp^2 -bonded carbon atoms, like graphite and can be viewed as rolled-up sheets of single layer graphite, or graphene (see figure 1.12). Their diameter, depending of their produced form, lies in the nanometre scale, while their length often exceeds microns, sometimes centimetres [Vajtai, 2013], thus making them 1-D nanostructures. There are several forms of carbon nanotubes, all depending on the number of concentric tubes that are arranged.

The types of CNTs are:

- Single-walled SWCNTs
- Double-walled DWCNTs
- Multi-walled MWCNTs

Single-walled Carbon nanotubes

Single-walled carbon nanotubes *(SWCNTs)* are hollow, long cylinders with extremely large aspect ratios, made of on atomic sheet of carbon atoms in a honeycomb lat-

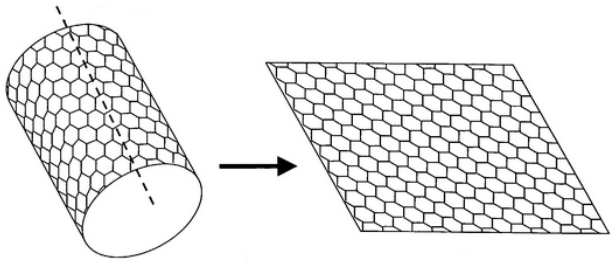

Figure 1.12: Rolled up graphene sheet to form a single wall carbon nanotube SWCNT

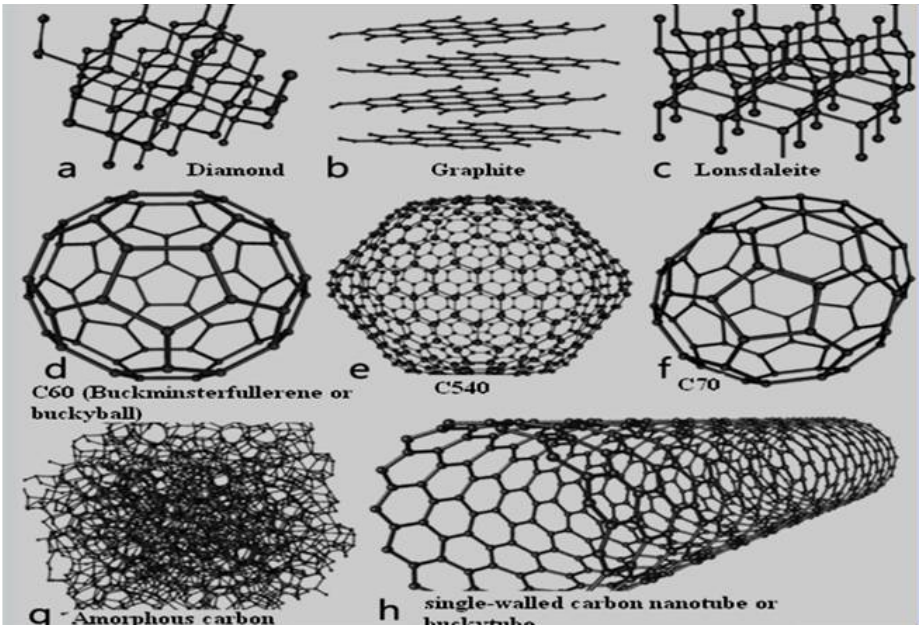

Figure 1.13: Various carbon nano structures

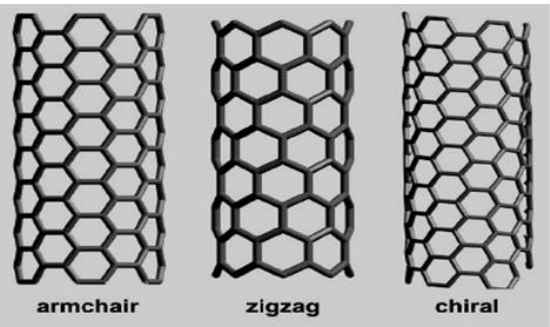

Figure 1.14: Different type of chirality

tice. They were originally discovered by S. Iiijima in 1993 [Iijima and Ichihashi, 1993]. A SWCNT has a diameter of $\approx$ 1nm and it can be pictured as a rolled-up version of graphene. Because of possessing extraordinary mechanical, thermal and electrical properties, they are considered as one of the most promising nanomaterials for future industrial applications and basic research.

Due to its intrinsic strength of the sp^2 C-C bonds and the special structure, a SWCNT show high mechanical strength and very large Young's modulus, with values near 1TPa, which is 5 times higher than the modulus of steel. Depending on their microscopic atomic arrangements and symmetry, also known as chirality (see figure 1.14), SWCNTs can be metallic or semiconducting. This electronic structural feature is extremely easy to change, by altering the geometric configuration of the tube.

Applications of carbon nanotubes are still under development and it is expected that the cost and availability of consistent quality's nanotubes will soon become more in line with industrial needs and out of the research labs. Future applications utilising SWCNTs are transparent electrodes, sensors and nanoelectromechanical devices and as filer reinforcements in polymer based nanocomposites [D. Resasco].

Multi-walled Carbon nanotubes

Multi-walled carbon nanotubes (MWCNTs), originally discovered by Iijima [1991] are elongated cylindrical nano objects made of sp^3 carbon. Their diameter is 3 to 30 nm and they can grow several cm long, thus their aspect ratio can vary between 10 to 10^6 [Vajtai, 2013]. The wall thickness of a MWCNT is fairly constant along the axis and therefore the inner channel is straight. This channel is not directly accessible from the outside because the ends of perfect MWCNTs are capped by half fullerene spheres [Vajtai, 2013]. They can easily be distinguished by SWCNTs on the basis of their multi-walled Russian-doll structure and rigidity. An other major difference between those two types of carbon nanotubes is that MWCNTs are stiff, rigid, rod-like structures whereas SWCNTs are flexible [Vajtai, 2013].

A broad variety of synthesis methods have been developed regarding the produc-

tion of multi-walled carbon nanotubes in the past 20 years. Now, synthesis of MWCNTs is a well established industrial scale process, with global production over 1700 metric tones per year [Vajtai, 2013]. Most known preparation processes are chemical vapour deposition (CVD), laser ablation and arc discharge [Y. Ando, 2002, C. Journet, 1998, 1997, S. Karthikeyan, 2009].

The appearance of MWCNTs is a fluffy black powder with very low apparent density between 0.03 g/cm^3 and 0.22 g/cm^3. This form is full of agglomerates, due to high tube-tube van der Waals interaction energy (500 $eV/\mu m$) [Vajtai, 2013] and can be separated by physical (ultrasonication, milling, shear strength) or chemical methods (surfactants, functionalisation). Purification and functionalisation in solution result in an agglomerated, dense material which is difficult to disperse. MWCNTs solubility is extremely low [Vajtai, 2013] in all liquids.

Focusing on the mechanical properties of MWCNTs, we can conclude of being impressive in the axial direction, with Young's modulus in the TPa range [M.M.J. Treacy, 1996] and tensile strength of 60 GPa [M. F. Yu, 2000a]. MWCNTs present soft characteristics in the radial direction, as indicated by a radial Young's modulus of 30 GPa[I. Palaci, 2005] and up to 40% radial deformability [M. F. Yu, 2000b]. It is suspected that defects on the surface or the whole structure of the tube, decrease the strength of the individual shells but improve the load transfer between walls [M. Locascio, 2009], therefore showing a complex overall effect on the mechanical properties of the MWCNT.

As mentioned earlier, applications produced with CNTs as a component, are sparse in industrial scale. Current projects involve applications as sensors/instruments, electromagnetic shielding, conducting polymer composites in automotive and electronics industries and sporting goods, as the tennis racket and sport bicycles. In the mid and long term, CNT's usage in applications as catalysts (petrochemical), fuel cells, coatings, drug delivery, medical implants, in aerospace industry and microwave antennas, are some of in future to come.

1.6 Hybrid composite materials

Major industries, such as aerospace and aeronautical, in which materials with excellent mechanical and structural properties are needed, are focusing on stretching the properties of advanced materials that are currently used towards their limits. A route of exploiting advanced structural materials is by using enabling technologies for additional functionalities, without compromising structural integrity. A strong candidate for providing an integral approach towards enhanced structural integrity and multifunctionality, is the usage of carbon nanotubes (CNTs) [Kostopoulos, 2013]. The hierarchical approach, of utilising CNTs may be translated into two results:

- Reinforcement in a nanoscale will enhance structural properties of an otherwise conventional composite
- Exploitation of the unique properties of CNTs will provide functionalities as real-time strain sensing, structural health monitoring and actuation capabilities [E. T. Thostenson, 2001]

Structural defiances of the composite laminates, such as interlaminar shear strength and toughness may be amended or even disappear by through thickness reinforcement at the nanoscale with mechanisms such as crack bridging, which can result in increased toughness via energy dissipation mechanisms activated by the additional interface between matrix and CNTs [L. Sun, 2009]. In order for the hybrid composite to achieve its enhanced predicted mechanical properties and fulfil its structural task, good dispersion of the nano filler on the matrix must be done [L. Zhang, 2007]. This can be done by utilising several dispersion techniques that will be discussed later in this chapter.

A particular new and exciting aspect of this kind of material is the additional functionalities that were discovered, in the field of strain and damage sensing, employing the real-time changes in the resistivity of the material [Kostopoulos, 2013]. Reversible changes are due to strain and irreversible ones are due to damage [C. Li, 2008] [Kostopoulos, 2013]. The structural health monitoring lies with the principle of a percolated network within the structure, created by the dispersed CNTs [W. Bauhofer, 2009], that follows the applied strain field and is disrupted at any discontinuity induced due to damage initiation and accumulation [F. Deng, 2009].

Damage tolerance relates to the ability to perform to required standards within damage limits, which at a the same time define the structures remaining life [A. Nettles, 2011]. This criterion is used in any composite structure that is exposed to a number of in-service loadings, which can cause initiation and structural degradation. Due to its good fatigue resistance, a composite material, has increased durability and damage tolerance [L. Lazzeri, 2009].

Regarding, though, the damage initiation and propagation, the main concern lies with the design of composite structural components. As the reinforcing phase is extremely brittle, especially that of carbon fibre's, the task of increasing damage tolerance lies with the matrix material. However, most matrix resin materials are also brittle and hence have limited resistance damage, which leads to cracks and delamination. These damage mechanisms may occur as a result of an out-off plane fatigue load, an impact event, or from some form of environmental degradation. Because of an increase in size of structural composite parts with a subsequent reduction of joints, a major drawback, that mainly exist in aerospace and aeronautical applications,is the case of passive damping [Kostopoulos, 2013] [Z. Li, 2005].

Damping is influenced by matrix properties and consequently research has been focused on resin systems (matrix additives, interleaves etc.) [Kostopoulos, 2013]. Modification of matrix properties is a key factor in improving the damage tolerance of the composites, which is, in our case, improved delamination fracture toughness. Hybrid resin systems as thermosets and thermoplastics blends, for example, are reported to improve the interlaminar fracture toughness of composite systems [D. Olmos, 2011]. However, brittle resins may exhibit high mode II delamination toughness which is attributed to the formation of microcracks ahead of the crack tip. These microcracks dissipate the energy and redistribute the load [M. Hojo, 1997].

An alternative approach to interfacial modification that combines the modification of the matrix properties as a macroscopically homogeneous material with the addi-

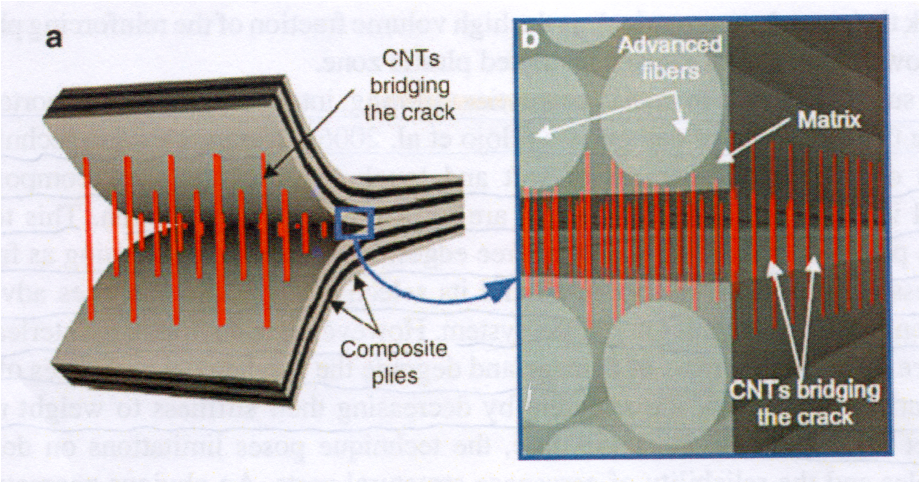

[E. J. Garcia, 2008]

Figure 1.15: Toughening in multi-scale reinforced composites

tional benefits of interfacial energy dissipation mechanisms is the inclusion of other phases in the matrix material which are not of the same order of magnitude of the reinforcing phase. This is a well-known technique ranging from carbon black modified rubbers to the use of other modifiers, such as piezoceramic materials [Kostopoulos, 2013] [S. Tsantzalis, 2007]. These additives change the toughness as well as the dynamic properties of the material (e.g. both modulus and damping properties) [Kostopoulos, 2013]. The use of CNTs as an additive [J. Cho, 2003], due to their nanoscale size, their huge aspect ratio and free surface, is a very interesting scenario. This is because CNTS are expected to enhance significantly the interfacial area in the composite system. Moreover, a minimum addition of the order of a few percent can dramatically change the properties of the matrix materials [Colbert, 2003]. The issue of compatibility of CNTs in a resin matrix material, is the basis of current research and development of new technologies and can lead to spectacular improvements in structural material properties. A particular example of utilising CNTs in a polymer matrix, is that of PBO fibres that were doped with CNTs and have been reported of exhibiting twice the energy absorbing capability in relation to conventional PBO fibres [S. Kumar, 2002], [Shelley, 2003]. In figure 1.15 we exhibit a schematic representation of aligned CNTs inside a composite material, acting as a bridge, increasing in that manner the interfacial bonding between the layers.

Commercial carbon nanotubes come in many lengths, diameters and difference levels of entanglement. Especially, MWCNTs which are generally entangled in a form of curved agglomerates. As a result, reaching the highest potential possible, a hybrid composite material must have its nano fillers, in this case CNTs, fully dispersed inside the polymer matrix. The dispersion of CNTs is not a simple process, since CNTs tend to agglomerate to each other due to van der Waal force attractions that exist between

the tubes as a result of their significant areas and high aspect ratios [M. Cadek, 2004, A. Thess, 1996, Kostopoulos, 2013]. Their very stable chemical characteristics as well as their lack of functional sites on the surface perplexes the dispersion process. An other issue regarding the CNTs dispersion is their length. Although, longer nanotubes could lead to better mechanical properties of composites even if dispersion is not good as desired [Kostopoulos, 2013], they are creating stronger interactions and entanglements between them. Along with the length parameter of the CNTs , is the adhesion between those and the polymer matrix. Knowledge of how nanotubes adhere to dispersion media could lead to better understanding and a potential full scale production of properly dispersed nanocomposites ready to be utilised in various applications. Similar to conventional fibre-reinforced composites, a load transfer across the CNT/matrix interface is required in order to increase the mechanical properties of reinforced composites [W. Ma, 2009, J. H. Du, 2007]. In addition to that, the interfacial load transfer can be governed by three mechanisms: **van der Waals forces**, **mechanical interlocking** and **covalent bonding**. The van der Waals forces, despite the fact that are relatively weak and CNTs do not bond well to matrix, which results to low transfer efficiency, are the most common between CNTs and polymer matrices [L. Jiang, 2007, K. T. Lau, 2002, C. Li, 2008]. Regarding the mechanical interlocking, it is created from defects around the interface, therefore it hardly occurs in CNTs because of their near to defect-free structure [L. Jiang, 2007]. Finally, the covalent bonding mechanism requires functionalisation of the CNT/matrix interface, which may lead to the introduction of defects to CNTs structure, reducing in that manner the mechanical properties of the composite and make the processing more difficult [L. Jiang, 2007].

1.6.1 Methods of dispersion

There are various techniques that are being investigated, regarding CNTs dispersion in a polymer matrix. The ideal case is to obtain as a final product a stable dispersion of independent separated nanotubes that can further be manipulated in order to have the preferred orientations of CNTs, in 1- , 2- and 3-dimensions, for production of fibre, flat sheets or bulk objects [Kostopoulos, 2013]. There are two main approaches to nanotube dispersion:

- Mechanical (physical) methods
- Chemical methods

We will briefly mention the various methods for each category, giving extra attention to the ones that were used during the experimental section of this thesis.

Mechanical methods of dispersion

Physical dispersion methods generally include ultrasonication, high-shear mixing, milling, etc. Although, they can be utilised as main dispersion method, they are usually accompanied by open-end or side-wall chemical functionalisation.

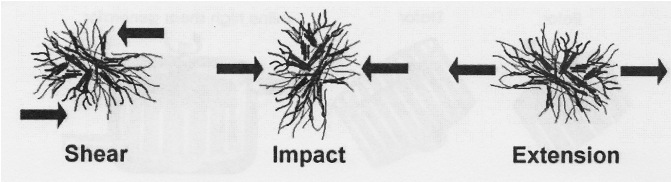

Figure 1.16: Main stress forces acting on CNT agglomerate [Kostopoulos, 2013]

High shear mixing

High-shear process can be distinguished into *distributive* and *dispersive* mixing. Distributive mixing aims to enhance the spatial distribution of the components. In dispersive mixing cohesive resistances have to be overcome to achieve finer levels of dispersion. Regarding the CNTs agglomerates, which were described above, they are acting as a cohesive component which need a certain minimum dress level in order for the rupture to occur. As Shown in the figure above, three primary stressing mechanisms take place during dispersion procedure:

- Shear stress forces
- Impact stress forces
- Extension stress forces

The problem with high-shear flow in a polymer matrix with CNT fillers, is that particles in the fluid are not only sheared but also rotated 1.16. In an elongation flow, particles undergo a stretching deformation without rotation. This is the reason why high-shear mixers, where shearing forces are dominant, are relatively ineffective for CNTs dispersion on a polymer based medium and are mostly used for distributive mixing [Kostopoulos, 2013]. There is a broad variety of shear mixer devices available in the market. The main ones are impellers, rotors, rotor-stator combinations, pump mixers, mills or special dispersers 1.17, 1.18 [Kostopoulos, 2013].

Milling

Mills primary role is to reduce particle size of solids which are suspended in fluids. The main mechanisms behind these devices to create dispersions, are the compressive and/or shear stresses that are generated. Therefore, mills can be divided into two mixing categories: *high shear* and *high impact* technologies.

High shear milling are constructed with two-roll and three-roll mills comprising two and three rotating cylinders respectively, to disperse materials between them. These rolls are usually equipped with heating and cooling systems for better controlling of the milling process. Such mills are also known as *roll calendars*.

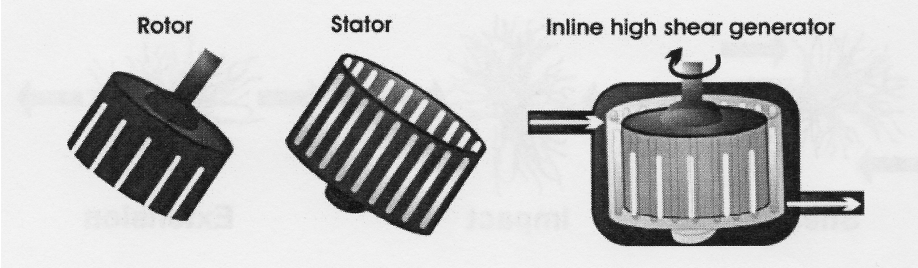

Figure 1.17: An example of rotor-stator combination
[Kostopoulos, 2013]

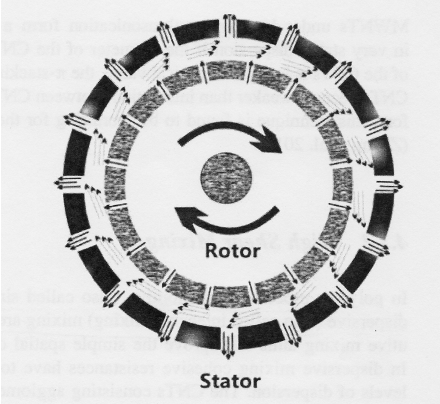

Figure 1.18: Shear forces in a rotor-stator combination
[Kostopoulos, 2013]

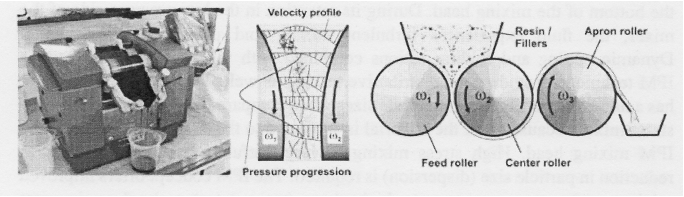

Figure 1.19: Three-roll calendar (left) and its working principle (right) [Kostopoulos, 2013]

Three-roll milling can be used for homogeneous CNTs dispersion within thermosetting resins with low level of damages and ruptures on CNTs, compared to other techniques [A. T. Seyhan, 2009]. However, dispersing them in a rubber system is usually accompanied with shortening them [B. M. Cho, 2010]. Therefore, care should be taken when utilising this technique regarding the final product's mechanical properties. An other advantage of this technique is that more viscous mixtures can be processed, which is especially important when dispersing nano fillers with large surface areas are used, such as CNTs. It should be noted that three-roll milling is more efficient for deagglomeration of the nanoclays and ceramic nano fillers , than for CNTs 1.19 [Kostopoulos, 2013].

In **high impact milling**, bead mills are used for grinding and dispersing solid particles. Usually, they consist of a grinding chamber filled with hardened beads, made of steel or zirconium dioxide, and supported by a stirring mechanism (a rotor). Ball milling is a mechanical dispersion method which generates local high impact areas between the balls resulting in a randomly crushing of the materials 1.20 [Kostopoulos, 2013]. It is a common processing technique for the agglomeration of CNTs both for dry and wet grinding, but with the danger of transferring CNTs into other forms of nanoparticles or even into amorphous graphite [J. H. Ahn, 2007, N. Pierard, 2004, Y. B. Li, 1999, S. Ghose, 2006], [M. Inkyo, 2008].

Ultrasonication

Ultrasonication is the most simple method used for dispersing CNTs in any polymer medium. The main mechanism behind this process includes three physical phenomena:

- Cavitations, with formation and collapse of bubbles
- Localised heating, with temperatures higher than $5000\ K$ and pressure up to $500\ atm$
- Formation of free radicals

The first is the acting dispersing process behind the deagglomeration of CNTs, while the other two reduce the efficiency of the ultrasonication. The frequency of ultrasound

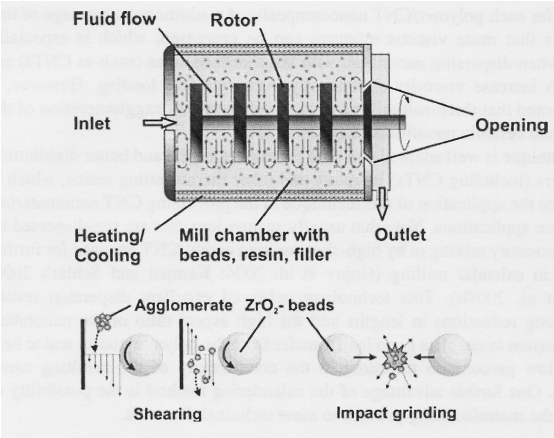

Figure 1.20: Ball mill (up) and schematic of its main action mechanisms (down) [Kostopoulos, 2013]

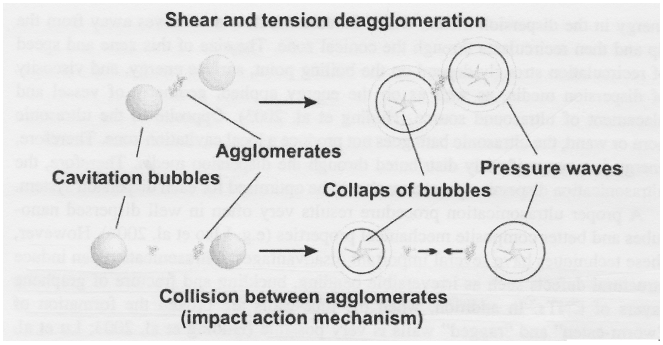

Figure 1.21: Main action mechanisms of ultrasonication [Kostopoulos, 2013]

is playing key role in the bubble size. Usage of this technique is most recommended for the dispersion of nanotubes in liquids with viscosities up to $100\ Pa \cdot s$. Cavitation is caused by periodical changing in the increased -pressure and reduced-pressure phases during the ultrasonication. During the increased-pressure phase, compressive forces are set on the fluid. By changing to the reduced-pressure phase, strong local pressures are dropped significantly under fluid vapour pressure resulting in the creation of cavitation bubbles. The next high pressure phase cause the collapsing of the cavitation bubbles with release of high energy forces able to start deagglomeration. Pressure-waves, then, propagate throughout the dispersing media, as shown in the figure below 1.21. In addition to the above, collisions between agglomerates, particles and the walls of the ultrasonic device are initiated, resulting in additional deagglomeration of the fillers [Kostopoulos, 2013].

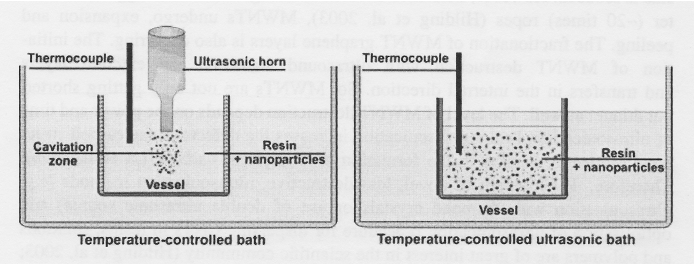

Figure 1.22: Ultrasonic horn (left) and ultrasonic bath (right) [Kostopoulos, 2013]

Two major ultrasonication procedures are used for dispersing CNTs in a polymer system: *ultrasonic horn/wand* and *ultrasonic bath* 1.22 .Rapid oscillation of the horn in the **Ultrasonication horn or wand** dispersing procedure, is responsible for the creation of a conical cavitation zone of high energy in the dispersing media. This conical zone induces the flow to move away from the tip and then recirculate through it. The size and the speed of that zone is strongly related to various parameters, such as the boiling point, the surface energy and the viscosity of the dispersion media, as well as, the geometry of the vessel, the placement of the tip and the energy applied [J. Hilding, 2003].The alternative ultrasonication method, called **ultrasonication bath**, does not produce a local cavitation zone. Therefore, energy is distributed uniformly through the dispersion media.

It is established that prolonged sonication increases the defects of the carbon structures ultimately leading to formation of amorphous carbon [K. L. Lu, 1996]. So, controlled mild ultrasonication treatment can result in minimised shortening of CNTs and is effective for dispersion of SWCNTs even in water, which is usually difficult to achieve due to the insolubility of SWCNTs in common organic solvents, caused by hydrophobic inert nature of SWCNTs and their high tendency to form agglomerated bundles. Accurate control of the ultrasonication amplitude allows limiting damages of SWCNTs.

Chemical methods of dispersion

In general, there are two main methods of chemical functionalisation for the dispersion of CNTs inside a polymer matrix. The first, involves covalent attachment of chemical groups, through reactions on the conjugated skeleton of CNTs, as amine-functionalisation. The second consists of non-covalent supramolecular absorption or wrapping of various functional molecules on the surface of the nanotubes, as surfactants.

Covalent functionalisation

The covalent approach includes various techniques. Certain of them will be fully discussed and analysed in the following pages, covering the experimental part of this thesis. The rest will be listed here as reference for the reader [Kostopoulos, 2013],

[N. Karousis, 2010]

- Oxidation reactions
- Esterification - amidation reactions on oxidised CNTs
- Halogenation
- Cycloaddition reactions
- Radical additions
- Nucleophilic additions
- Electrophilic additions
- Ozonolysis
- Electromechanical modification
- Plasma-activation
- Mechanochemical functionalisation
- Polymer grafting

Non-covalent functionalisation

In the non-covalent functionalisation [N. Karousis, 2010] , the CNT surface can be modified via $\pi - \pi$ interactions and van der Waals forces, by absorption or wrapping of:

- Polynuclear aromatic compounds, as phenyl, naphthalene, pyrene etc.
- Polymers, as epoxy, acrylic, aliphatic, conjugated etc.
- Biomolecules, as proteins
- Other substances, as surfactants, macrocyclic host molecules, ionic liquids, dyes, alkoxysilanes, phosphines etc.

Except from the above, chemical modification of the CNTs includes also the endohedral filling of CNTs with fullerenes and inorganic or organic substances [N. Karousis, 2010] [Kostopoulos, 2013].

Although, this path of functionalisation research continues with great results, we will focus our research, in this thesis, on the covalent techniques of chemical functionalisation, using oxidation reactions, amidation and their combination.

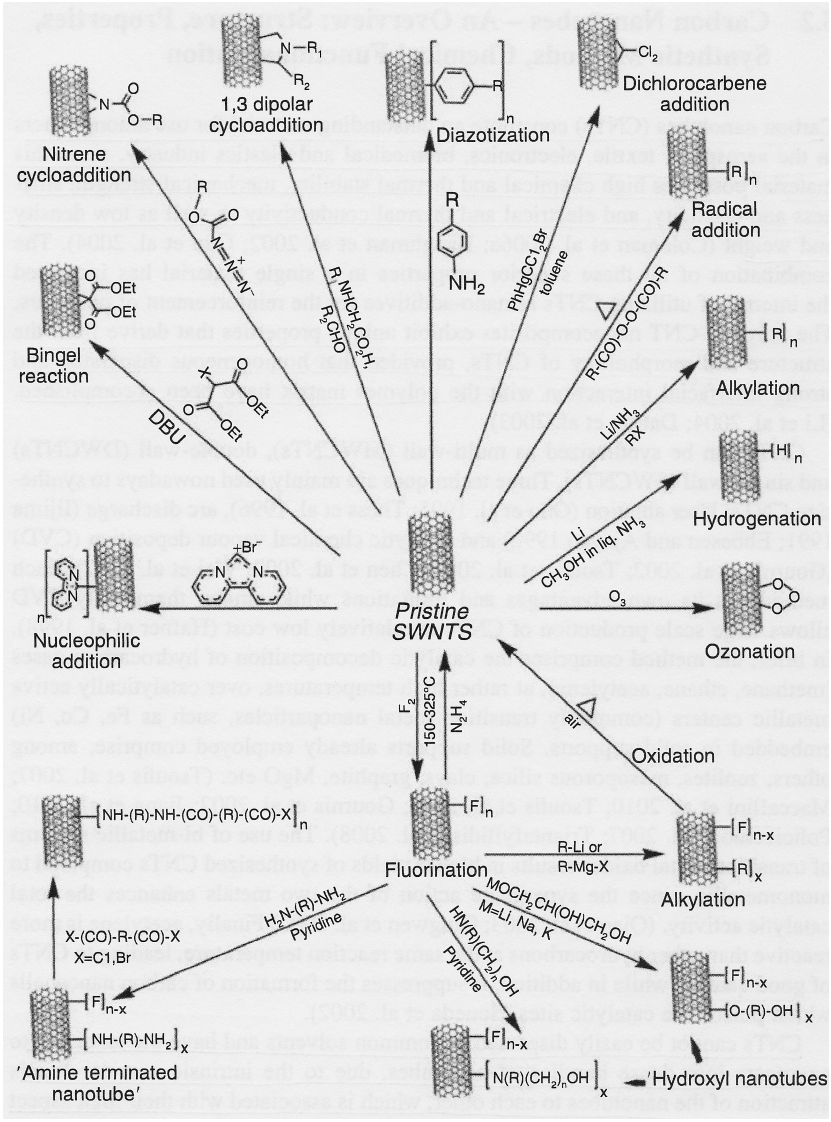

Figure 1.23: Schematic with various covalent sidewall functionalisation reactions of SWCNTs

[A. A. Gusev, 2000]

1.7 Scope of the present work: improvement of the compressive strength

The basic subject of this work is the establishing of new methods to enhance the mechanical properties of the polymeric matrix by adding nanoparticles and creating hybrid nano-macro-composites. Ordinary composite laminate materials show very low strength to compressive loads parallel to the fiber direction. Similar to a simple rope, the fibres, when compressed axially, will buckle at relatively low forces and the composite will fail. What will prevent them from buckling is the stiffness of the matrix. If this stiffness is increased, the resistance to buckling of the composite will be enhanced and the compressive strength will increase as well. In this work we are aiming at improving the compression strength of the continuous fibre composite by enhancing the elastic properties of the matrix. This is done by adding reinforcing nano-sized particles in the matrix.

The technique has been tried by Vlasveld [2005] at the Technical University of Delft. Vlasveld has used silicate clay nano-particles to enhance the stiffness of the polyamide-6 matrix used to prepare glass-fiber hybrid composites. In the present work we chose to use CNTs to reinforce the matrix because we expect better compatibility between the carbon particles, the matrix and the carbon fibre reinforcement. This may reduce the possible reduction of the tensile strength and toughness.

The focus, thus, of the thesis is in inserting CNTs in an epoxy resin matrix by using various chemical and mechanical dispersion techniques. Chemical treatment includes the functionalisation of the carbon nanotube surface with various functional groups and the addition of organic solvents, particularly that of acetone. Mechanical dispersion methods refer to continuous stirring and sonication with ultrasonication tip technique.

The present thesis deals also with the analysis of the tensile strength of the hybrid composite materials and the tensile strain / stress curves. Actual compression or three-point bending measurements were not possible due to lack of appropriate testing equipment. Thus, we tried to infer the possible improvement for the compression strength of the hybrid composite from tensile measurements of Young's modulus and strength. Obviously, further work is needed to verify these conclusions.

Chapter 2

EXPERIMENTAL

This chapter addresses the experimental section of this thesis project. It is divided in three parts, all of which refer to the experiments that were conducted at the Materials Laboratory of Assoc. Prof. A. D. Gotsis, the Analytical and Environmental Chemistry Laboratory of Prof. N. Kallithrakas - Kontos. and the Petroleum Engineering laboratory of Assoc. Prof. N. Pasadakis. The first two sections present the materials and the experimental procedures. The chapter closes with the characterisation methods of analysis that were implemented.

2.1 Materials

For the creation of the hybrid composites, certain raw materials were utilised. The three prime compounds of the final product are the carbon fibres, the epoxy polymeric system and the multi walled carbon nanotubes (MWCNTs). In the following tables, we present the type and properties of these materials, as well as certain assistive chemical compounds, which are crucial for the construction of the hybrid composite samples. The mechanical properties, such as as Young's modulus, strength and strain at break of the samples were measured in a tensile tester.

Carbon fibre fabric, with code C 160P, was purchased by *Fibermax Composites*. The texture style of the fabric is **plain**, thus the perpendicular positioning of the two main constituents of the fabric, the wrap and the weft. Each wrap yarn, on the carbon fabric, has 3,000 fibres, the same as for each weft. The **areal weight** of this type of carbon fabric is measured 160 g/m^2. All the important parameters and properties, regarding this material, are given in the table 2.1.

As presented earlier, carbon nanotubes are extremely strong and stiff materials in terms of tensile strength and elastic modulus, with values from 50 to 150 GPa and from 0.2 to 1 TPa respectively. This strength derives from the covalent sp^2 bonds formed between the individual carbon atoms. The type of CNTs used in our experiments is multi-walled carbon nanotubes or MWCNTs. The product comes in the form of a black

Table 2.1: Carbon fibre properties

Material:	Carbon Fiber - Pyrofil	
Company:	Grafil Inc. - Fibermax Composites	
Precursor:	PAN	
Fabric's texture:	Plain	
Properties:	Wrap:	3K TR30S
	Weft:	3K TR30S
	Aerial weight:	$160\ \frac{g}{m^2}$
	Elasticity Modulus:	$235\ GPa$
	Tensile Strength:	$4410\ MPa$
	Elongation at break:	1.9 %
	Density:	$1.79\ \frac{g}{cm^3}$
	Thermal Expansion:	$0.5 \cdot 10^{-6}\ K^{-1}$
	Filament Diameter:	$6.88625\ \mu m$

Table 2.2: Carbon nanotubes properties

Material:	Carbon Nanotubes - CNTs	
Company:	Fibermax Composites	
Type:	MWCNTs	
Properties:	Length:	$1 - 2\ \mu m$
	Av. diameter:	$10 - 40\ nm$
	Purity by weight:	93 %
	Specific surface area:	150-250 m^2/g
	Melting point (mp):	$3.652 - 3.697\ ^\circ C$
	Specific gravity ($25^\circ C$):	2.1 g/cm^3
	Bulk density:	0.03 - 0.06 g/cm^3

powder with apparent density between 0.03 to 0.06 g/cm^3. The average diameter of the nanotubes lies between 10 to 40 nm, whereas their length, between 1 to 2 µm, as it is shown in the table below 2.2.

The third main constituent of the hybrid composite material, is the epoxy system. It is composed of the epoxy resin R9330 and the acceleration agent H9054, also known as hardener. This system belongs to the thermosetting type of polymers, which is fully described in the above chapter. Both the resin and the hardener have a liquid yellowish form and once they are mix they form a dense cross linking network.

The epoxy resin is made of three ingredients as shown in the table below 2.3. It has 1.158 g/cm^3 density and approximately 1320 mPa·s viscosity.The hardener is composed of two substances (see the table below 2.4). It has 0.942 g/cm^3 density and approximately 6 mPa·s viscosity.

Tables 2.5 2.6 present some properties of the mixed epoxy system. The wt% ratio used in our experiments for the preparation of the polymer matrix for the composite was 78/22, epoxy to hardener.

Table 2.3: Constituents of the epoxy resin

Number:	Name:	percentage
1	Bisphenol F–(Epichlorhydrin) Epoxy Resin	$50\% \leq x \leq 100\%$
2	Bisphenol A–(Epichlorhydrin) Epoxy Resin	$25\% \leq x \leq 50\%$
3	Hexanediol Diglycidyl Ether	$10\% \leq x \leq 25\%$
	Ratio #1:#2:#3 = 5:2:1	

Table 2.4: Constituents of the hardener agent

Number:	Name:	percentage
1	Methylpentane diamine	$50\% \leq x \leq 100\%$
2	Metaxylene diamine	$50\% \leq x \leq 100\%$

Table 2.5: Epoxy system properties

Epoxy System		
Material:	Epoxy Resin	
Company:	Fibermax Composites	
Type:	R 9330	
Properties:	Aspect/Colour:	Yellowish liquid
	Viscosity ($20^{\circ}\mathrm{C}$):	1320$\pm$100 mPa·s
	Density($20^{\circ}\mathrm{C}$):	1.158 g/cm^3
Material:	Hardener	
Company:	Fibermax Composites	
Type:	H 9054	
Properties:	Aspect/Colour:	Light yellowish liquid
	Viscosity ($20^{\circ}\mathrm{C}$):	6$\pm$2 mPa·s
	Density($20^{\circ}\mathrm{C}$):	0.942 g/cm^3

Table 2.6: More epoxy system properties

Epoxy System		
Mix properties of R 9330 - H 9054 system		
Properties:	Mix viscosity ($20^{\circ}\mathrm{C}$):	300$\pm$100 mPa·s
	Mixing ratio by weight (in grams):	100 to 22
	Exothermic temp. on 500 g at $20\ ^{\circ}\mathrm{C}$:	$\geq$ 210 ?
	Time to reach exothermic peak:	1 h 27 min

Finally, in the next table we present the supportive chemical materials that were used during the construction of the hybrid composite samples. We experimented with different methods of dispersing the MWCNTs inside the epoxy matrix, as the organically solvent dispersion by using acetone, oxidation of the MWCNTs before dispersing them in the matrix by utilising nitric acid, the amine functionalisation with hexadecylamine and the combination of the last two. Excess of ethanol was used during the washing and filtration section of certain functionalisation recipes.

2.2 Sample preparation

The preparation of a hybrid composite material involves two main procedures. The first, often optional, is usually necessary for dispersing carbon nanotubes in a polymer medium, and refers to the functionalisation of the CNTs using various chemical compounds. The second, includes the basic process of constructing a composite material on a mould, e.g. by hand laying-up. Both of these will be described and analysed in this section.

After completing the construction of the hybrid composite materials, using different recipes, we employed a water jet cutting machine to cut the samples for the tensile measurements. The shape of the sample is standardised according to the *ASTM D 638 - 99*. The full data regarding the standard, used to measure the tensile properties of composite materials, is available in the Appendix .

2.2.1 CNT dispersing techniques

As mentioned in the previous chapter, a plethora of dispersion techniques exist either mechanical (physical), or chemical or the combination of both. In this thesis we set four different experiments of dispersing CNTs inside the epoxy matrix. The various techniques are listed below:

- Organically modified CNTs
- Carboxyl functionalisation
- Amine functionalisation
- Combination of carboxyl and amine functionalisation

The first method in our list features the mixture of CNTs inside an organic solvent. In this case we used **acetone** inside the epoxy resin in order to achieve an homogeneous dispersion. In this recipe we mixed $50g$ of acetone with $0.222\ g$ of CNTs or $0.2\%\ wt.$ of the total epoxy system, which was $110.04\ g$. We sonicated it for $1\ h$, using the UP 400S ultrasonicator at 60% amplitude and 1 full cycle. Then we added $90.32\ g$ of epoxy resin and continued sonication for $1\ h$ at the same amplitude. Before adding the hardener agent and initiating the polymerisation mechanism, we left the mixture under vacuum for the acetone to evaporate, for 2 days. The existence of acetone inside our final

Table 2.7: Characteristics of the chemical compounds used for the modification of the cnTs

Material:	Hexadecylamine - HDA	
Company:	Sigma - Aldrich Chemie GmbH	
Chemical type:	$CH_3(CH)_{15}NH_2$ 1-Aminohexadecane Cetylamine	
Properties:	Molecular weight:	$241.46\ \frac{g}{mol}$
	Vapor pressure:	< 1 mmHg (20 ?)
	Melting point (mp):	$43 - 45\ ^\circ\mathrm{C}$
	Boiling point (bp):	$330\ ^\circ\mathrm{C}$
	Grade:	Technical grade , 90%
Material:	Nitric Acid	
Company:	Sigma - Aldrich Chemie GmbH	
Chemical type:	HNO_3	
Properties:	Molecular weight:	$63.01\ \frac{g}{mol}$
	Vapor pressure:	$8\ mmHg$
	Assay:	$\geq 65\%$
	Density:	$1.37 - 1.41\ \frac{g}{mL}(20\ ^\circ\mathrm{C})$
	Boiling point (bp):	$120.5\ ^\circ\mathrm{C}$
	Grade:	for determination w ith dithiozone reag. ISO, reag. Ph. Eur.
Material:	Ethanol	
Company:	Fischer - Scientific	
Chemical type:	C_2H_5OH	
Properties:	Molecular weight:	$46.07\ \frac{g}{mol}$
	Density:	$0.789\ \frac{g}{cm^3}$
	Boiling point (bp):	$78.37\ ^\circ\mathrm{C}$
Material:	Acetone	
Company:	Sigma - Aldrich Chemie GmbH	
Chemical type:	C_3H_6O	
Properties:	Molecular weight:	$58.08\ \frac{g}{mol}$
	Density:	$0.791\ \frac{g}{cm^3}$
	Boiling point (bp):	$56\ ^\circ\mathrm{C}$

product will cause defects and alter the mechanical properties of the constituents. After that we laid the matrix mixture on one pile of carbon fibre, manufacturing the final product.

For the rest methods we changed the number of carbon fibre piles from one to three, giving a stronger and stiff attribute to our final product's structure. So on the second method we tried to modify the surface of the carbon nanotube by grafting on it a **carboxyl group**. This chemical functionalisation method in accordance with the use of ultrasonication technique, acts either as single step of functionalisation or as a precursor for further chemical treatment of the nanotubes surface with amine. Therefore, in order to prepare the oxidised CNTs, we stirred $1\ g$ of CNTs on a magnetic stirrer in a 5M HNO_3 solution for $1\ h$. Then, we washed and filtered the nanotubes with den-ionised water for 5 times. Before adding the functionalised CNTs in the epoxy for sonication, we dried them overnight in an oven at $100\ ^{\circ}\mathrm{C}$ [Sreejarani K. Pillai]. As already mentioned, we sonicated the mixture of only $0.445\ g$ functionalised CNTs , or again $0.2\%\ wt.$ of the total epoxy system, which was $222.1\ g$, with the resin ($180.65\ g$) for $1\ h$, at 60% amplitude and 1 full cycle, and added the hardener agent to initiate the polymerisation mechanism. Finally the matrix material was laid on the three plies of carbon fibres and left overnight until full cure was achieved.

Regarding the **amine** functionalisation method, we used $0.645\ g$ of CNTs and $7,00\ g$ of **hexadecylamine** (HDA). After mixed in a flask, we heated the mixture in a oil bath at $180\ ^{\circ}\mathrm{C}$ for $6\ h$ [Sreejarani K. Pillai] and we washed and filtered it with excess of ethanol for 5 times. Then, we left the sample in an oven overnight to dry at $100^{\circ}\mathrm{C}$. The weight of the functionalised CNTs produced was $0.820\ g$. For that reason we utilised $0.555\ g$, which is the $0.445\ g$ CNTs that we needed for a $0.2\%\ wt.$ of the total $222.1\ g$ epoxy system and the $0.110\ g$ of the amount of amine grafted on the surface of the nanotubes [Sreejarani K. Pillai]. At the final stage we sonicated the mixture of the amine-functionalised CNTs with the resin ($180.65\ g$) for $1\ h$ at 60% amplitude and 1 full cycle and then added the hardener agent before applying the material on the three plies of carbon fibre.

As a final amine treatment for the two-step functionalisation method [Sreejarani K. Pillai] we used the rest of the oxidised CNTs that we created in the carboxyl functionalisation recipe and added them in a flask with $20\ g$ of HDA. We heated the flask for $24\ h$ in an oil bath at $140^{\circ}\mathrm{C}$ and then washed and filtered the functionalised CNTs with excess of ethanol 5 times. As an next step we added those CNTs in $180.65\ g$ resin and sonicated this mixture for $1\ h$. Then we applied the hardener and laid the mixture on the three carbon fibre plies.

Finally, we created an extra sample of unmodified CNT hybrid composite. This time we sonicated $0.445\ g$ (or $0.2\%\ wt.$) for $1\ h$ with epoxy resin and after applying the hardener agent we competed the specimen by laying the mixture of each carbon fibre ply with a brush. For each ply we laid the same amount of matrix material for better distribution inside the composite and we were careful not creating any gaps of misalignment to the fibres. For further information see the Hand lay - up technique.

2.2.2 Hand lay - up technique to prepare composite samples

Hand lay-up is the simplest open mould method of the composite fabrication processes. It is essential for low volume, labor intensive method suited especially for large components. It takes place on a plain of glass, which is initially cleaned from any debris that will cause defects on the final product's surface and then sprayed at least three times with a release agent, which in our case is wax. Each time we wax the glass we have to brush it with a mat afterwards, cleaning any large particles or debris. Then we cut the carbon fabric to the needed dimensions and spay it with glue, which eventually evaporates, to stabilise the fibres in the preferred direction. When the matrix material is ready (with the hardener agent inside) we lay it on the first carbon fibre ply using a brush. We brush it carefully and at all directions, considering any voids that may pop out. After completing the first ply we continue with the next plies following the same procedure, brushing the mixed material and squeezing it to enter between plies. So for the final stage of this method, we leave the hybrid composite cure overnight at room temperature.

2.2.3 Vacuum-bag composite preparation technique

Vacuum bagging (or vacuum bag laminating) is a clamping method that uses atmospheric pressure to hold the adhesive or resin-coated components of a lamination in place until the adhesive cures. Modern room-temperature-cure adhesives have helped to make vacuum bag laminating techniques available to the average builder by eliminating the need for much of the sophisticated and expensive equipment required for laminating in the past. The effectiveness of vacuum bagging permits the laminating of a wide range of materials from traditional wood veneers to synthetic fibres and core materials.[1]

Vacuum bagging uses atmospheric pressure as a clamp to hold laminate plies together. The laminate is sealed within an airtight envelope. The envelope may be an airtight mould on one side and an airtight bag on the other. When the bag is sealed to the mould, pressure on the outside and inside of this envelope is equal to atmospheric pressure. As a vacuum pump evacuates air from the inside of the envelope, air pressure inside of the envelope is reduced. Atmospheric pressure forces the sides of the envelope and everything within the envelope together, putting equal and even pressure over the surface of the envelope. The vacuum induces the flow of the resin from an external reservoir through the fibre cloth and the impregnation of the fibres.

More details on this method can be found in the MSc thesis of Antonogiannakis [2013].

[1] http://www.westsystem.com/ss/assets/HowTo-Publications/Vacuum-Bagging-Techniques.pdf

2.3 Characterisation

2.3.1 Fourier Transform InfraRed spectroscopy - FTIR

Fourier Transform InfraRed spectroscopy is a qualitative technique which is used to obtain an infrared spectrum of absorption of a solid, liquid or gas. The vibrational spectrum of a molecule is considered to be a unique physical property and is characteristic of the molecule. As such, infrared spectrum can be used as ”fingerprint” for identification by comparison of the spectrum from unknown with previously recorded reference spectra.Thus, in infrared spectroscopy, IR radiation is passed through the sample. Some of this radiation is absorbed by the sample and some is transmitted. The resulting spectrum represents the molecular absorption and transmission of the sample.

We employed FTIR analysis as a method of qualitative measurement of the functionalisation treatments, on the surface of MWCNTs. As amine and carboxyl groups are grafted on CNT's surface, vibrational spectrum of the bonds of each molecule are recorded via this method. We intend to identify the intensity peaks of these substances in order to prove the proper realisation of the functionalisation procedure.For that reason, in the following chapter, plots of the intensity at each individual frequency, for every treatment used, are presented and discussed.

2.3.2 Scanning Electron Microscope - SEM

Scanning Electron Microscope or SEM is an electron microscope device that produces images of the sample's surface by scanning it with a focused electron beam. The advantages over other methods of microscopy, such as light microscopy, is that SEM includes much higher magnification, nearly up to $100,000$ times, and greater depth of field (100 times higher than light microscopy's).

Images produced by the SEM analysis for each sample with different chemical treatment will be assessed and analysed in order to drew solid conclusions, in conjunction with FTIR analysis, about the type of dispersion of CNTs inside the epoxy resin. Except of samples containing CNTs (0.2% wt), a base sample of pure epoxy will be utilised as a reference. As in the previous method of characterisation, images and extended analysis will be held in the following chapter.

2.3.3 Tensile measurements

Following the production of plain hybrid composite panels, samples of certain geometry are cut, using the water jet cutter. The geometry of the specimens follows the Standard Test Method for Tensile Properties of Plastics (*ASTM D 638 - 99*) as seen in the figure 2.1. The reason of using this type of specimen, is because of the inability of our tensile test machine to to exceed the 5,000 Kg. The proper specimen type that is currently used for tensile measurements of composite materials, has much larger width, which in accordance with the thickness of the three plies of carbon, increases

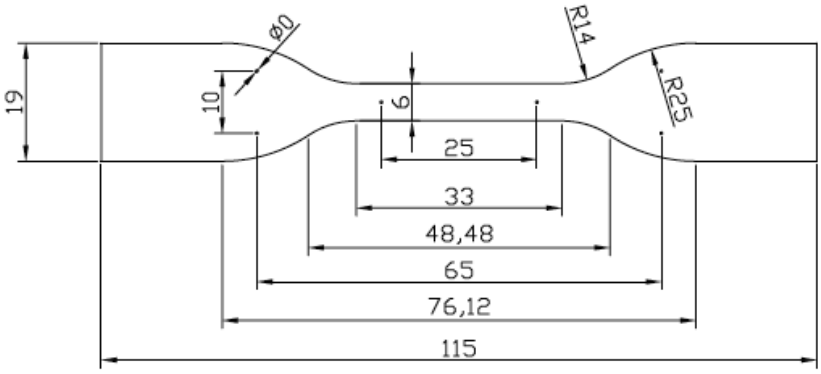

[ast]

Figure 2.1: ASTM D $638 - 99$ specimen type IV

the strength needed to reach a break point. Despite, any inconvenience we might faced, we were able to drew solid conclusions regarding our experiment. Additional information regarding the standard utilised in this thesis is in the Appendix.

For the measurement of the tensile properties of the specimens we used an INSTRON® tensile testing machine at the Applied Mechanics Lab of the Technical University of Crete. The instrument is able to measure forces up to $5000N$ at a stable rate of displacement of the grips. In our experiments we used 0.05 mm/s velocity deformation. The instrument produces a voltage value proportional of the displacement and the force, which was calibrated and located by using known number of weights and externally measured displacements of between the grips. The produced electric signal is transferred to a computer through a data collection device and is processed by a specialised software.

$$Force = 470.22 \times Voltage + 0.029$$

$$\Delta l = 99.93 \times Voltage + 0.16$$

The tables with the calibration values for both the force and the elongation, are listed in the tables section further below in this document.

Chapter 3

Results

This section presents the results of the experimental measurements. First a full scale analysis of the FTIR and SEM results is done, in order to test the success of the functionalisation techniques that were used and the the quality of the dispersion of the CNTs in the epoxy resin and the hybrid composites (carbon fibre-resin-CNT). Then, the sample characteristics are presented for all sample series. The mechanical properties measured during the tensile tests of both the hybrid and the basic samples (w/o CNT) are shown.

3.1 FTIR Analysis

The FTIR technique was used in an attempt to verify the grafting of the functionalisation groups on the surface of the CNTs. The spectra of the pure resin, the modified CNTs and the nanocomposites (cured resin with CNTs) are shown in the Appendix.

Having identified the peaks that correspond to the epoxy resin and the carbon nanotubes we were able to isolate the relevant peaks in the nanocomposites (Table 3.1. The peaks around 1500 cm^{-1} are indications of the amine group's presence.

In the pure epoxy sample C.2 a strong peak corresponding to the amines present in the hardener is evident at 1508 cm^{-1}. In the samples, where the CNTs were treated by the 1-step or the 2-step functionalisation treatment we are able to identify the peaks of amine groups at 1584 cm^{-1} and 1510 cm^{-1} respectively, and they are much stronger than those in the pure resin. This establishes the presence of the hexadecylamine (HDA) group on the CNT surface.

The peak that corresponds to the carbonyl group at around 1700 cm^{-1} is only present in the samples treated by acetone and it is probably due to remnants of acetone in the system. Thus, the presence of carboxylic groups on the surface of the CNTs cannot be proven by these FTIR measurements. It seems, therefore, that the oxidation of the carbon surface by the strong acid in the sample series #6 does not yield the carbonyls that were expected. Nevertheless, even in the 2-step functionalisation tech-

Table 3.1: FTIR analysis of pure epoxy sample

Wavenumber cm^{-1}	**Description**
3401.63	stretching O−H
3061.47 , 3032.78	stretching C−H of oxirane ring
2934.42 , 2864.75	stretching C−H of CH_2 and CH aromatic and aliphatic
2352.45	small band of CO_2
1607.66	stretching C≡C of aromatic rings
1509.57	stretching C−C of aromatic rings
1039.59 , 1243.93 , 1111.11	stretching C−O−C of ethers
937.42	stretching C−O of oxirane group
831	stretching C−O−C of oxirane groups
772	rocking CH_2

nique, where it is assumed that the HDA reacts with the carboxyl group on the surface, it seems that the amine gets indeed grafted on the nanotubes, even if the carboxyl is not obvious. The compatibilisation of the reinforcement with the matrix, therefore, is successful. Evidence for this can be seen also in the following SEM pictures.

3.2 SEM analysis

In this section we present some scanning electron micrographs of our samples. As we can see in the Fig. 3.1 we have our pure epoxy sample (without any nano filler inserted), while in the rest of figures we exhibit samples of CNT/epoxy nanocomposite, as created by the recipes described above. In figure 3.4 and 3.5 we can see that the grafted CNTs with amine groups for the 1-step and 2-step chemical treatments, respectively. These samples seem to be well dispersed inside the resin, contrary to the samples where the CNT were treated with acetone (Fig. 3.2) or nitric acid (Fig. 3.3), which show the existence of more clusters.

3.3 Sample characteristics

Eight series of samples were constructed. Each series differed from the others regarding the existence of nanotubes in the matrix, the type and the technique used for the functionalisation, and the method used to incorporate the macroscopic carbon fibres (CF) into the hybrid composite. Each series comprises 15 samples. The geometry and the mass of each sample were measured precisely for the calculation of the volume fraction of CF, f:

$$f = \frac{nc}{\rho t} \ ,$$

where the parameter n corresponds to the number of plies of carbon cloth used, $\rho = 1.97$ g/cm^3 is the density of the fibre, t is the average thickness of the sample in cm

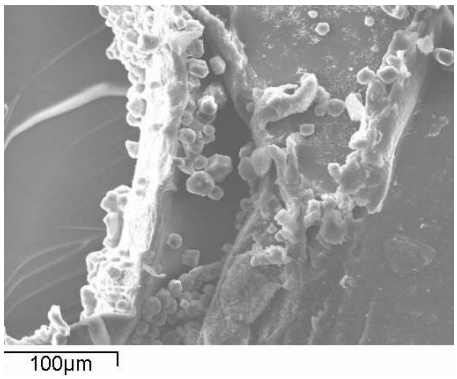

Figure 3.1: SEM picture of pure epoxy

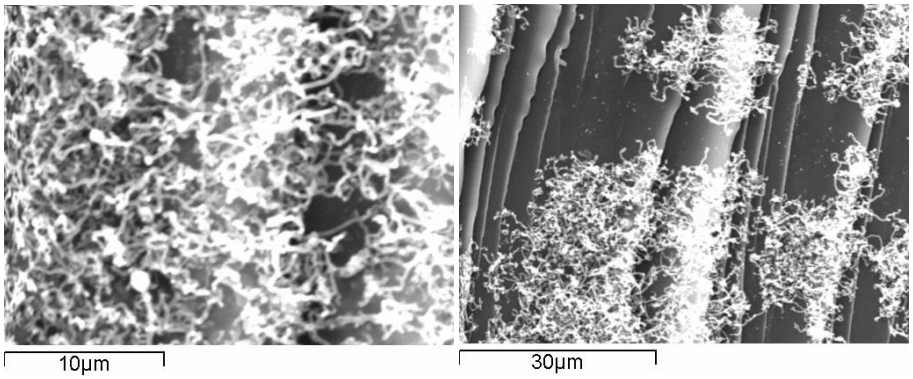

Figure 3.2: SEM picture of CNTs initially dispersed in acetone and then in the epoxy matrix

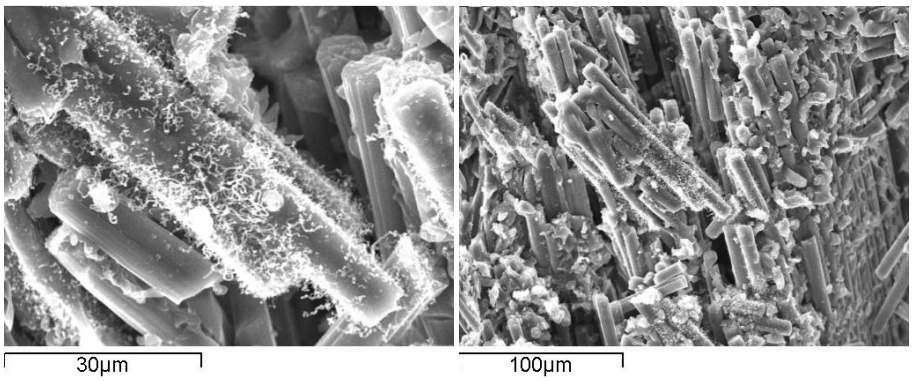

Figure 3.3: SEM picture of CNTs treated with nitric acid in an epoxy matrix

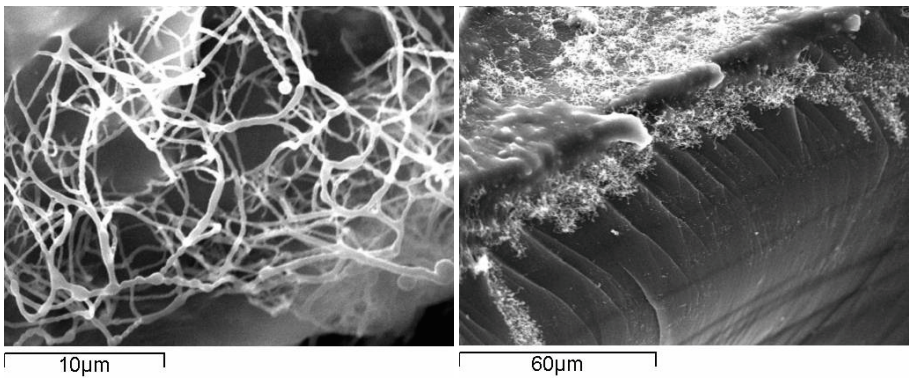

Figure 3.4: SEM pictures of functionalised CNTs treated using the 1-step procedure and then dispersed in the epoxy matrix

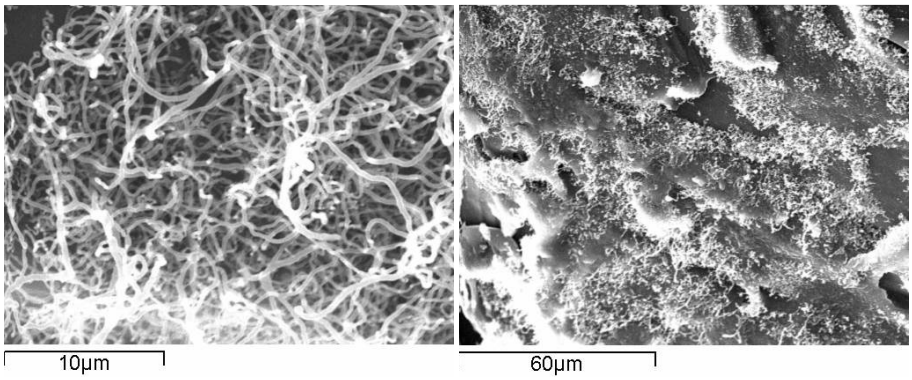

Figure 3.5: SEM pictures of functionalised CNTs treated using the 2-step procedure and then dispersed in the epoxy matrix

Table 3.2: Description of the samples

Series #	**Description**	CF plies	constr. method
1	Basic CF composite	3	vacuum-bag
2	Basic CF composite	1	vacuum-bag
3	Hybrid CF/CNT (in acetone) composite	1	vacuum-bag
4	Hybrid CF/CNT (in acetone) composite	1	hand lay-up
5	Unsuccessful		
6	Hybrid CF/CNT (oxidised) composite	3	hand lay-up
7	Hybrid CF/CNT (one-step funct.) composite	3	hand lay-up
8	Hybrid CF/CNT (two-step funct.) composite	3	hand lay-up
9	Hybrid CF/CNT (unmodified) composite	3	hand lay-up
10	Basic CF composite	3	hand lay-up

Table 3.3: General characteristics of the samples. In all hybrid samples, the amount of the CNT is 0.4 phr (wt.%)

Series #	**Avg.Thickness** cm	**Avg.vol.fraction** V_f, %
1	0.0082	40.93
2	0.0031	36.00
3	0.0037	29.80
4	0.0054	32.60
5	-	-
6	0.0111	30.27
7	0.0110	30.47
8	0.0108	31.67
9	0.0103	30.20
10	0.0109	32.

and $c = 0.02$ is a constant describing the cloth weave characteristics. Tables 3.2 and 3.3 present the full description of each series and their average thickness and volume fractions.

Some observations that can be extracted from these tables are the following:

1. Hand lay-out gives thicker samples and lower CF volume fractions

2. The thickness of composites with three plies is smaller than three times the thickness of composites with one ply.

3. The samples for which acetone was used give composites with lower volume fractions.

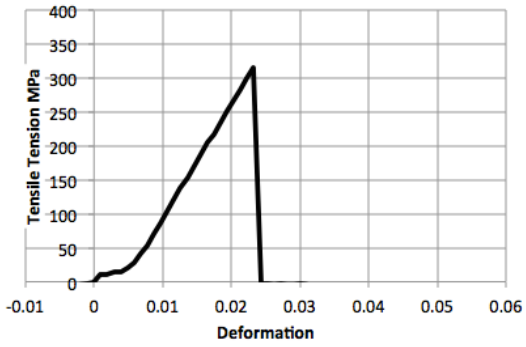

Figure 3.6: Stress-deformation graph of the reference composite sample 11 - Series 2

3.4 Mechanical measurements

Typical stress vs. deformation diagrams are presented below for each series of samples. The values of strength, Young's modulus (E) and elongation at break were determined, in order to compare the mechanical behaviour of the basic and the hybrid composites. The graphs for all samples are available in the appendix.

3.4.1 Samples with a single CF ply

Three samples were constructed with only one carbon fibre ply. Sample #2 is a basic sample (without CNTs). Samples #2 and #3 contain 0.4 phr CNT (parts CNT per hundred parts resin [wt.]) and were treated with acetone, an organic solvent. They differ in the manufacturing process of the composite: #2, was made by utilising the vacuum process, while #3, was carried out using the Hand lay-up method. The CF volume fraction in these samples are 36, 29.8 and 32.6 %.

From the graphs in Fig. 3.6, 3.7 and 3.8 we extract the strength, the stress at which the sample break, the Young's modulus, which is derived from the slope of the curve, and the elongation at break. These values are presented as an histogram in Fig. 3.9. Even though quantitative conclusions cannot be made from these graphs, as the CF volume fractions of the samples are not equal, it seems that the insertion of CNTs using acetone as a dispersion medium in composites consisting of one ply of carbon fibres decreases both the strength and the modulus of the composite. The hand lay-up method seems to give better results than the vacuum-bag method. Similar observations are made also for the values of the elongation at break.

3.4.2 Samples with 3 CF plies

All other sample series were manufactured using 3 carbon fibre plies. Series #1 acts as the reference sample. i.e. the one that does not contain CNT. The rest refer to various

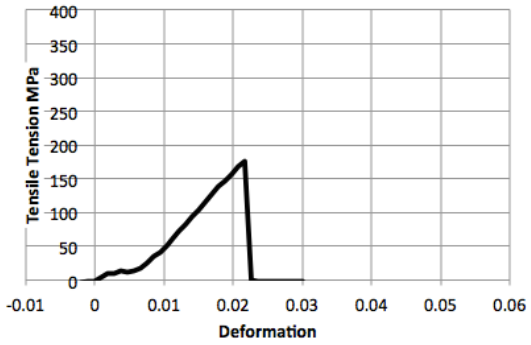

Figure 3.7: Stress-deformation graph of the hybrid composite sample 14 - Series 3

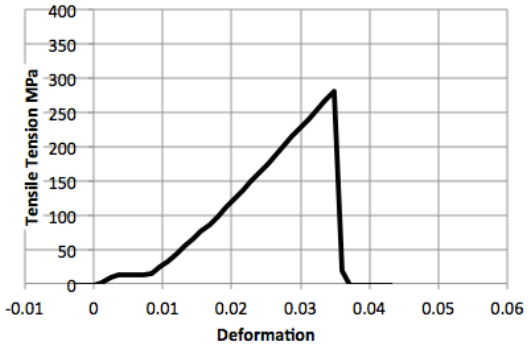

Figure 3.8: Stress-deformation graph of the hybrid composite sample 7 - Series 4

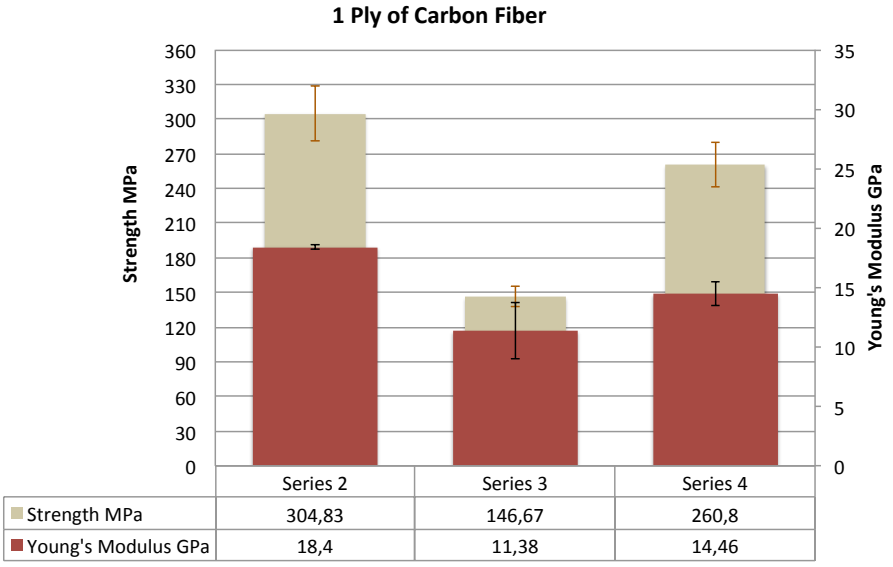

Figure 3.9: Comparison between samples with one ply of carbon fibres - Strength at break/ and Young's modulus

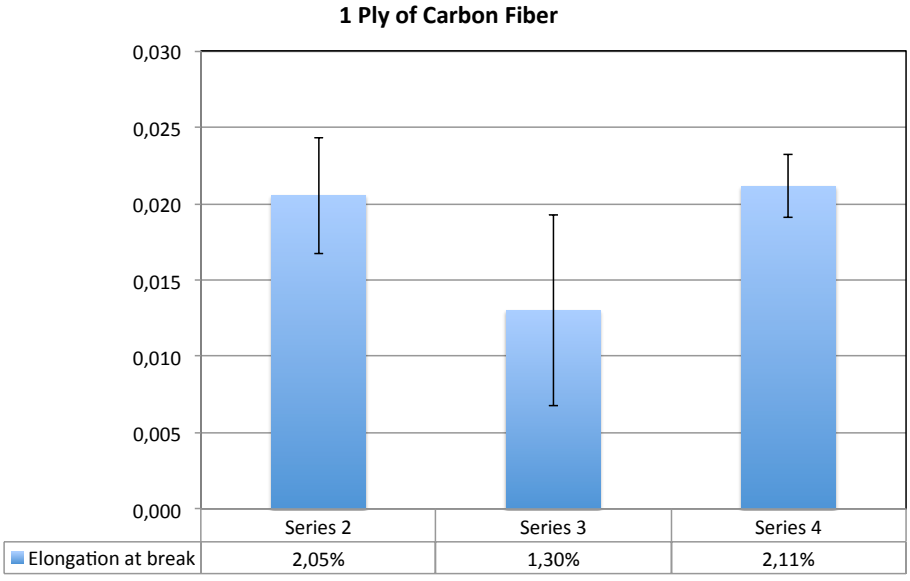

Figure 3.10: Comparison between samples with a single ply of carbon fibres - Elongation at break

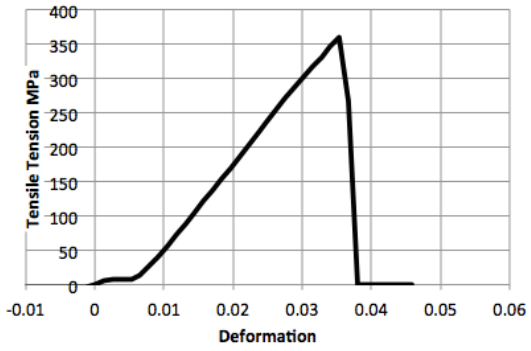

Figure 3.11: Stress-deformation graph of the reference composite sample 7 - Series 1

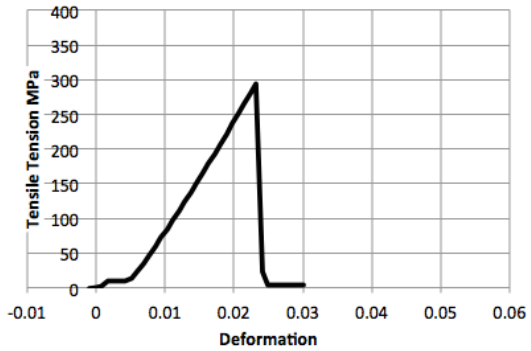

Figure 3.12: Stress-deformation graph of the hybrid composite sample 2 - Series 6

techniques used to improve the dispersion of the CNT's, according to Table 3.2.

The difference between samples #1 and #10 is that the former was made by the vacuum-bag technique, while the latter was laid-up mahually with the help of a brush. Th first obvious result is that the former technique leads to higher volume fraction of CF in the composite with the accompanying higher mechanical properties. However, if the comparison is done on the same CF content basis, then the mechanical properties are not much different. On the other hand, the technique of the vacuum bag gives in general more uniform samples. However, it is not possible to use this technique efficiently for the hybrid composites. When nanotubes are dispersed in the matrix the viscosity of the matrix increases and the pumping system for the preparation of the composite may not be able to cope. Further, the particles may be filtered out by the layers of the breather fabric that is used to distribute the flow of the liquid matrix over the reinforcement fabric.

Coming back to the mechanical properties of the composites, the reference sample that was made by the vacuum-bag method, Figure 3.11 contains 40% CF and no CNTs

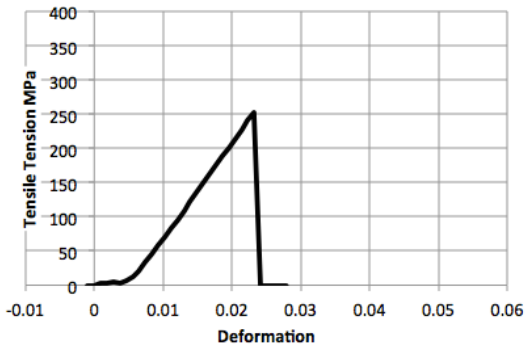

Figure 3.13: Stress-deformation graph of the hybrid composite sample 1 - Series 7

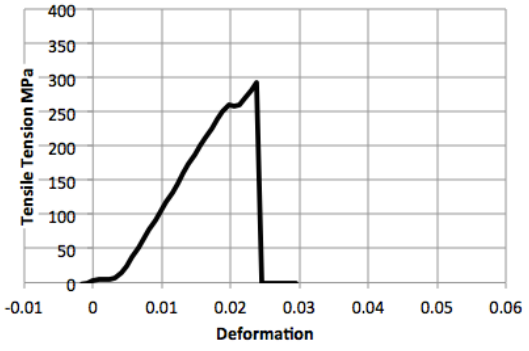

Figure 3.14: Stress-deformation graph of the hybrid composite sample 13 - Series 8

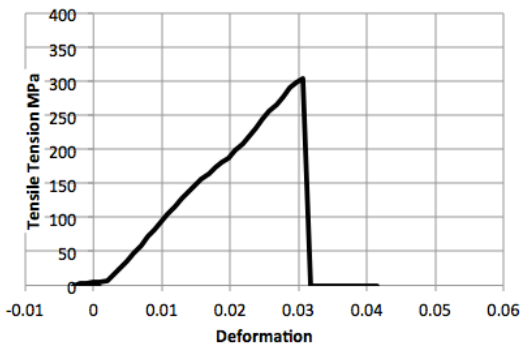

Figure 3.15: Stress-deformation graph of the hybrid composite sample 7 - Series 9

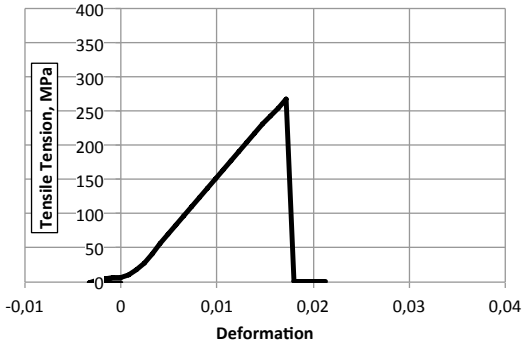

Figure 3.16: Stress-deformation graph of the basic composite sample 2 - Series 10

but shows similar values for the E-modulus to the hybrid ones that contain around 30% CF. This is an evidence that the addition of carbon nano tubes increase the stiffness of the matrix and, thus, the composite. The two step functionalisation technique applied to the CNT gives the stiffest composites for the same amount of CNT.

On the other hand, the vacuum-bag prepared sample without CNT fillers, exhibits higher strength than the hybrid samples (Fig.3.17). The difference is partly due to the higher volume fraction of the high-strength reinforcement and partly due to the better adhesion between the matrix and the fibres that is caused by the vacuum. When the volume fractions as well as the preparation methods are similar, as in the cases of series #6 - #10, then the differences in strength are small. The best strength is shown by the the #8 series, i.e. by the hybrid composite in which the CNTs were treated by the 2-step functionalisation method, even though the differences is not spectacular.

The addition of CNT has a complicated effect on the the elongation at break of the composites, Fig. 3.18. The hybrid composites with unmodified CNTs present an increase of around 20 % in their elongation at break relative to the samples of series #10. This elongation at break is larger than the elongation at break of the individual carbon fibres. We will discuss this in the following chapter. Treating the CNTs to improve the degree of dispersion and their affinity with the organic matrix results in lower values of the elongation at break. Hybrid composites with treated CNTs are more brittle than the basic composite.

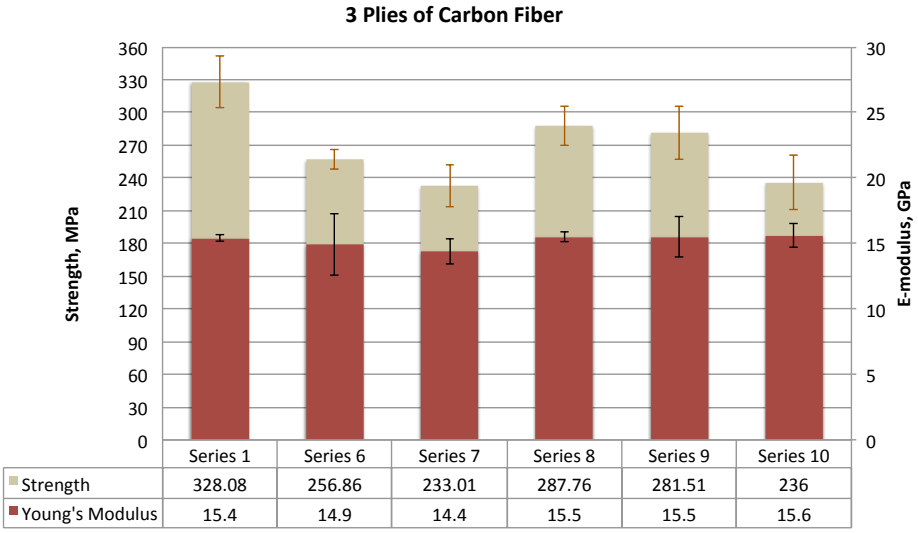

Figure 3.17: Comparison between samples with 3 plies of carbon fibres - Strength at break/Young's modulus

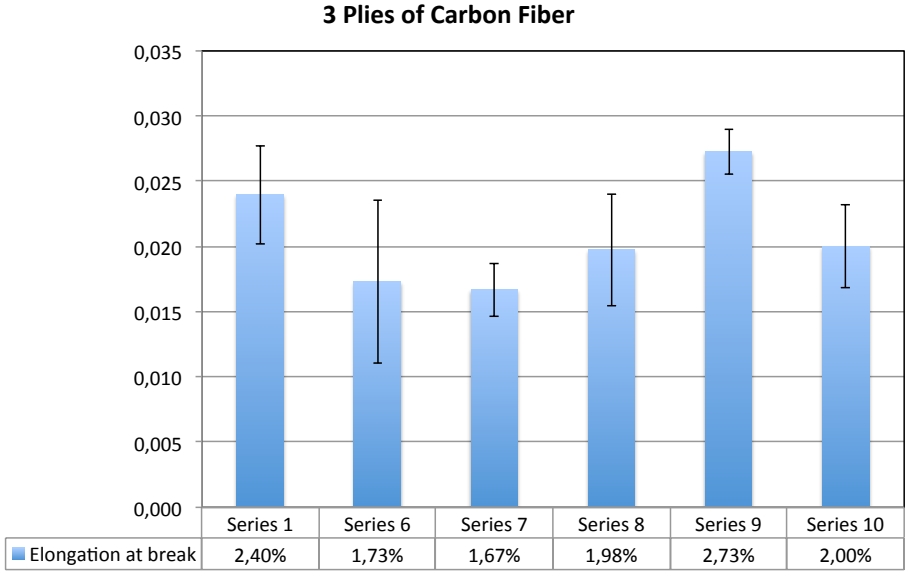

Figure 3.18: Comparison between samples with 3 plies of carbon fibres - Elongation at break

Chapter 4

Discussion

4.1 The dispersion of the carbon nanotubes and the functionalisation methods

As we initially created samples with one ply of carbon fiber we started by one reference sample, without CNTs, and we continued our experiments by testing the limitations of the vacuum-bag technique in conjunction with the use of organic solvent, which assisted in inserting CNTs inside the matrix. As it turned out, severe problems, caused by the high viscosity values, determined by the insertion of CNTs inside the resin, and by the occurrence of extreme filtration of CNT/epoxy, caused by the number of assistive sheet layers needed for the implementation of this technique, made it impossible for us to continue our experiments with this technique. Therefore, we utilised the hand lay-up technique.

In order to increase the thickness of our samples we proceeded with the construction of three-ply composite samples. As we have seen by our previous experiments of dispersing CNTs inside the epoxy with the assistance of acetone, we figured out that great amount of acetone had remained inside our mixture, unable to evaporate. This result, as shown in the mechanical test results, decreases the mechanical properties of the final product, especially the stiffness and the fracture strength. This may happened due to an increase of the plasticity of our samples, caused by the remained acetone in them.

The quality of dispersion of the nanoparticles in the matrix can be estimated both from the SEM photos and the results of the mechanical properties, especially the stiffness. The SEM photos indicate some level of dispersion for the 1-step and 2-step functionalisation methods of dispersion. Specifically for the 2-step chemical treatment, we we have seen pictures of homogeneous dispersion of the functionalised CNTs inside the epoxy resin and in accordance we our mechanical results on strength and stiffness, we can conclude that the quality of dispersion can be considered high enough.

The mechanical properties indicate that the 2-step method gives the highest mod-

ulus when it comes to compare it the other hybrid samples and with the reference sample, created by the vacuum-bag technique. As a result, one would expect, that this technique produces the best, so far, dispersion of the nanotubes in the hybrid composite.

On the other hand, the results of the FTIR spectroscopy cannot confirm the existence of the bond that should exist between the carbon surfaces and the amine functionalisation agent. Or the existence of carboxylic groups on the CNTs.

4.2 E-modulus

4.2.1 Basic carbon textile composites

From the graphs of stress vs. deformation, initially it seems strange that we measure so low values for the E-modulus. The stiffness of the carbon fibres by themselves are in the order of 235 GPa, while the pure epoxy matrix has a modulus of around 3 GPa. If 40 vol.% fibres are added to the matrix and get oriented along the load direction, then one would expect that the composite could have a modulus of around 95 GPa, much higher than the 15 - 18 GPa that is measured for the present composites.

Of course, the present composites have been constructed using woven carbon fibres in the form of fabric, where half the fibres are oriented perpendicular to the load direction. Further, as these fibres are woven in a plain fashion, their actual form is not straight. Rather, they have an undulating form, as one strand of fibres of the warp climbs over one strand of the weft and then goes under the next one.

When under load, the undulating form will start stretching towards a straight line together with the extension of the fibres. Assuming that the warp direction is parallel to the load direction, the resistance to its straightening comes from the weft: in order for these strands to straighten, the perpendicular strands must bend more. The strands of the weft in the dog-bone sample, however, are much shorter than in the warp and have free ends. They are kept together by shearing stresses in the matrix and the friction between the fibres.

The resistance to this type of deformation, thus, is much lower than the resistance of the fibre to extend parallel to its axis. The straightening of the fibres is easier than their stretching and the resistance of the composite sample to the global deformation is less than what it would be for pure stretching of the fibres. The measured modulus for the present composites corresponds to this effective modulus.

Antonogiannakis [2013] has developed a theory that estimates the macroscopic modulus of fabric reinforced composites and it is described in a previous chapter. The theory needs the knowledge of many details of the geometry, weave type and characteristics of the fabric and the stacking of the plies. For systems similar to the one used in this work with 30 - 50% fabric content the effective modulus along the main directions of the fabric in the composite seems to be around 1/4 the value of the fibre modulus.

A simpler approach could be the following: Let us assume that the composite is

loaded at the warp direction. The contribution of half of the composite volume, the one that includes the weft fibres, to the stiffness in the warp direction is small and it is given by a series model as:

$$\frac{1}{E_{weft}} = \frac{V_f}{E_f} + \frac{1-V_f}{E_m} \approx \frac{1-V_f}{E_m} \ .$$

This contribution is added to the contribution of the other half where the fibres are oriented parallel to the warp:

$$E_{warp} = E_{fabric}V_f + E_m(1-V_f) \ ,$$

where E_{fabric} is the effective modulus of the fibres in the fabric and incorporates their resistance to extension and the hindrance of their environment to their straightening.

The modulus of the composite is estimated by adding these contributions:

$$E_1 = \frac{E_{warp}}{2} + \frac{E_{weft}}{2} = \frac{1}{2}\left(E_{fabric}V_f + E_m(1-V_f)\right) + \frac{1}{2}\frac{E_m}{1-V_f} \ . \qquad (4.1)$$

For the samples of series 1 ($E_1 \approx 15.5$ GPa, $V_f = 0.4$ and $E_m = 2.7$ GPa) this can be solved for E_{fabric} at either the weft or the warp direction (equivalent in our case) and gives a value of 65 GPa. This indicates that the stress on the fibres acts simultaneously to straighten and extend them gradually. About 40-50% of the deformation of the composite up to the breaking point goes into the straightening of the fibres in the fabric. This value for E_{fabric} is confirmed by the data of the samples of series 10, which also do not contain CNTs in the matrix.

4.2.2 Hybrid composites

The same arguments should hold to some degree also for the hybrid composites. The contribution of the CNTs in the elastic properties of the composite comes through the enhancement of the stiffness of the matrix. However, given the large difference in the moduli of the matrix and the carbon fibres, even when the former triples in value due to the nano-reinforcement, one could safely assume that the fabric contribution to the composite modulus, E_{fabric} in eq. 4.1, will not change significantly. Keeping thus the same value for E_{fabric} we can now solve eq. 4.1 and estimate the value of E_m for every hybrid sample series. The results are listed in Table 4.1.

The values of the matrix modulus calculated in this way are in relative agreement with the results of the theory for randomly oriented short fibres of 1TPa modulus and $L/D < 100$ in a soft matrix of 2.7 GPa modulus. It is interesting to note that the highest increase of the modulus is obtained when no treatment is conducted and the lowest when the surface of the CNTs are oxidised by strong acid.

Apparently the amine that gets grafted on the surface of the carbon tubes creates a soft phase around the CNTs and reduces their overall stiffness. Thus, the final effective modulus of the nano-reinforcement is lower than what is assumed for pristine CNTs. In practice, this can be accounted for if this phase is considered as another phase with a lower modulus, which contributes negatively to the total stiffness of the matrix.

Table 4.1: Estimated values of the matrix E-modulus

Series #	description	E_m (GPa)
1	no CNT, vacuum	3
10	no CNT, hand lay-up	3
9	untreated CNT	5.3
6	oxidised CNT	4.2
7	1-step treated CNT	4.7
8	2-step treated CNT	4.9

The lower stiffness of the partly oxidised CNTs could be due to damaged surfaces of the CNTs or lower values of the L/D ratio due to agglomeration. On the other hand, the SEM picture of these samples show a fragmented morphology, where the continuity of the matrix is broken in many places also outside the fracture plane. This, in combination with the absence of FTIR evidence that carboxylic groups are indeed created on the CNT surfaces, suggests that these samples should be prepared and studied again for verification.

4.3 Strength

It can be seen in Fig.3.17 when we compare the basic composite samples of series #1 and #10 that the vacuum-bag techniques produces composites with higher strength than the hand lay-up technique. This is true even when the properties of the materials are adjusted for the difference in the volume fractions (by 20%). It seems, therefore, that the vacuum applied during the flow of the uncured resin for the preparation of the composite leads to more intimate adhesion between the carbon fibres and the epoxy matrix.

The addition of CNT improves the tensile strength of the composite in general. The direct comparison of the hybrid composite samples should be done with sample series #10, which has almost the same volume fraction of CF and it was prepared in the same way. Whether the functionalisation treatment is necessary for the improvement of stress is not clear.

The best improvement comes for the samples, for which the CNTs were treated by the 2-step technique. The difference between the strength of these samples and the untreated is very small. Even though the increase of the strength is not spectacular, however, it is obvious that the addition of very stiff particles in the matrix (the ratio of the modulus of the CNTs over the resin is $>$ 300!) is not detrimental for its strength and toughness, as we see in the following when looking at the strain at break of these materials.

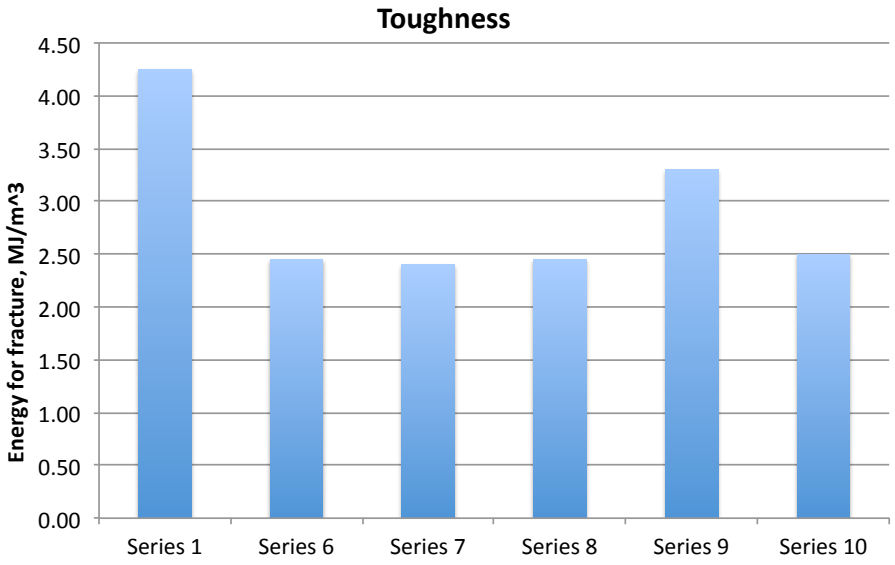

Figure 4.1: The toughness (energy needed for fracture) for the 3-ply samples

4.4 Strain at break and toughness

The most remarkable observation that can be done from Fig. 3.18 is that the strain at break of the most composites is larger than the strain at break of the carbon fibres. This is a result of the mechanism of straightening and extending of the woven fibres that also gives the lower apparent values of the modulus of the fabric. I.e., the undulating shape of the woven fibres at the direction of the load become gradually straight and, at the same time, are extended axially. The final length of the fibre when it breaks should be the sum of the elongation at break of the graphitic material increased by a factor:

$$1.14\alpha_{weft}/2\ , \tag{4.2}$$

where α_{weft} is the relative (dimensionless) width of the strands of the weft, over and under which the warp has to pass in the initial fabric. This in our case could add an extra 20% prolongation to the estimated 1.9% deformation at break of the carbon fibres that we used.

Figure 4.1 shows the surface area under the stress-strain curves of the several samples that contained three plies. Theses values correspond to the integral $\int \sigma d\varepsilon$ and give the energy needed for the fracture of the composite. They give, that is, an estimate of the toughness of the material.

The first thing that the comparison of the samples shows is, again, that, even when normalised for the same reinforcement load, the composites produced by the vacuum-bagging technique show higher toughness than the ones made by the hand lay-up

method. This follows the higher strength that was measured for of these composites and enforces the idea of the more efficient adhesion between the the CF fibres and the matrix.

The addition of untreated CNTs also improves the toughness of the composite, as it can be seen in Fig. 4.1 by comparing the samples of series #9 with series #10 for similar CF volume fractions. The treatment of the CNTs cancels this improvement but does not deteriorate the toughness.

The latter is significant because the CNTs are so much stiffer than the matrix, that they could also create stress concentration points in the material and nucleate and accelerate the growth of possible cracks. Fortunately, the reduction of the strain at break due to CNTs is not very large and the toughness of the composite is not sacrificed.

4.5 The reinforcing in the hybrid composite

From the above analysis it seems that the addition of the nanotubes and the creation of the hybrid composites has more advantages than disadvantages for the mechanical properties of the material. While the tensile properties of the composite do not improve very much, the stiffness of the matrix increases.

As mentioned in the introduction, ordinary continuous fibre composite materials show very low strength in compressive loads parallel to the fiber direction. When compressed axially, the fibres will buckle at relatively low forces and the composite fails. What will prevent them from buckling is the stiffness of the matrix. Since this stiffness is increased in the present hybrid composites by the addition of CNTs, the resistance to buckling of the composite will be enhanced and the compressive strength will increase.

We did not have the proper equipment to measure compressive strength in the laboratory and we will suffice to show some results that support this idea from the literature. Fig. 4.2 shows the increase of the compressive strength of several composites as a function of the stiffness of the matrix. The latter was controlled by the amount of the nano-particles.

It should be reiterated here that the tensile properties of the composites produced using the vacuum-bag method are better than the ones made by the hand lay-out technique. The compressive strength, however, depends on the stiffness of the matrix. The best way to increase this stiffness and, thus, delay the buckling of the fibres is the addition of CNTs. Therefore, if the improvement of the compressive strength is desired, then the extra cost of incorporating the CNTs may be justified but the vacuum-bag technique may not be possible to apply.

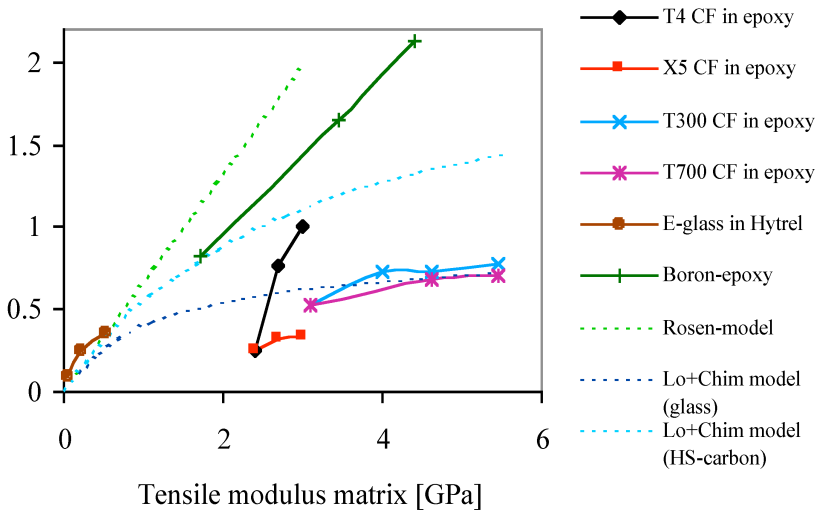

[Vlasveld, 2005]

Figure 4.2: Improvement of the compressive strength as a function of the matrix stiffness for several continuous fibre composites.

Chapter 5

Conclusions and recommendations

After conducting our experiments and finishing the analysis of the results, we are able to come to certain conclusions and recommendations for a future research.

- The vacuum-bag technique produces samples with higher strength than hand lay-up does. Despite that, the former is considered as inappropriate to insert and disperse CNTs inside an epoxy resin, due to the high viscosity and possible problems of particle filtration that may occur. It seems that the simple vacuum-bag technique can not be used for the construction of hybrid composite materials.

- When acetone or another organic solvent is used for the dispersion medium of the nanoparticles, the mechanical properties of the composite worsen, due to the excess of solvent that remains trapped inside the resin.

- By analysing the data from both the mechanical test measurements and the SEM pictures we are in a position to state that samples treated with the 2-step functionalisation method exhibited the best level of dispersion inside the epoxy matrix.

- It was observed that due to the undulating form of the fibers inside the plain carbon fabric , the straightening of the fibers is easier than their stretching. The resistance of the sample to the global deformation is less that it would have been only for pure stretching of the fibers. Thus, we conclude that the measured modulus is the effective modulus and is much lower than the modulus contribution of straight fibres.

- According to the elastic deformation theory of textile reinforced composites, introduced by [Antonogiannakis, 2013], for the stiffness values that we measured for the reference sample's fabric, E_{fabric}, it is clear that the stress on the fibers

acts simultaneously to straighten and extend them. For that reason from 40% up to 50% of the deformation until the breaking point, goes to straightening the fibers in the fabric.

- As for the hybrid composites, regarding the stiffness of the samples, assuming that the effective modulus of the fabric, E_{fabric}, remains unchanged, we are able to conclude that at the samples of 1-step and 2-step functionalisation treatment, the hexadecylamine grafted on the surface of the CNTs created a soft phase. This phase has lower stiffness and plays a negative role on the total stiffness of the matrix. Regarding the oxidised-CNT samples, damaged surfaces of CNTs or the formation of agglomerates may be the reason for their poor results on Young's modulus. It is clear that further research must be done for the cases of the amine and for the acid treatment, in order to obtain solid evidence, which will lead us to final conclusions.

- It is to mention the we observed the best results on stiffness by the mechanically dispersed CNT samples, or best known as unmodified CNT samples. Although further study and experiments must be carried out in order to conclude if the mechanical methods of dispersion are more appropriate for inserting and dispersing CNTs inside an epoxy matrix.

- Regarding the strength of the hybrid composites, although the unmodified CNT samples exhibit very small differences from the 2-step functionalised samples, the latter present better results.

- We concluded that the strain at break of most composite samples is larger than that of carbon fibers alone. This can be explained by the straightening and extending of the woven fibers. Additionally, we observe that in certain hybrid composite samples, elongation at break is decreased.

- The toughness of the composites improves when CNTs are added. The treatment of the nanoparticles by any of the techniques tried does not lead to improvement of the toughness.

- The CNTs added to the matrix increase the stiffness of the matrix. This will lead to enhancement of the resistance of the hybrid composite to buckling of the CF fibres and improvement of the compressive strength.

- Actual measurements of the compressive strength is needed to verify these conclusions

- If high tensile properties are needed, then the vacuum-bag technique with no CNTs will produce the best material but at the cost of low compressive strength. If the compressive strength is the important parameter, then CNTs can be the solution. In the latter case, however, the technique of vacuum-bagging may not be possible with the result of losing the exceptional tensile properties that accompany it.

Bibliography

Standard test method for astm d 638 – 99 tensile properties of plastics.

I. M. Ward A. A. Gusev, P. J. Hine. Fiber packing and elastic properties of a transversely random unidirectional glass/epoxy composite. *Composite Science and Technology*, 60(4):535–541, 2000.

J. Jackson A. Nettles, A. Hodge. An examination of the compressive cyclic loading aspects of damage tolerance for polymer matrix launch vehicle hardware. *Journal of Composite Materials*, 1445(4):437–458, 2011.

K. Shulte A. T. Seyhan, M. Tanoglu. Tensile mechanical behaviour and fracture toughness of mwcnt and dwcnt modified vinyl-ester/polyesterhybrid nanocompositesproduced by 3-roll milling. *Mater. Sci. Eng.*, A(523):85–92, 2009.

P. Nikolaev h. Dai P. Petit J. Robert C. Xu Y. H. Lee S. G. Kim A. G. Rinzler D. T. Colbert G. E. Scuseria D. Tamanek J. E. Fischer R. E. Samlley A. Thess, R. Lee. Crystalline ropes of metallic carbon nanotubes. *Science*, 273:483–487, 1996.

G. H. Kim B. M. Cho. Effect of the processing parameters on the surface resistivity of acrilonitrile-butadiene rubber/multiwalled carbon nanotube nanocomposites. *J. Appl. Polym. Sci.*, 116:555–561, 2010.

M.P. Bacos. Carbon-carbon composites:oxidation behavior and coatings protection. *JOURNAL DE PHYSIQUE IV*, 1993.

J.A. Barreto, W.Õ' Malley, M. Kubeil, B. Graham, H. Stephon, and L. Spiccia. Nanomaterials:applications in cancer imaging. *Advanced Materilas*, 23(12), March 2011.

P. Bernier C. Journet. Production of carbon nanotubes. *Appl. Phys. A. Mater. Sci. Proc.*, 67:1–9, 1998.

P. Bernier A. Loiseau M. Lammy de la Chapelle S.Lefrant P. Deniard R. Lee J. E. Fischer C. Journet, W. K. Maiser. Large-scale production of single-walled carbon nanotubes by the electric-arc technique. *Nature*, 388:756–758, 1997.

T. W. Chou C. Li, E. T. Thostenson. Sensors and actuators based on carbon nanotubes and their composites: a review. *Composite Science and Technology*, 68:1227–1249, 2008.

F.C. Campbell. *Manufacturing Technology for Aerospace Structural Materials*. Elsevier, 2nd edition, 2008.

D. T. Colbert. Single-wall nanotubes: a new option for conductive plastics and engineering polymers. *Plastics Addit Compound*, 5(1):18–25, 2003.

J. Mozco B. Pukanszky J. Gonzalez-Benito D. Olmos, K. Bagdi. Morphology interphase formation in epoxy/pmma/glass fiber composites:effect of the molecular weight of pmma. *Journal of Colloid Interface Science*, 360:289–299, 2011.

R.P. Silvy D. Resasco. *Structure and Applications of Single-Walled Carbon Nanotubes (SWCNTs)*. SWeNT.

A. John Hart E. J. Garcia, B. L. Wardle. Joining prepreg composite interfaces with aligned carbon nanotubes. *Composites Part A: Applied Science Manufacturing*, 39(6):1065–1070, 2008.

T. W. Chou E. T. Thostenson, Z. Ren. Advnaces in the science and technology of carbon nanotubes and their composites:a review. *Composite Science and Technology*, 61 (13):1899–1912, 2001.

Q. Zheng F. Deng. Interaction models for effective thermal and electric conductivites of carbon nanotubes. *Acta Mechanica Solida Sinica*, 22(1):1–17, 2009.

A.D. Gotsis. *Σημειώσεις Τεχνολογίας Πολυμερών*. Dept. of Science, Technical University of Crete, 2008.

D. Hull and T.W. Clyne. *An Introduction to Composite Materials*. Cambribge Solid State Science Series, 2nd edition, 1996.

H. Brune C. Klinke M. Chen-E. Riedo I. Palaci, S. Fedrigo. Radial elasticity of multiwalled carbon nanotubes. *Physics Review Letters*, 94, 2005.

S. Iijima. Helical microtubules of graphitic carbon. *Nature*, 354:56–58, 1991.

S. Iijima and T. Ichihashi. Single-shell carbon nanotubes of 1-nm diameter. *Nature*, 363:603–605, June 1993.

M. S. P. Shafer J. Cho, A. R. Boccaccini. Ceramic matrix compositesconatining carbon nanotubes. *J. Mater. Sci.*, 44(8):1934–1951, 2003.

S. J. Hwang H. Chung J. H. Ahn, Y. J. Kim. High energy ball milling of catalytically synthesized carbon nanotubes. *Mater. Sci. Forum*, 534-536:193–196, 2007.

H. M. Cheng J. H. Du, j. Bai. The present status and key problems of carbon nanotubes based on polymer composites. *eXPRESS Polym. Lett.*, 1(5):253–273, 2007.

Z. G. Zhang F. Lockwood J. Hilding, E. A. Grulke. Dispersion of carbon nanotubes in liquids. *J. Disper. Sci. Technol.*, 24(1):1–41, 2003.

Y. K. Chen M. H. L. Green P. J. F. Harris S. C. Tsang K. L. Lu, R. M. Lago. Mechanical damage of carbon nanotubes by ultrasonication. *Carbon*, 34(6):814–816, 1996.

Q. Shi K. T. Lau, S. Failure mechanisms of carbon nanotube/epoxy composites pre-treated in different temperature environments. *Carbon*, 40(15):2965–2968, 2002.

A. Paipetis; V. Kostopoulos. *Carbon Nanotube Enhanced Aerospace Composite Materials*, volume 188 of *Solid Mechanics and Its Applications*. Springer, 2013.

J. Wu Y. Huang K. C. Hwang L. Jiang, H. Tan. Continuum modeling of interfaces in polymer matrix composites reinforced by carbon nanotubes. *Nano Letters*, 2(3): 139–148, 2007.

U. Mariani L. Lazzeri. Applications of damage tolerance principles to the design of helicopters. *International Journal of Fatigue*, 31(6):1039–1045, 2009.

F. Gordaninejad J. Suhr L. Sun, R. F. Gibson. Energy absorption capability of nanocomposites: a review. *Composite Science and Technology*, 69(14):2392–2409, 2009.

M. Kausala L. Zhang. Fabrication and application of polymer composites comprising carbon nanotubes. *Recent Patents on Nanotechnology*, 1(1):59–65, 2007.

K. P. Ryan V. Nicolosi G. Bister A. Fonseca J. B. Nagy K. Szostak F. Beguin W. J. Blau M. Cadek, J. N. Coleman. Reinforcement of polymers with carbon nanotubes: the role of the nanotube surface area. *Nano Letters*, 4(2):353–356, 2004.

M. J. Dyer K. Moloni T. F. Kelly R. S. Ruoff M. F. Yu, O. lourie. Strength and breaking mechanism of multiwalled carbon nanotubes under tensile load. *Science*, 287:637–640, 2000a.

R. S. Ruoff M. F. Yu, T. Kowalewski. Investigation of the radial deformability of individual carbon nanotubes under controlled indentation force. *Physics Review Letters*, 85, 2000b.

T. Higuchi S. Oschiai M. Hojo, S. Matsuda. Fracture mechanism for mode ii propagation of delamination fatigue cracks in cf/peek laminates. *Zairyo/J. Soc. Mater. Sci. Jpn.*, 46(4):366–373, 1997.

T. Tahara T. Iwaki F. Iskandar C. J. Hogan Jr K. Okuyama M. Inkyo, Y. Tokunaga. Beads mill-assisted synthesis of poly methyl methacrylate (pmma)-tio2 nanoparticle composites. *Ind. Eng. Chem.*, 47:2597–2604, 2008.

P. Zapol Y.Zhu S. Li T. Belytschko H. D. Espinosa M. Locascio, B. Peng. Tailoring the load carrying capacity of mwcnts through inter-shell atomic bridging. *Experimental Mechanics*, 49, 2009.

J.M. Gibson M.M.J. Treacy, T.W. Ebbesen. Exceptionally high young's modulus observed for individual carbon nanotubes. *Nature*, 381:678–680, 1996.

D. Tasis N. Karousis, N. Tagmatarchis. Currents progress on the chemical modification of carbon nanotubes. *Chem. Rev.*, 110(9):5366–5397, 2010.

J. F. Colomer C. Bossuot J. M. Benoit G. Van Tendeloo J. P. Pirard J. B. Nagy N. Pierard, A. Fonseca. Ball milling effect on the structure of single-wall carbon nanotubes. *Carbon*, 42:1691–1697, 2004.

J.F. Nye. *Physical Properties of Crystals: Their Representation by Tensors and Matrices*. Oxford Science Publications, 1985.

K. J. Sun K. M. Criss E. J. Siochi J. W. Connell S. Ghose, K. A. Watson. High temperature resin/carbon nanotube composite fabrication. *Comput. Sci. Tech.*, 66:1995–2002, 2006.

M. Karthik S. Karthikeyan, P. Mahalingam. Large scale synthesisof carbon nanotubes. *E-J Chem.*, 6(1):1–12, 2009.

A. R. Bhattacharyya B. G. Min X. Zhang R. A. Vaia C. Park W. Wade Adams R. H. Hauge R. E. Smalley S. Ramesh P. A. Willis S. Kumar, T. D. Deng F. E. Arnold. Synthesis, structure and propertiesof pbo/swcnt composites. *Macromolecules*, 35(24):9039–9043, 2002.

A. Vavouliotis P. Tsotra V. Kostopoulos T. Tanimoto K. Friedrich S. Tsantzalis, P. Karappas. On the improvement of toughness of cfrps with resin doped with cnf and pzt particles. *Composites Part A: Applied Science Manufacturing*, 38(4):1159–1162, 2007.

S. Shelley. Newsfront: carbon nanotubes: a small scale wonder. *Chem. Eng.*, 110(1): 27–29, 2003.

Suprakas Sinha Ray Sreejarani K. Pillai, James Ramontja. Amine functionalization of carbon nanotubes for the preparation of cnt based polylactide composites- a comparative study. *American Ceramic Society*.

R. Vajtai, editor. *Springer Handbook of Nanomaterials*. Springer, 2013.

D.P.N. Vlasveld. *Fibre reinforced polymer nanocomposites*. PhD thesis, Delft University of Technology, Delft, the Netherlands, 2005.

J. Z. Kovacs W. Bauhofer. A review and analysis of electrical percolation in carbon nanotube polymer composites. *Composite Science and Technology*, 69(10):1486–1498, 2009.

Z. Zhang R. Yang G. Liu T> Zhang X. An X. Yi Y. Ren Z. Niu J. Li H. Dong W. Zhou P. M. Ajayan S. Xie W. Ma, L. Liu. High-strength composite fibers: realizing true potential of carbon nanotubes on polymer matrix through continuous reticulate architecture and molecular level coupling. *Nano Letters*, 9(8):2855–2861, 2009.

S. Inoue S. Iijima Y. Ando, X. Zhao. Mass production of multiwalled carbon nanotubes by hydrogen arc discharge. *J. Cryst. Growth*, 237-239:1926–1930, 2002.

J. Liang Q. Yu D. H. Wu Y. B. Li, B. Q. Wei. Transformation of carbon nanotubesto nanoparticlesby ball milling process§. *Carbon*, 37:493–497, 1999.

M. J. Crocker Z. Li. A review on vibration damping in sandwich composite structures. *International Journal of Accoustics*, 10(4):159–169, 2005.

A. Antonogiannakis. Μελέτη της επίδρασης της ύφανσης των ινών στις μηχανικές ιδιότητες ινοπλισμένων σύνθετων υλικών. Master's thesis, Science Dept. ,Technical University of Crete, 2013.

Appendix A

ASTM Standard Test Method for Tensile Properties of Plastics

Designation: D 638 – 99

An American National Standard

Standard Test Method for Tensile Properties of Plastics[1]

This standard is issued under the fixed designation D 638; the number immediately following the designation indicates the year of original adoption or, in the case of revision, the year of last revision. A number in parentheses indicates the year of last reapproval. A superscript epsilon (ε) indicates an editorial change since the last revision or reapproval.

This standard has been approved for use by agencies of the Department of Defense.

1. Scope *

1.1 This test method covers the determination of the tensile properties of unreinforced and reinforced plastics in the form of standard dumbbell-shaped test specimens when tested under defined conditions of pretreatment, temperature, humidity, and testing machine speed.

1.2 This test method can be used for testing materials of any thickness up to 14 mm (0.55 in.). However, for testing specimens in the form of thin sheeting, including film less than 1.0 mm (0.04 in.) in thickness, Test Methods D 882 is the preferred test method. Materials with a thickness greater than 14 mm (0.55 in.) must be reduced by machining.

1.3 This test method includes the option of determining Poisson's ratio at room temperature.

NOTE 1—This test method and ISO 527-1 are technically equivalent.

NOTE 2—This test method is not intended to cover precise physical procedures. It is recognized that the constant rate of crosshead movement type of test leaves much to be desired from a theoretical standpoint, that wide differences may exist between rate of crosshead movement and rate of strain between gage marks on the specimen, and that the testing speeds specified disguise important effects characteristic of materials in the plastic state. Further, it is realized that variations in the thicknesses of test specimens, which are permitted by these procedures, produce variations in the surface-volume ratios of such specimens, and that these variations may influence the test results. Hence, where directly comparable results are desired, all samples should be of equal thickness. Special additional tests should be used where more precise physical data are needed.

NOTE 3—This test method may be used for testing phenolic molded resin or laminated materials. However, where these materials are used as electrical insulation, such materials should be tested in accordance with Test Methods D 229 and Test Method D 651.

NOTE 4—For tensile properties of resin-matrix composites reinforced with oriented continuous or discontinuous high modulus >20-GPa ($>3.0 \times 10^6$-psi) fibers, tests shall be made in accordance with Test Method D 3039/D 3039M.

1.4 Test data obtained by this test method are relevant and appropriate for use in engineering design.

1.5 The values stated in SI units are to be regarded as the standard. The values given in parentheses are for information only.

1.6 *This standard does not purport to address all of the safety concerns, if any, associated with its use. It is the responsibility of the user of this standard to establish appropriate safety and health practices and determine the applicability of regulatory limitations prior to use.*

2. Referenced Documents

2.1 *ASTM Standards:*

D 229 Test Methods for Rigid Sheet and Plate Materials Used for Electrical Insulation[2]

D 412 Test Methods for Vulcanized Rubber and Thermoplastic Rubbers and Thermoplastic Elastomers— Tension[3]

D 618 Practice for Conditioning Plastics for Testing[4]

D 651 Test Method for Tensile Strength of Molded Electrical Insulating Materials[5]

D 882 Test Methods for Tensile Properties of Thin Plastic Sheeting[4]

D 883 Terminology Relating to Plastics[4]

D 1822 Test Method for Tensile-Impact Energy to Break Plastics and Electrical Insulating Materials[4]

D 3039/D 3039M Test Method for Tensile Properties of Polymer Matrix Composite Materials[6]

D 4000 Classification System for Specifying Plastic Materials[7]

D 4066 Specification for Nylon Injection and Extrusion Materials[7]

D 5947 Test Methods for Physical Dimensions of Solid Plastic Specimens[8]

E 4 Practices for Force Verification of Testing Machines[9]

E 83 Practice for Verification and Classification of Extensometers[9]

E 132 Test Method for Poisson's Ratio at Room Temperature[9]

E 691 Practice for Conducting an Interlaboratory Study to Determine the Precision of a Test Method[10]

2.2 *ISO Standard:*

[1] This test method is under the jurisdiction of ASTM Committee D-20 on Plastics and is the direct responsibility of Subcommittee D 20.10 on Mechanical Properties.

Current edition approved Nov. 10, 1999. Published February 2000. Originally published as D 638 – 41 T. Last previous edition D 638 – 98.

[2] *Annual Book of ASTM Standards*, Vol 10.01.

[3] *Annual Book of ASTM Standards*, Vol 09.01.

[4] *Annual Book of ASTM Standards*, Vol 08.01.

[5] Discontinued; see *1994 Annual Book of ASTM Standards*, Vol 10.01.

[6] *Annual Book of ASTM Standards*, Vol 15.03.

[7] *Annual Book of ASTM Standards*, Vol 08.02.

[8] *Annual Book of ASTM Standards*, Vol 08.03.

[9] *Annual Book of ASTM Standards*, Vol 03.01.

[10] *Annual Book of ASTM Standards*, Vol 14.02.

96

***A Summary of Changes section appears at the end of this standard.**

ISO 527-1 Determination of Tensile Properties[11]

3. Terminology

3.1 *Definitions*—Definitions of terms applying to this test method appear in Terminology D 883 and Annex A2.

4. Significance and Use

4.1 This test method is designed to produce tensile property data for the control and specification of plastic materials. These data are also useful for qualitative characterization and for research and development. For many materials, there may be a specification that requires the use of this test method, but with some procedural modifications that take precedence when adhering to the specification. Therefore, it is advisable to refer to that material specification before using this test method. Table 1 in Classification D 4000 lists the ASTM materials standards that currently exist.

4.2 Tensile properties may vary with specimen preparation and with speed and environment of testing. Consequently, where precise comparative results are desired, these factors must be carefully controlled.

4.2.1 It is realized that a material cannot be tested without also testing the method of preparation of that material. Hence, when comparative tests of materials per se are desired, the greatest care must be exercised to ensure that all samples are prepared in exactly the same way, unless the test is to include the effects of sample preparation. Similarly, for referee purposes or comparisons within any given series of specimens, care must be taken to secure the maximum degree of uniformity in details of preparation, treatment, and handling.

4.3 Tensile properties may provide useful data for plastics engineering design purposes. However, because of the high degree of sensitivity exhibited by many plastics to rate of straining and environmental conditions, data obtained by this test method cannot be considered valid for applications involving load-time scales or environments widely different from those of this test method. In cases of such dissimilarity, no reliable estimation of the limit of usefulness can be made for most plastics. This sensitivity to rate of straining and environment necessitates testing over a broad load-time scale (including impact and creep) and range of environmental conditions if tensile properties are to suffice for engineering design purposes.

NOTE 5—Since the existence of a true elastic limit in plastics (as in many other organic materials and in many metals) is debatable, the propriety of applying the term "elastic modulus" in its quoted, generally accepted definition to describe the "stiffness" or "rigidity" of a plastic has been seriously questioned. The exact stress-strain characteristics of plastic materials are highly dependent on such factors as rate of application of stress, temperature, previous history of specimen, etc. However, stress-strain curves for plastics, determined as described in this test method, almost always show a linear region at low stresses, and a straight line drawn tangent to this portion of the curve permits calculation of an elastic modulus of the usually defined type. Such a constant is useful if its arbitrary nature and dependence on time, temperature, and similar factors are realized.

97

[11] Available from American National Standards Institute, 11 W. 42nd St., 13th Floor, New York, NY 10036.

4.4 *Poisson's Ratio*—When uniaxial tensile force is applied to a solid, the solid stretches in the direction of the applied force (axially), but it also contracts in both dimensions lateral to the applied force. If the solid is homogeneous and isotropic, and the material remains elastic under the action of the applied force, the lateral strain bears a constant relationship to the axial strain. This constant, called Poisson's ratio, is defined as the negative ratio of the transverse (negative) to axial strain under uniaxial stress.

4.4.1 Poisson's ratio is used for the design of structures in which all dimensional changes resulting from the application of force need to be taken into account and in the application of the generalized theory of elasticity to structural analysis.

NOTE 6—The accuracy of the determination of Poisson's ratio is usually limited by the accuracy of the transverse strain measurements because the percentage errors in these measurements are usually greater than in the axial strain measurements. Since a ratio rather than an absolute quantity is measured, it is only necessary to know accurately the relative value of the calibration factors of the extensometers. Also, in general, the value of the applied loads need not be known accurately.

5. Apparatus

5.1 *Testing Machine*—A testing machine of the constant-rate-of-crosshead-movement type and comprising essentially the following:

5.1.1 *Fixed Member*—A fixed or essentially stationary member carrying one grip.

5.1.2 *Movable Member*—A movable member carrying a second grip.

5.1.3 *Grips*—Grips for holding the test specimen between the fixed member and the movable member of the testing machine can be either the fixed or self-aligning type.

5.1.3.1 Fixed grips are rigidly attached to the fixed and movable members of the testing machine. When this type of grip is used extreme care should be taken to ensure that the test specimen is inserted and clamped so that the long axis of the test specimen coincides with the direction of pull through the center line of the grip assembly.

5.1.3.2 Self-aligning grips are attached to the fixed and movable members of the testing machine in such a manner that they will move freely into alignment as soon as any load is applied so that the long axis of the test specimen will coincide with the direction of the applied pull through the center line of the grip assembly. The specimens should be aligned as perfectly as possible with the direction of pull so that no rotary motion that may induce slippage will occur in the grips; there is a limit to the amount of misalignment self-aligning grips will accommodate.

5.1.3.3 The test specimen shall be held in such a way that slippage relative to the grips is prevented insofar as possible. Grip surfaces that are deeply scored or serrated with a pattern similar to those of a coarse single-cut file, serrations about 2.4 mm (0.09 in.) apart and about 1.6 mm (0.06 in.) deep, have been found satisfactory for most thermoplastics. Finer serrations have been found to be more satisfactory for harder plastics, such as the thermosetting materials. The serrations should be kept clean and sharp. Breaking in the grips may occur at times, even when deep serrations or abraded specimen surfaces are used; other techniques must be used in these cases.

Other techniques that have been found useful, particularly with smooth-faced grips, are abrading that portion of the surface of the specimen that will be in the grips, and interposing thin pieces of abrasive cloth, abrasive paper, or plastic, or rubber-coated fabric, commonly called hospital sheeting, between the specimen and the grip surface. No. 80 double-sided abrasive paper has been found effective in many cases. An open-mesh fabric, in which the threads are coated with abrasive, has also been effective. Reducing the cross-sectional area of the specimen may also be effective. The use of special types of grips is sometimes necessary to eliminate slippage and breakage in the grips.

5.1.4 *Drive Mechanism*—A drive mechanism for imparting to the movable member a uniform, controlled velocity with respect to the stationary member, with this velocity to be regulated as specified in Section 8.

5.1.5 *Load Indicator*—A suitable load-indicating mechanism capable of showing the total tensile load carried by the test specimen when held by the grips. This mechanism shall be essentially free of inertia lag at the specified rate of testing and shall indicate the load with an accuracy of ±1 % of the indicated value, or better. The accuracy of the testing machine shall be verified in accordance with Practices E 4.

NOTE 7—Experience has shown that many testing machines now in use are incapable of maintaining accuracy for as long as the periods between inspection recommended in Practices E 4. Hence, it is recommended that each machine be studied individually and verified as often as may be found necessary. It frequently will be necessary to perform this function daily.

5.1.6 The fixed member, movable member, drive mechanism, and grips shall be constructed of such materials and in such proportions that the total elastic longitudinal strain of the system constituted by these parts does not exceed 1 % of the total longitudinal strain between the two gage marks on the test specimen at any time during the test and at any load up to the rated capacity of the machine.

5.2 *Extension Indicator* (extensometer)—A suitable instrument shall be used for determining the distance between two designated points within the gage length of the test specimen as the specimen is stretched. For referee purposes, the extensometer must be set at the full gage length of the specimen, as shown in Fig. 1. It is desirable, but not essential, that this instrument automatically record this distance, or any change in it, as a function of the load on the test specimen or of the elapsed time from the start of the test, or both. If only the latter is obtained, load-time data must also be taken. This instrument shall be essentially free of inertia at the specified speed of testing. Extensometers shall be classified and their calibration periodically verified in accordance with Practice E 83.

5.2.1 *Modulus-of-Elasticity Measurements*—For modulus-of-elasticity measurements, an extensometer with a maximum strain error of 0.0002 mm/mm (in./in.) that automatically and continuously records shall be used. An extensometer classified by Practice E 83 as fulfilling the requirements of a B-2 classification within the range of use for modulus measurements meets this requirement.

5.2.2 *Low-Extension Measurements*—For elongation-at-yield and low-extension measurements (nominally 20 % or less), the same above extensometer, attenuated to 20 % extension, may be used. In any case, the extensometer system must meet at least Class C (Practice E 83) requirements, which include a fixed strain error of 0.001 strain or ±1.0 % of the indicated strain, whichever is greater.

5.2.3 *High-Extension Measurements*—For making measurements at elongations greater than 20 %, measuring techniques with error no greater than ±10 % of the measured value are acceptable.

5.2.4 *Poisson's Ratio*—Bi-axial extensometer or axial and transverse extensometers capable of recording axial strain and transverse strain simultaneously. The extensometers shall be capable of measuring the change in strains with an accuracy of 1 % of the relevant value or better.

NOTE 8—Strain gages can be used as an alternative method to measure axial and transverse strain; however, proper techniques for mounting strain gages are crucial to obtaining accurate data. Consult strain gage suppliers for instruction and training in these special techniques.

5.3 *Micrometers*—Suitable micrometers for measuring the width and thickness of the test specimen to an incremental discrimination of at least 0.025 mm (0.001 in.) should be used. All width and thickness measurements of rigid and semirigid plastics may be measured with a hand micrometer with ratchet. A suitable instrument for measuring the thickness of nonrigid test specimens shall have: *(1)* a contact measuring pressure of 25 ± 2.5 kPa (3.6 ± 0.36 psi), *(2)* a movable circular contact foot 6.35 ± 0.025 mm (0.250 ± 0.001 in.) in diameter, and *(3)* a lower fixed anvil large enough to extend beyond the contact foot in all directions and being parallel to the contact foot within 0.005 mm (0.0002 in.) over the entire foot area. Flatness of the foot and anvil shall conform to Test Method D 5947.

5.3.1 An optional instrument equipped with a circular contact foot 15.88 ± 0.08 mm (0.625 ± 0.003 in.) in diameter is recommended for thickness measuring of process samples or larger specimens at least 15.88 mm in minimum width.

6. Test Specimens

6.1 *Sheet, Plate, and Molded Plastics*:

6.1.1 *Rigid and Semirigid Plastics*—The test specimen shall conform to the dimensions shown in Fig. 1. The Type I specimen is the preferred specimen and shall be used where sufficient material having a thickness of 7 mm (0.28 in.) or less is available. The Type II specimen may be used when a material does not break in the narrow section with the preferred Type I specimen. The Type V specimen shall be used where only limited material having a thickness of 4 mm (0.16 in.) or less is available for evaluation, or where a large number of specimens are to be exposed in a limited space (thermal and environmental stability tests, etc.). The Type IV specimen should be used when direct comparisons are required between materials in different rigidity cases (that is, nonrigid and semirigid). The Type III specimen must be used for all materials with a thickness of greater than 7 mm (0.28 in.) but not more than 14 mm (0.55 in.).

6.1.2 *Nonrigid Plastics*—The test specimen shall conform to the dimensions shown in Fig. 1. The Type IV specimen shall be used for testing nonrigid plastics with a thickness of 4 mm (0.16 in.) or less. The Type III specimen must be used for all materials with a thickness greater than 7 mm (0.28 in.) but not

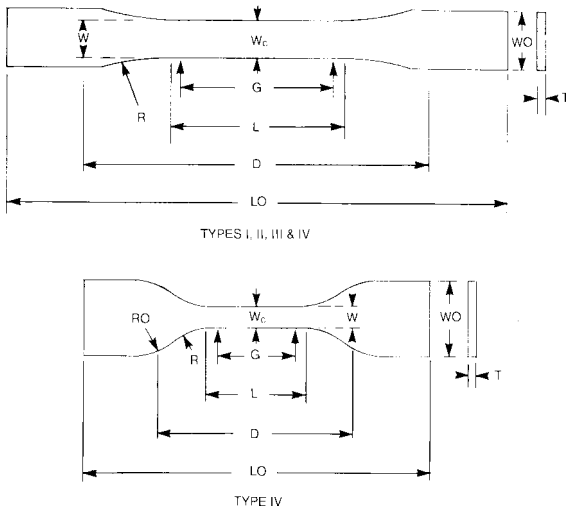

Specimen Dimensions for Thickness, *T*, mm (in.)[A]

Dimensions (see drawings)	7 (0.28) or under		Over 7 to 14 (0.28 to 0.55), incl	4 (0.16) or under		Tolerances
	Type I	Type II	Type III	Type IV[B]	Type V[C,D]	
W—Width of narrow section[E,F]	13 (0.50)	6 (0.25)	19 (0.75)	6 (0.25)	3.18 (0.125)	±0.5 (±0.02)[B,C]
L—Length of narrow section	57 (2.25)	57 (2.25)	57 (2.25)	33 (1.30)	9.53 (0.375)	±0.5 (±0.02)[C]
WO—Width overall, min[G]	19 (0.75)	19 (0.75)	29 (1.13)	19 (0.75)	...	+ 6.4 (+ 0.25)
WO—Width overall, min[G]	...	...	...	...	9.53 (0.375)	+ 3.18 (+ 0.125)
LO—Length overall, min[H]	165 (6.5)	183 (7.2)	246 (9.7)	115 (4.5)	63.5 (2.5)	no max (no max)
G—Gage length[I]	50 (2.00)	50 (2.00)	50 (2.00)	...	7.62 (0.300)	±0.25 (±0.010)[C]
G—Gage length[I]	...	...	...	25 (1.00)	...	±0.13 (±0.005)
D—Distance between grips	115 (4.5)	135 (5.3)	115 (4.5)	65 (2.5)[J]	25.4 (1.0)	±5 (±0.2)
R—Radius of fillet	76 (3.00)	76 (3.00)	76 (3.00)	14 (0.56)	12.7 (0.5)	±1 (±0.04)[C]
RO—Outer radius (Type IV)	...	...	...	25 (1.00)	...	±1 (±0.04)

[A] Thickness, *T*, shall be 3.2± 0.4 mm (0.13 ± 0.02 in.) for all types of molded specimens, and for other Types I and II specimens where possible. If specimens are machined from sheets or plates, thickness, *T*, may be the thickness of the sheet or plate provided this does not exceed the range stated for the intended specimen type. For sheets of nominal thickness greater than 14 mm (0.55 in.) the specimens shall be machined to 14 ± 0.4 mm (0.55 ± 0.02 in.) in thickness, for use with the Type III specimen. For sheets of nominal thickness between 14 and 51 mm (0.55 and 2 in.) approximately equal amounts shall be machined from each surface. For thicker sheets both surfaces of the specimen shall be machined, and the location of the specimen with reference to the original thickness of the sheet shall be noted. Tolerances on thickness less than 14 mm (0.55 in.) shall be those standard for the grade of material tested.

[B] For the Type IV specimen, the internal width of the narrow section of the die shall be 6.00 ± 0.05 mm (0.250± 0.002 in.). The dimensions are essentially those of Die C in Test Methods D 412.

[C] The Type V specimen shall be machined or die cut to the dimensions shown, or molded in a mold whose cavity has these dimensions. The dimensions shall be:
W = 3.18 ± 0.03 mm (0.125 ± 0.001 in.),
L = 9.53 ± 0.08 mm (0.375 ± 0.003 in.),
G = 7.62 ± 0.02 mm (0.300 ± 0.001 in.), and
R = 12.7 ± 0.08 mm (0.500 ± 0.003 in.).
The other tolerances are those in the table.

[D] Supporting data on the introduction of the L specimen of Test Method D 1822 as the Type V specimen are available from ASTM Headquarters. Request RR:D20-1038.

[E] The width at the center W_c shall be +0.00 mm, −0.10 mm (+0.000 in., −0.004 in.) compared with width *W* at other parts of the reduced section. Any reduction in *W* at the center shall be gradual, equally on each side so that no abrupt changes in dimension result.

[F] For molded specimens, a draft of not over 0.13 mm (0.005 in.) may be allowed for either Type I or II specimens 3.2 mm (0.13 in.) in thickness, and this should be taken into account when calculating width of the specimen. Thus a typical section of a molded Type I specimen, having the maximum allowable draft, could be as follows:

[G] Overall widths greater than the minimum indicated may be desirable for some materials in order to avoid breaking in the grips.

[H] Overall lengths greater than the minimum indicated may be desirable either to avoid breaking in the grips or to satisfy special test requirements.

[I] Test marks or initial extensometer span.

[J] When self-tightening grips are used, for highly extensible polymers, the distance between grips will depend upon the types of grips used and may not be critical if maintained uniform once chosen.

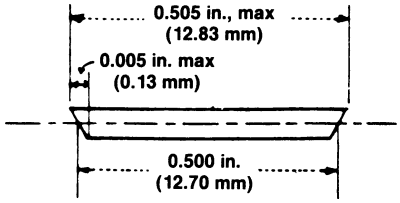

FIG. 1 Tension Test Specimens for Sheet, Plate, and Molded Plastics

more than 14 mm (0.55 in.).

6.1.3 *Reinforced Composites*—The test specimen for reinforced composites, including highly orthotropic laminates, shall conform to the dimensions of the Type I specimen shown in Fig. 1.

6.1.4 *Preparation*—Test specimens shall be prepared by machining operations, or die cutting, from materials in sheet, plate, slab, or similar form. Materials thicker than 14 mm (0.55 in.) must be machined to 14 mm (0.55 in.) for use as Type III

specimens. Specimens can also be prepared by molding the material to be tested.

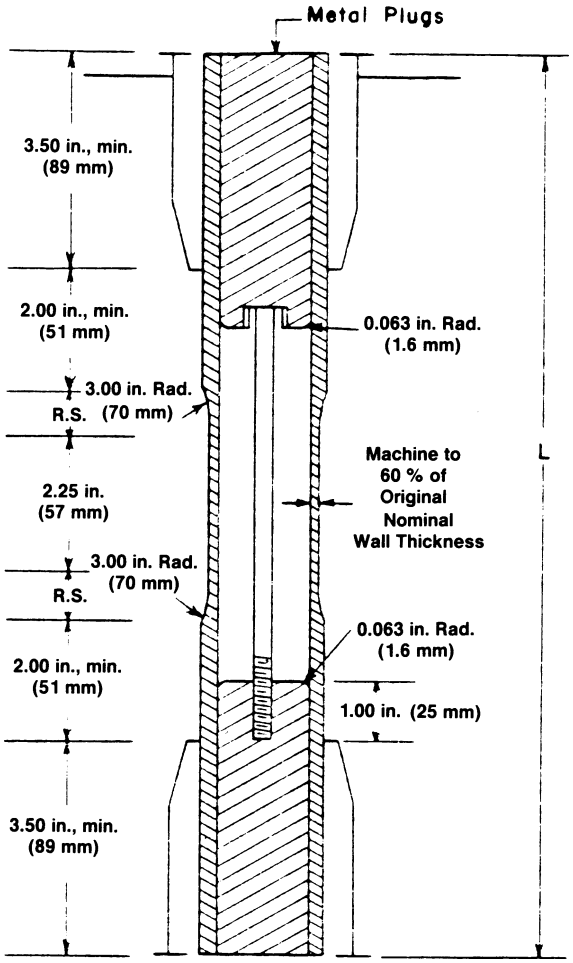

DIMENSIONS OF TUBE SPECIMENS

Nominal Wall Thickness	Length of Radial Sections, 2R.S.	Total Calculated Minimum Length of Specimen	Standard Length, *L*, of Specimen to Be Used for 89-mm (3.5-in.) Jaws[A]
	mm (in.)		
0.79 (1/32)	13.9 (0.547)	350 (13.80)	381 (15)
1.2 (3/64)	17.0 (0.670)	354 (13.92)	381 (15)
1.6 (1/16)	19.6 (0.773)	356 (14.02)	381 (15)
2.4 (3/32)	24.0 (0.946)	361 (14.20)	381 (15)
3.2 (1/8)	27.7 (1.091)	364 (14.34)	381 (15)
4.8 (3/16)	33.9 (1.333)	370 (14.58)	381 (15)
6.4 (1/4)	39.0 (1.536)	376 (14.79)	400 (15.75)
7.9 (5/16)	43.5 (1.714)	380 (14.96)	400 (15.75)
9.5 (3/8)	47.6 (1.873)	384 (15.12)	400 (15.75)
11.1 (7/16)	51.3 (2.019)	388 (15.27)	400 (15.75)
12.7 (1/2)	54.7 (2.154)	391 (15.40)	419 (16.5)

[A] For other jaws greater than 89 mm (3.5 in.), the standard length shall be increased by twice the length of the jaws minus 178 mm (7 in.). The standard length permits a slippage of approximately 6.4 to 12.7 mm (0.25 to 0.50 in.) in each jaw while maintaining the maximum length of the jaw grip.

FIG. 2 Diagram Showing Location of Tube Tension Test Specimens in Testing Machine

NOTE 9—Test results have shown that for some materials such as glass cloth, SMC, and BMC laminates, other specimen types should be considered to ensure breakage within the gage length of the specimen, as mandated by 7.3.

NOTE 10—When preparing specimens from certain composite laminates such as woven roving, or glass cloth, care must be exercised in cutting the specimens parallel to the reinforcement. The reinforcement will be significantly weakened by cutting on a bias, resulting in lower laminate properties, unless testing of specimens in a direction other than parallel with the reinforcement constitutes a variable being studied.

NOTE 11—Specimens prepared by injection molding may have different tensile properties than specimens prepared by machining or die-cutting because of the orientation induced. This effect may be more pronounced in specimens with narrow sections.

6.2 *Rigid Tubes*—The test specimen for rigid tubes shall be as shown in Fig. 2. The length, *L*, shall be as shown in the table in Fig. 2. A groove shall be machined around the outside of the specimen at the center of its length so that the wall section after machining shall be 60 % of the original nominal wall thickness. This groove shall consist of a straight section 57.2 mm (2.25 in.) in length with a radius of 76 mm (3 in.) at each end joining it to the outside diameter. Steel or brass plugs having diameters such that they will fit snugly inside the tube and having a length equal to the full jaw length plus 25 mm (1 in.) shall be placed in the ends of the specimens to prevent crushing. They can be located conveniently in the tube by separating and supporting them on a threaded metal rod. Details of plugs and test assembly are shown in Fig. 2.

6.3 *Rigid Rods*—The test specimen for rigid rods shall be as shown in Fig. 3. The length, *L*, shall be as shown in the table in Fig. 3. A groove shall be machined around the specimen at the center of its length so that the diameter of the machined portion shall be 60 % of the original nominal diameter. This groove shall consist of a straight section 57.2 mm (2.25 in.) in length with a radius of 76 mm (3 in.) at each end joining it to the outside diameter.

6.4 All surfaces of the specimen shall be free of visible flaws, scratches, or imperfections. Marks left by coarse machining operations shall be carefully removed with a fine file or abrasive, and the filed surfaces shall then be smoothed with abrasive paper (No. 00 or finer). The finishing sanding strokes shall be made in a direction parallel to the long axis of the test specimen. All flash shall be removed from a molded specimen, taking great care not to disturb the molded surfaces. In machining a specimen, undercuts that would exceed the dimensional tolerances shown in Fig. 1 shall be scrupulously avoided. Care shall also be taken to avoid other common machining errors.

6.5 If it is necessary to place gage marks on the specimen, this shall be done with a wax crayon or India ink that will not affect the material being tested. Gage marks shall not be scratched, punched, or impressed on the specimen.

6.6 When testing materials that are suspected of anisotropy, duplicate sets of test specimens shall be prepared, having their long axes respectively parallel with, and normal to, the suspected direction of anisotropy.

7. Number of Test Specimens

7.1 Test at least five specimens for each sample in the case of isotropic materials.

7.2 Test ten specimens, five normal to, and five parallel with, the principle axis of anisotropy, for each sample in the case of anisotropic materials.

7.3 Discard specimens that break at some obvious fortuitous

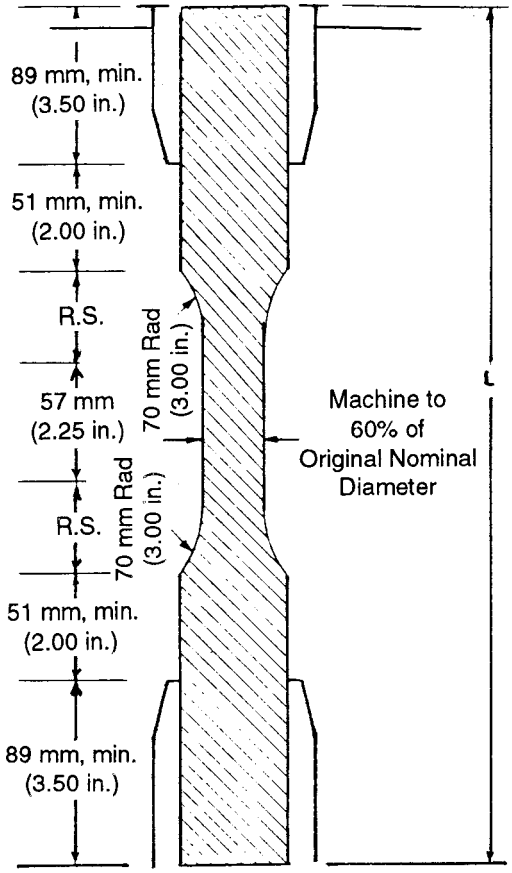

DIMENSIONS OF ROD SPECIMENS

Nominal Diameter	Length of Radial Sections, 2R.S.	Total Calculated Minimum Length of Specimen	Standard Length, *L*, of Specimen to Be Used for 89-mm (3½-in.) Jaws[A]
		mm (in.)	
3.2 (⅛)	19.6 (0.773)	356 (14.02)	381 (15)
4.7 (3/16)	24.0 (0.946)	361 (14.20)	381 (15)
6.4 (¼)	27.7 (1.091)	364 (14.34)	381 (15)
9.5 (⅜)	33.9 (1.333)	370 (14.58)	381 (15)
12.7 (½)	39.0 (1.536)	376 (14.79)	400 (15.75)
15.9 (⅝)	43.5 (1.714)	380 (14.96)	400 (15.75)
19.0 (¾)	47.6 (1.873)	384 (15.12)	400 (15.75)
22.2 (⅞)	51.5 (2.019)	388 (15.27)	400 (15.75)
25.4 (1)	54.7 (2.154)	391 (15.40)	419 (16.5)
31.8 (1¼)	60.9 (2.398)	398 (15.65)	419 (16.5)
38.1 (1½)	66.4 (2.615)	403 (15.87)	419 (16.5)
42.5 (1¾)	71.4 (2.812)	408 (16.06)	419 (16.5)
50.8 (2)	76.0 (2.993)	412 (16.24)	432 (17)

[A] For other jaws greater than 89 mm (3.5 in.), the standard length shall be increased by twice the length of the jaws minus 178 mm (7 in.). The standard length permits a slippage of approximately 6.4 to 12.7 mm (0.25 to 0.50 in.) in each jaw while maintaining the maximum length of the jaw grip.

FIG. 3 Diagram Showing Location of Rod Tension Test Specimen in Testing Machine

flaw, or that do not break between the predetermined gage marks, and make retests, unless such flaws constitute a variable to be studied.

101

NOTE 12—Before testing, all transparent specimens should be inspected in a polariscope. Those which show atypical or concentrated strain patterns should be rejected, unless the effects of these residual strains constitute a variable to be studied.

8. Speed of Testing

8.1 Speed of testing shall be the relative rate of motion of the grips or test fixtures during the test. The rate of motion of the driven grip or fixture when the testing machine is running idle may be used, if it can be shown that the resulting speed of testing is within the limits of variation allowed.

8.2 Choose the speed of testing from Table 1. Determine this chosen speed of testing by the specification for the material being tested, or by agreement between those concerned. When the speed is not specified, use the lowest speed shown in Table 1 for the specimen geometry being used, which gives rupture within ½ to 5-min testing time.

8.3 Modulus determinations may be made at the speed selected for the other tensile properties when the recorder response and resolution are adequate.

8.4 Poisson's ratio determinations shall be made at the same speed selected for modulus determinations.

9. Conditioning

9.1 *Conditioning*—Condition the test specimens at 23 ± 2°C (73.4 ± 3.6°F) and 50 ± 5 % relative humidity for not less than 40 h prior to test in accordance with Procedure A of Practice D 618, for those tests where conditioning is required. In cases of disagreement, the tolerances shall be± 1°C (1.8°F) and ±2 % relative humidity.

9.1.1 Note that for some hygroscopic materials, such as nylons, the material specifications (for example, Specification D 4066) call for testing "dry as-molded specimens." Such requirements take precedence over the above routine preconditioning to 50 % relative humidity and require sealing the specimens in water vapor-impermeable containers as soon as molded and not removing them until ready for testing.

9.2 *Test Conditions*—Conduct tests in the Standard Laboratory Atmosphere of 23 ± 2°C (73.4 ± 3.6°F) and 50 ± 5 % relative humidity, unless otherwise specified in the test methods. In cases of disagreement, the tolerances shall be ± 1°C (1.8°F) and ±2 % relative humidity.

TABLE 1 Designations for Speed of Testing[A]

Classification[B]	Specimen Type	Speed of Testing, mm/min (in./min)	Nominal Strain[C] Rate at Start of Test, mm/mm· min (in./in.·min)
Rigid and Semirigid	I, II, III rods and tubes	5 (0.2) ± 25 %	0.1
		50 (2) ± 10 %	1
		500 (20) ± 10 %	10
	IV	5 (0.2) ± 25 %	0.15
		50 (2) ± 10 %	1.5
		500 (20) ± 10 %	15
	V	1 (0.05) ± 25 %	0.1
		10 (0.5) ± 25 %	1
		100 (5)± 25 %	10
Nonrigid	III	50 (2) ± 10 %	1
		500 (20) ± 10 %	10
	IV	50 (2) ± 10 %	1.5
		500 (20) ± 10 %	15

[A] Select the lowest speed that produces rupture in ½ to 5 min for the specimen geometry being used (see 8.2).

[B] See Terminology D 883 for definitions.

[C] The initial rate of straining cannot be calculated exactly for dumbbell-shaped specimens because of extension, both in the reduced section outside the gage length and in the fillets. This initial strain rate can be measured from the initial slope of the tensile strain-versus-time diagram.

NOTE 13—The tensile properties of some plastics change rapidly with small changes in temperature. Since heat may be generated as a result of straining the specimen at high rates, conduct tests without forced cooling to ensure uniformity of test conditions. Measure the temperature in the reduced section of the specimen and record it for materials where self-heating is suspected.

10. Procedure

10.1 Measure the width and thickness of rigid flat specimens (Fig. 1) with a suitable micrometer to the nearest 0.025 mm (0.001 in.) at several points along their narrow sections. Measure the thickness of nonrigid specimens (produced by a Type IV die) in the same manner with the required dial micrometer. Take the width of this specimen as the distance between the cutting edges of the die in the narrow section. Measure the diameter of rod specimens, and the inside and outside diameters of tube specimens, to the nearest 0.025 mm (0.001 in.) at a minimum of two points 90° apart; make these measurements along the groove for specimens so constructed. Use plugs in testing tube specimens, as shown in Fig. 2.

TABLE 2 Modulus, 10^6 psi, for Eight Laboratories, Five Materials

	Mean	S_r	S_R	I_r	I_R
Polypropylene	0.210	0.0089	0.071	0.025	0.201
Cellulose acetate butyrate	0.246	0.0179	0.035	0.051	0.144
Acrylic	0.481	0.0179	0.063	0.051	0.144
Glass-reinforced nylon	1.17	0.0537	0.217	0.152	0.614
Glass-reinforced polyester	1.39	0.0894	0.266	0.253	0.753

10.2 Place the specimen in the grips of the testing machine, taking care to align the long axis of the specimen and the grips with an imaginary line joining the points of attachment of the grips to the machine. The distance between the ends of the gripping surfaces, when using flat specimens, shall be as indicated in Fig. 1. On tube and rod specimens, the location for the grips shall be as shown in Fig. 2 and Fig. 3. Tighten the grips evenly and firmly to the degree necessary to prevent slippage of the specimen during the test, but not to the point where the specimen would be crushed.

10.3 Attach the extension indicator. When modulus is being determined, a Class B-2 or better extensometer is required (see 5.2.1).

NOTE 14—Modulus of materials is determined from the slope of the linear portion of the stress-strain curve. For most plastics, this linear portion is very small, occurs very rapidly, and must be recorded automatically. The change in jaw separation is never to be used for calculating modulus or elongation.

10.3.1 *Poisson's Ratio Determination:*

10.3.1.1 When Poisson's ratio is determined, the speed of testing and the load range at which it is determined shall be the same as those used for modulus of elasticity.

10.3.1.2 Attach the transverse strain measuring device. The transverse strain measuring device must continuously measure the strain simultaneously with the axial strain measuring device.

10.3.1.3 Make simultaneous measurements of load and strain and record the data. The precision of the value of Poisson's ratio will depend on the number of data points of axial and transverse strain taken.

TABLE 3 Tensile Stress at Yield, 10^3 psi, for Eight Laboratories, Three Materials

	Mean	S_r	S_R	I_r	I_R
Polypropylene	3.63	0.022	0.161	0.062	0.456
Cellulose acetate butyrate	5.01	0.058	0.227	0.164	0.642
Acrylic	10.4	0.067	0.317	0.190	0.897

TABLE 4 Elongation at Yield, %, for Eight Laboratories, Three Materials

	Mean	S_r	S_R	I_r	I_R
Cellulose acetate butyrate	3.65	0.27	0.62	0.76	1.75
Acrylic	4.89	0.21	0.55	0.59	1.56
Polypropylene	8.79	0.45	5.86	1.27	16.5

10.4 Set the speed of testing at the proper rate as required in Section 8, and start the machine.

10.5 Record the load-extension curve of the specimen.

10.6 Record the load and extension at the yield point (if one exists) and the load and extension at the moment of rupture.

NOTE 15—If it is desired to measure both modulus and failure properties (yield or break, or both), it may be necessary, in the case of highly extensible materials, to run two independent tests. The high magnification extensometer normally used to determine properties up to the yield point may not be suitable for tests involving high extensibility. If allowed to remain attached to the specimen, the extensometer could be permanently damaged. A broad-range incremental extensometer or hand-rule technique may be needed when such materials are taken to rupture.

11. Calculation

11.1 *Tensile Strength*—Calculate the tensile strength by dividing the maximum load in newtons (or pounds-force) by the original minimum cross-sectional area of the specimen in square metres (or square inches). Express the result in pascals (or pounds-force per square inch) and report it to three significant figures as tensile strength at yield or tensile strength at break, whichever term is applicable. When a nominal yield or break load less than the maximum is present and applicable, it may be desirable also to calculate, in a similar manner, the corresponding tensile stress at yield or tensile stress at break and report it to three significant figures (see Note A2.8).

11.2 *Percent Elongation*—If the specimen gives a yield load that is larger than the load at break, calculate percent elongation at yield. Otherwise, calculate percent elongation at break. Do this by reading the extension (change in gage length) at the moment the applicable load is reached. Divide that extension by the original gage length and multiply by 100. Report percent elongation at yield or percent elongation at break to two significant figures. When a yield or breaking load less than the maximum is present and of interest, it is desirable to calculate and report both percent elongation at yield and percent elongation at break (see Note A2.2).

11.3 *Modulus of Elasticity*—Calculate the modulus of elasticity by extending the initial linear portion of the load-extension curve and dividing the difference in stress corresponding to any segment of section on this straight line by the corresponding difference in strain. All elastic modulus values shall be computed using the average initial cross-sectional area of the test specimens in the calculations. The result shall be expressed in pascals (pounds-force per square inch) and

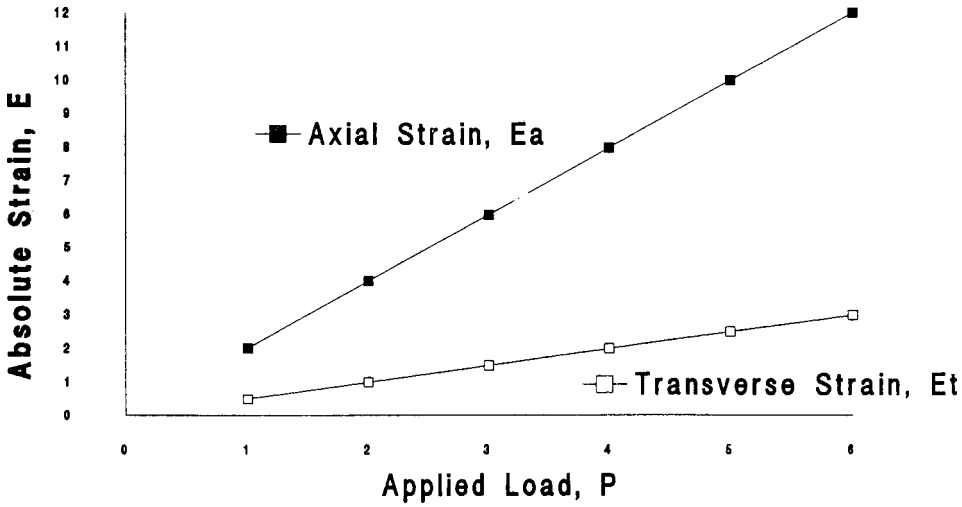

FIG. 4 Plot of Strains Versus Load for Determination of Poisson's Ratio

reported to three significant figures.

11.4 *Secant modulus*—At a designated strain, this shall be calculated by dividing the corresponding stress (nominal) by the designated strain. Elastic modulus values are preferable and shall be calculated whenever possible. However, for materials where no proportionality is evident, the secant value shall be calculated. Draw the tangent as directed in A1.3 and Fig. A1.2, and mark off the designated strain from the yield point where the tangent line goes through zero stress. The stress to be used in the calculation is then determined by dividing the load-extension curve by the original average cross-sectional area of the specimen.

11.5 *Poisson's Ratio*—The axial strain, ϵ_a, indicated by the axial extensometer, and the transverse strain, ϵ, indicated by the transverse extensometers, are plotted against the applied load, *P*, as shown in Fig. 4. A straight line is drawn through each set of points, and the slopes, $d\epsilon_a / dP$ and $d\epsilon_t / dP$, of these lines are determined. Poisson's ratio, μ, is then calculated as follows:

$$\mu = -(d\epsilon_t / dP)/(d\epsilon_a / dP) \quad (1)$$

where:
$d\epsilon_t$ = change in transverse strain,
$d\epsilon_a$ = change in axial strain, and
dP = change in applied load;
or

$$\mu = -(d\epsilon_t) / (d\epsilon_a) \quad (2)$$

11.5.1 The errors that may be introduced by drawing a straight line through the points can be reduced by applying the method of least squares.

11.6 For each series of tests, calculate the arithmetic mean of all values obtained and report it as the "average value" for the particular property in question.

11.7 Calculate the standard deviation (estimated) as follows and report it to two significant figures:

$$s = \sqrt{(\Sigma X^2 - n\bar{X}^2) / (n - 1)} \quad (3)$$

where:
s = estimated standard deviation,
X = value of single observation,
n = number of observations, and
$\bar{X}$ = arithmetic mean of the set of observations.

11.8 See Annex A1 for information on toe compensation.

TABLE 5 Tensile Strength at Break, 10^3 psi, for Eight Laboratories, Five Materials[A]

	Mean	S_r	S_R	I_r	I_R
Polypropylene	2.97	1.54	1.65	4.37	4.66
Cellulose acetate butyrate	4.82	0.058	0.180	0.164	0.509
Acrylic	9.09	0.452	0.751	1.27	2.13
Glass-reinforced polyester	20.8	0.233	0.437	0.659	1.24
Glass-reinforced nylon	23.6	0.277	0.698	0.784	1.98

[A] Tensile strength and elongation at break values obtained for unreinforced propylene plastics generally are highly variable due to inconsistencies in necking or "drawing" of the center section of the test bar. Since tensile strength and elongation at yield are more reproducible and relate in most cases to the practical usefulness of a molded part, they are generally recommended for specification purposes.

TABLE 6 Elongation at Break, %, for Eight Laboratories, Five Materials[A]

	Mean	S_r	S_R	I_r	I_R
Glass-reinforced polyester	3.68	0.20	2.33	0.570	6.59
Glass-reinforced nylon	3.87	0.10	2.13	0.283	6.03
Acrylic	13.2	2.05	3.65	5.80	10.3
Cellulose acetate butyrate	14.1	1.87	6.62	5.29	18.7
Polypropylene	293.0	50.9	119.0	144.0	337.0

[A] Tensile strength and elongation at break values obtained for unreinforced propylene plastics generally are highly variable due to inconsistencies in necking or "drawing" of the center section of the test bar. Since tensile strength and elongation at yield are more reproducible and relate in most cases to the practical usefulness of a molded part, they are generally recommended for specification purposes.

12. Report

12.1 Report the following information:

12.1.1 Complete identification of the material tested, including type, source, manufacturer's code numbers, form, principal dimensions, previous history, etc.,

12.1.2 Method of preparing test specimens,

12.1.3 Type of test specimen and dimensions,

12.1.4 Conditioning procedure used,

TABLE 7 Tensile Yield Strength, for Ten Laboratories, Eight Materials

Material	Test Speed, in./min	Values Expressed in psi Units				
		Average	S_r	S_R	r	R
LDPE	20	1544	52.4	64.0	146.6	179.3
LDPE	20	1894	53.1	61.2	148.7	171.3
LLDPE	20	1879	74.2	99.9	207.8	279.7
LLDPE	20	1791	49.2	75.8	137.9	212.3
LLDPE	20	2900	55.5	87.9	155.4	246.1
LLDPE	20	1730	63.9	96.0	178.9	268.7
HDPE	2	4101	196.1	371.9	549.1	1041.3
HDPE	2	3523	175.9	478.0	492.4	1338.5

12.1.5 Atmospheric conditions in test room,

12.1.6 Number of specimens tested,

12.1.7 Speed of testing,

12.1.8 Classification of extensometers used. A description of measuring technique and calculations employed instead of a minimum Class-C extensometer system,

12.1.9 Tensile strength at yield or break, average value, and standard deviation,

12.1.10 Tensile stress at yield or break, if applicable, average value, and standard deviation,

12.1.11 Percent elongation at yield or break, or both, as applicable, average value, and standard deviation,

12.1.12 Modulus of elasticity, average value, and standard deviation,

12.1.13 Date of test, and

12.1.14 Revision date of Test Method D 638.

13. Precision and Bias [12]

13.1 *Precision*—Tables 2-6 are based on a round-robin test conducted in 1984, involving five materials tested by eight laboratories using the Type I specimen, all of nominal 0.125-in. thickness. Each test result was based on five individual determinations. Each laboratory obtained two test results for each material.

TABLE 8 Tensile Yield Elongation, for Eight Laboratories, Eight Materials

Material	Test Speed, in./min	Values Expressed in Percent Units				
		Average	S_r	S_R	r	R
LDPE	20	17.0	1.26	3.16	3.52	8.84
LDPE	20	14.6	1.02	2.38	2.86	6.67
LLDPE	20	15.7	1.37	2.85	3.85	7.97
LLDPE	20	16.6	1.59	3.30	4.46	9.24
LLDPE	20	11.7	1.27	2.88	3.56	8.08
LLDPE	20	15.2	1.27	2.59	3.55	7.25
HDPE	2	9.27	1.40	2.84	3.91	7.94
HDPE	2	9.63	1.23	2.75	3.45	7.71

13.1.1 Tables 7-10 are based on a round-robin test conducted by the polyolefin subcommittee in 1988, involving eight polyethylene materials tested in ten laboratories. For each material, all samples were molded at one source, but the individual specimens were prepared at the laboratories that tested them. Each test result was the average of five individual determinations. Each laboratory obtained three test results for each material. Data from some laboratories could not be used for various reasons, and this is noted in each table.

TABLE 9 Tensile Break Strength, for Nine Laboratories, Six Materials

Material	Test Speed, in./min	Values Expressed in psi Units				
		Average	S_r	S_R	r	R
LDPE	20	1592	52.3	74.9	146.4	209.7
LDPE	20	1750	66.6	102.9	186.4	288.1
LLDPE	20	4379	127.1	219.0	355.8	613.3
LLDPE	20	2840	78.6	143.5	220.2	401.8
LLDPE	20	1679	34.3	47.0	95.96	131.6
LLDPE	20	2660	119.1	166.3	333.6	465.6

TABLE 10 Tensile Break Elongation, for Nine Laboratories, Six Materials

Material	Test Speed, in./min	Values Expressed in Percent Units				
		Average	S_r	S_R	r	R
LDPE	20	567	31.5	59.5	88.2	166.6
LDPE	20	569	61.5	89.2	172.3	249.7
LLDPE	20	890	25.7	113.8	71.9	318.7
LLDPE	20	64.4	6.68	11.7	18.7	32.6
LLDPE	20	803	25.7	104.4	71.9	292.5
LLDPE	20	782	41.6	96.7	116.6	270.8

13.1.2 In Tables 2-10, for the materials indicated, and for test results that derived from testing five specimens:

13.1.2.1 S_r is the within-laboratory standard deviation of the average; $I_r = 2.83\ S_r$. (See 13.1.2.3 for application of I_r.)

13.1.2.2 S_R is the between-laboratory standard deviation of the average; $I_R = 2.83\ S_R$. (See 13.1.2.4 for application of I_R.)

13.1.2.3 *Repeatability*—In comparing two test results for the same material, obtained by the same operator using the same equipment on the same day, those test results should be judged not equivalent if they differ by more than the I_r value for that material and condition.

13.1.2.4 *Reproducibility*—In comparing two test results for the same material, obtained by different operators using different equipment on different days, those test results should be judged not equivalent if they differ by more than the I_R value for that material and condition. (This applies between different laboratories or between different equipment within the same laboratory.)

13.1.2.5 Any judgment in accordance with 13.1.2.3 and 13.1.2.4 will have an approximate 95 % (0.95) probability of being correct.

13.1.2.6 Other formulations may give somewhat different results.

13.1.2.7 For further information on the methodology used in this section, see Practice E 691.

13.1.2.8 The precision of this test method is very dependent upon the uniformity of specimen preparation, standard practices for which are covered in other documents.

13.2 *Bias*—There are no recognized standards on which to base an estimate of bias for this test method.

14. Keywords

14.1 modulus of elasticity; percent elongation; plastics;

[12] Supporting data are available from ASTM Headquarters. Request RR:D20-1125 for the 1984 round robin and RR:D20-1170 for the 1988 round robin.

tensile properties; tensile strength

ANNEXES

(Mandatory Information)

A1. TOE COMPENSATION

A1.1 In a typical stress-strain curve (Fig. A1.1) there is a toe region, *AC*, that does not represent a property of the material. It is an artifact caused by a takeup of slack and alignment or seating of the specimen. In order to obtain correct values of such parameters as modulus, strain, and offset yield point, this artifact must be compensated for to give the corrected zero point on the strain or extension axis.

A1.2 In the case of a material exhibiting a region of-Hookean (linear) behavior (Fig. A1.1), a continuation of the linear (*CD*) region of the curve is constructed through the zero-stress axis. This intersection (*B*) is the corrected zero-strain point from which all extensions or strains must be measured, including the yield offset (*BE*), if applicable. The elastic modulus can be determined by dividing the stress at any point along the line *CD* (or its extension) by the strain at the same point (measured from Point *B*, defined as zero-strain).

A1.3 In the case of a material that does not exhibit any linear region (Fig. A1.2), the same kind of toe correction of the zero-strain point can be made by constructing a tangent to the maximum slope at the inflection point (*H′*). This is extended to intersect the strain axis at Point *B′*, the corrected zero-strain point. Using Point *B′* as zero strain, the stress at any point (*G′*) on the curve can be divided by the strain at that point to obtain a secant modulus (slope of Line *B′ G′*). For those materials with no linear region, any attempt to use the tangent through the inflection point as a basis for determination of an offset yield point may result in unacceptable error.

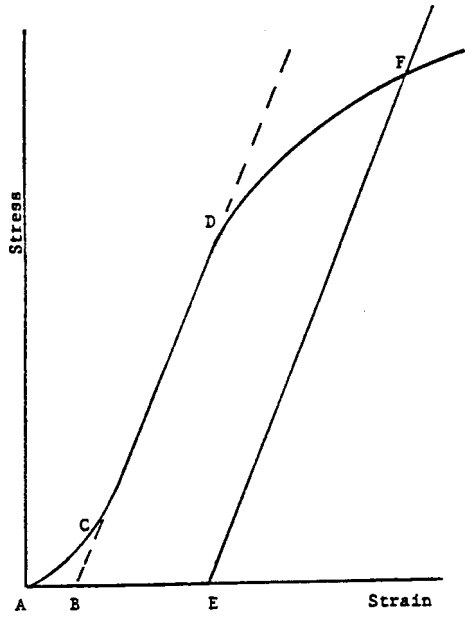

NOTE 1—Some chart recorders plot the mirror image of this graph.

FIG. A1.1 Material with Hookean Region

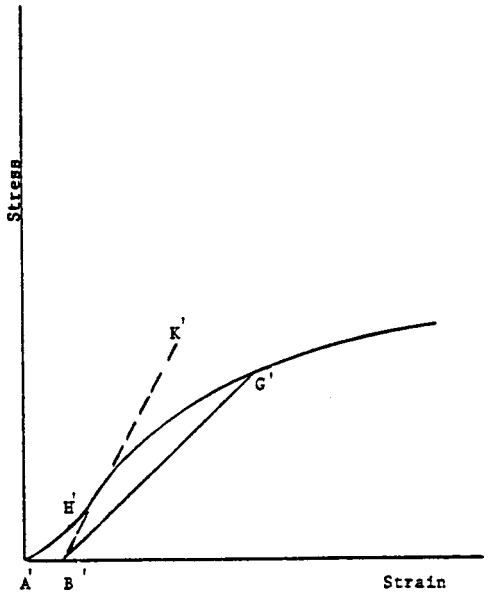

NOTE 1—Some chart recorders plot the mirror image of this graph.

FIG. A1.2 Material with No Hookean Region

A2. DEFINITIONS OF TERMS AND SYMBOLS RELATING TO TENSION TESTING OF PLASTICS

A2.1 *elastic limit*—the greatest stress which a material is capable of sustaining without any permanent strain remaining upon complete release of the stress. It is expressed in force per unit area, usually pounds-force per square inch (megapascals).

NOTE A2.1—Measured values of proportional limit and elastic limit vary greatly with the sensitivity and accuracy of the testing equipment, eccentricity of loading, the scale to which the stress-strain diagram is plotted, and other factors. Consequently, these values are usually replaced by yield strength.

A2.2 *elongation*—the increase in length produced in the gage length of the test specimen by a tensile load. It is expressed in units of length, usually inches (millimetres). (Also known as *extension*.)

NOTE A2.2—Elongation and strain values are valid only in cases where

uniformity of specimen behavior within the gage length is present. In the case of materials exhibiting necking phenomena, such values are only of qualitative utility after attainment of yield point. This is due to inability to ensure that necking will encompass the entire length between the gage marks prior to specimen failure.

A2.3 *gage length*—the original length of that portion of the specimen over which strain or change in length is determined.

A2.4 *modulus of elasticity*—the ratio of stress (nominal) to corresponding strain below the proportional limit of a material. It is expressed in force per unit area, usually megapascals (pounds-force per square inch). (Also known as *elastic modulus* or *Young's modulus*).

NOTE A2.3—The stress-strain relations of many plastics do not conform to Hooke's law throughout the elastic range but deviate therefrom even at stresses well below the elastic limit. For such materials the slope of the tangent to the stress-strain curve at a low stress is usually taken as the modulus of elasticity. Since the existence of a true proportional limit in plastics is debatable, the propriety of applying the term "modulus of elasticity" to describe the stiffness or rigidity of a plastic has been seriously questioned. The exact stress-strain characteristics of plastic materials are very dependent on such factors as rate of stressing, temperature, previous specimen history, etc. However, such a value is useful if its arbitrary nature and dependence on time, temperature, and other factors are realized.

A2.5 *necking*—the localized reduction in cross section which may occur in a material under tensile stress.

A2.6 *offset yield strength*—the stress at which the strain exceeds by a specified amount (the offset) an extension of the initial proportional portion of the stress-strain curve. It is expressed in force per unit area, usually megapascals (pounds-force per square inch).

NOTE A2.4—This measurement is useful for materials whose stress-strain curve in the yield range is of gradual curvature. The offset yield strength can be derived from a stress-strain curve as follows (Fig. A2.1):

On the strain axis lay off *OM* equal to the specified offset.

Draw *OA* tangent to the initial straight-line portion of the stress-strain curve.

Through *M* draw a line *MN* parallel to *OA* and locate the intersection of *MN* with the stress-strain curve.

The stress at the point of intersection *r* is the "offset yield strength." The specified value of the offset must be stated as a percent of the original gage length in conjunction with the strength value. *Example:* 0.1 % offset yield strength = ... MPa (psi), or yield strength at 0.1 % offset ... MPa (psi).

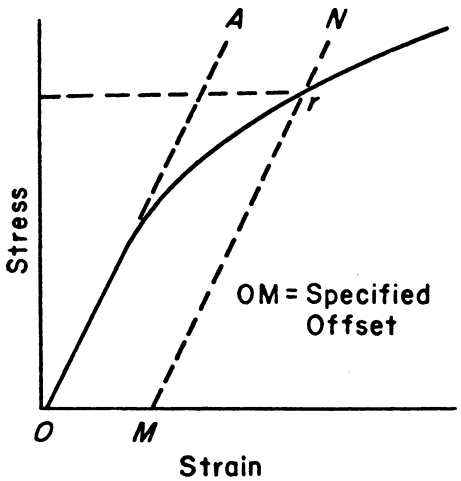

FIG. A2.1 Offset Yield Strength

A2.7 *percent elongation*—the elongation of a test specimen expressed as a percent of the gage length.

A2.8 *percent elongation at break and yield:*

A2.8.1 *percent elongation at break*

the percent elongation at the moment of rupture of the test specimen.

A2.8.2 *percent elongation at yield*

the percent elongation at the moment the yield point (A2.21) is attained in the test specimen.

A2.9 *percent reduction of area (nominal)*—the difference between the original cross-sectional area measured at the point of rupture after breaking and after all retraction has ceased, expressed as a percent of the original area.

A2.10 *percent reduction of area (true)*—the difference between the original cross-sectional area of the test specimen and the minimum cross-sectional area within the gage boundaries prevailing at the moment of rupture, expressed as a percentage of the original area.

A2.11 *proportional limit*—the greatest stress which a material is capable of sustaining without any deviation from proportionality of stress to strain (Hooke's law). It is expressed in force per unit area, usually megapascals (pounds-force per square inch).

A2.12 *rate of loading*—the change in tensile load carried by the specimen per unit time. It is expressed in force per unit time, usually newtons (pounds-force) per minute. The initial rate of loading can be calculated from the initial slope of the load versus time diagram.

A2.13 *rate of straining*—the change in tensile strain per unit time. It is expressed either as strain per unit time, usually metres per metre (inches per inch) per minute, or percent elongation per unit time, usually percent elongation per minute. The initial rate of straining can be calculated from the initial slope of the tensile strain versus time diagram.

NOTE A2.5—The initial rate of straining is synonymous with the rate of crosshead movement divided by the initial distance between crossheads only in a machine with constant rate of crosshead movement and when the specimen has a uniform original cross section, does not "neck down," and does not slip in the jaws.

A2.14 *rate of stressing (nominal)*—the change in tensile stress (nominal) per unit time. It is expressed in force per unit area per unit time, usually megapascals (pounds-force per square inch) per minute. The initial rate of stressing can be calculated from the initial slope of the tensile stress (nominal) versus time diagram.

NOTE A2.6—The initial rate of stressing as determined in this manner has only limited physical significance. It does, however, roughly describe the average rate at which the initial stress (nominal) carried by the test specimen is applied. It is affected by the elasticity and flow characteristics of the materials being tested. At the yield point, the rate of stressing (true) may continue to have a positive value if the cross-sectional area is decreasing.

A2.15 *secant modulus*—the ratio of stress (nominal) to corresponding strain at any specified point on the stress-strain curve. It is expressed in force per unit area, usually megapascals (pounds-force per square inch), and reported together with the specified stress or strain.

NOTE A2.7—This measurement is usually employed in place of modulus of elasticity in the case of materials whose stress-strain diagram does not demonstrate proportionality of stress to strain.

A2.16 *strain*—the ratio of the elongation to the gage length of the test specimen, that is, the change in length per unit of original length. It is expressed as a dimensionless ratio.

A2.17 *tensile strength (nominal)*—the maximum tensile stress (nominal) sustained by the specimen during a tension test. When the maximum stress occurs at the yield point (A2.21), it shall be designated tensile strength at yield. When the maximum stress occurs at break, it shall be designated tensile strength at break.

A2.18 *tensile stress (nominal)*—the tensile load per unit area of minimum original cross section, within the gage boundaries, carried by the test specimen at any given moment. It is expressed in force per unit area, usually megapascals (pounds-force per square inch).

NOTE A2.8—The expression of tensile properties in terms of the minimum original cross section is almost universally used in practice. In the case of materials exhibiting high extensibility or necking, or both (A2.15), nominal stress calculations may not be meaningful beyond the yield point (A2.21) due to the extensive reduction in cross-sectional area that ensues. Under some circumstances it may be desirable to express the tensile properties per unit of minimum prevailing cross section. These properties are called true tensile properties (that is, true tensile stress, etc.).

A2.19 *tensile stress-strain curve*—a diagram in which values of tensile stress are plotted as ordinates against corresponding values of tensile strain as abscissas.

A2.20 *true strain* (see Fig. A2.2) is defined by the following equation for ϵ_T:

$$\epsilon_T = \int_{L_o}^{L} dL/L = \ln L/L_o \qquad (A2.1)$$

where:

dL = increment of elongation when the distance between the gage marks is L,
L_o = original distance between gage marks, and
L = distance between gage marks at any time.

A2.21 *yield point*—the first point on the stress-strain curve at which an increase in strain occurs without an increase in stress (Fig. A2.2).

NOTE A2.9—Only materials whose stress-strain curves exhibit a point of zero slope may be considered as having a yield point.

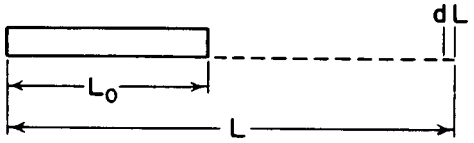

FIG. A2.2 Illustration of True Strain Equation

NOTE A2.10—Some materials exhibit a distinct "break" or discontinuity in the stress-strain curve in the elastic region. This break is not a yield point by definition. However, this point may prove useful for material characterization in some cases.

A2.22 *yield strength*—the stress at which a material exhibits a specified limiting deviation from the proportionality of stress to strain. Unless otherwise specified, this stress will be the stress at the yield point and when expressed in relation to the tensile strength shall be designated either tensile strength at yield or tensile stress at yield as required in A2.17 (Fig. A2.3). (See *offset yield strength.*)

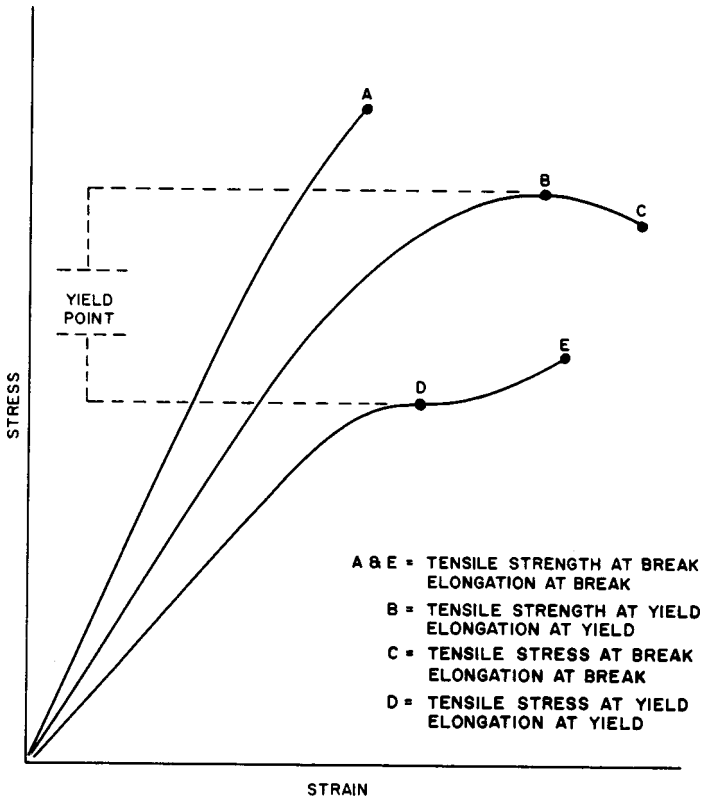

FIG. A2.3 Tensile Designations

A2.23 *Symbols*—The following symbols may be used for the above terms:

Symbol	Term
W	Load
ΔW	Increment of load
L	Distance between gage marks at any time
L_o	Original distance between gage marks
L_u	Distance between gage marks at moment of rupture
ΔL	Increment of distance between gage marks = elongation
A	Minimum cross-sectional area at any time
A_o	Original cross-sectional area
ΔA	Increment of cross-sectional area
A_u	Cross-sectional area at point of rupture measured after breaking specimen
A_T	Cross-sectional area at point of rupture, measured at the moment of rupture
t	Time
Δt	Increment of time
σ	Tensile stress
$\Delta\sigma$	Increment of stress
σ_T	True tensile stress
σ_U	Tensile strength at break (nominal)
σ_{UT}	Tensile strength at break (true)
ϵ	Strain
$\Delta\epsilon$	Increment of strain
ϵ_U	Total strain, at break
ϵ_T	True strain
%El	Percentage elongation
Y.P.	Yield point
E	Modulus of elasticity

A2.24 Relations between these various terms may be defined as follows:

$\sigma = W/A_o$
$\sigma_T = W/A$
$\sigma_U = W/A_o$ (where W is breaking load)
$\sigma_{UT} = W/A_T$ (where W is breaking load)
$\epsilon = \Delta L/L_o = (L - L_o)/L_o$
$\epsilon_U = (L_u - L_o)/L_o$
$\epsilon_T = \int_{L_o}^{L} dL/L = \ln L/L_o$
%$El = [(L - L_o)/L_o] \times 100 = \epsilon \times 100$

Percent reduction of area (nominal) = $[(A_o - A_u)/A_o] \times 100$
Percent reduction of area (true) = $[(A_o - A_T)/A_o] \times 100$
Rate of loading = $\Delta W/\Delta t$
Rate of stressing (nominal) = $\Delta\sigma/\Delta = (\Delta W]/A_o)/\Delta t$
Rate of straining = $\Delta\epsilon/\Delta t = (\Delta L/L_o)\Delta t$

For the case where the volume of the test specimen does not change during the test, the following three relations hold:

$$\sigma_T = \sigma(1 + \epsilon) = \sigma L/L_o \quad \text{(A2.2)}$$
$$\sigma_{UT} = \sigma_U(1 + \epsilon_U) = \sigma_U L_u/L_o$$
$$A = A_o/(1 + \epsilon)$$

SUMMARY OF CHANGES

This section identifies the location of selected changes to this test method. For the convenience of the user, Committee D-20 has highlighted those changes that may impact the use of this test method. This section may also include descriptions of the changes or reasons for the changes, or both.

D 638–98:
(1) Revised 10.3 and added 12.1.8 to clarify extensometer usage.
(2) Added 12.1.14.
(3) Replaced reference to Test Methods D 374 with Test Method D 5947 in 2.1 and 5.3.
D 638–99:
(1) Added and clarified extensometer classification requirements.

Appendix B

Stress-strain data for the composites

.

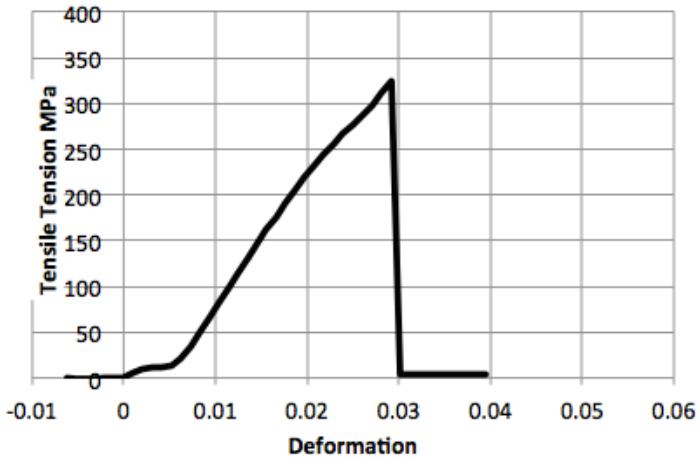

Figure B.1: A stress/deformation chart - sample 2 series 1

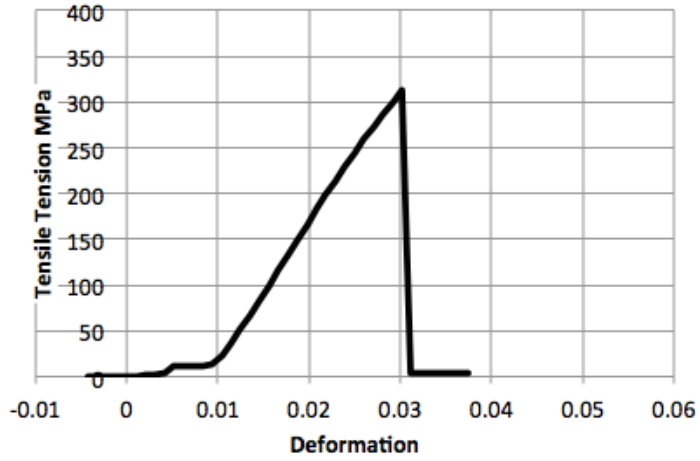

Figure B.2: A stress/deformation chart - sample 10 series 1

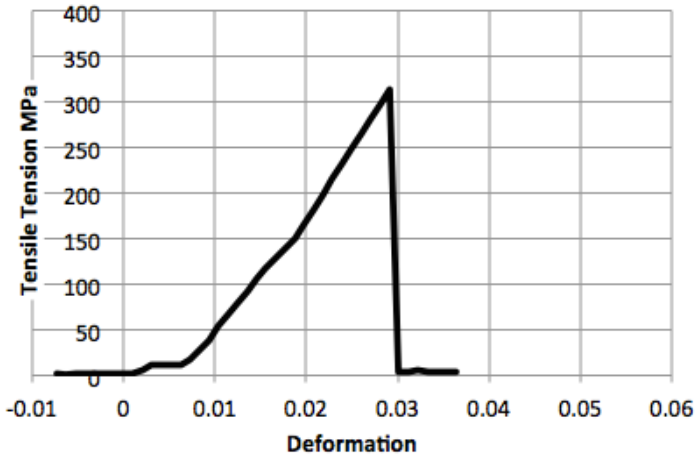

Figure B.3: A stress/deformation chart - sample 11 series 1

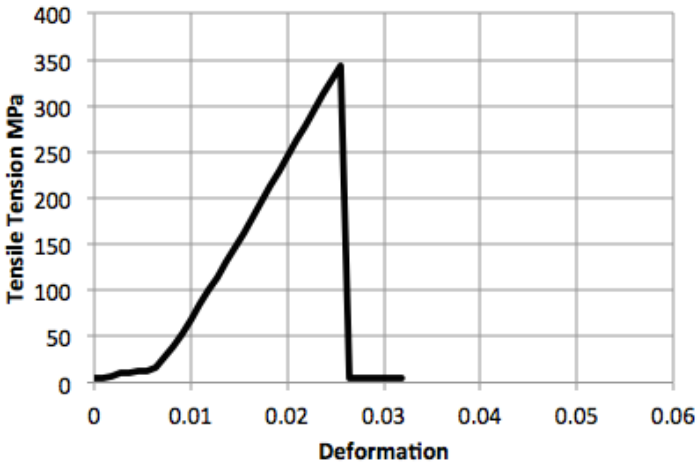

Figure B.4: A stress/deformation chart - sample 13 series 1

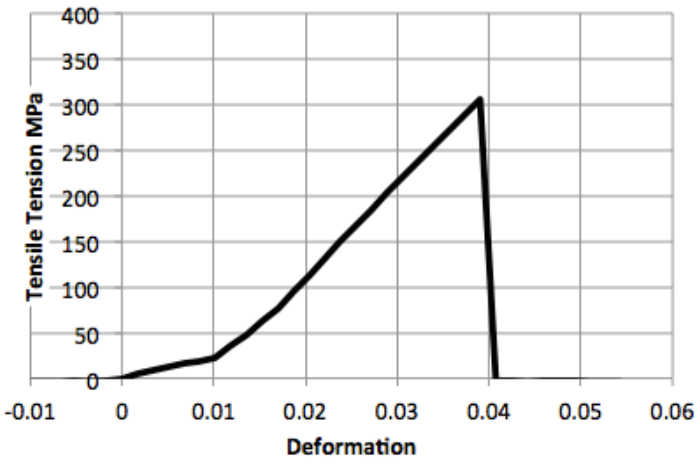

Figure B.5: A stress/deformation chart - sample 1 series 2

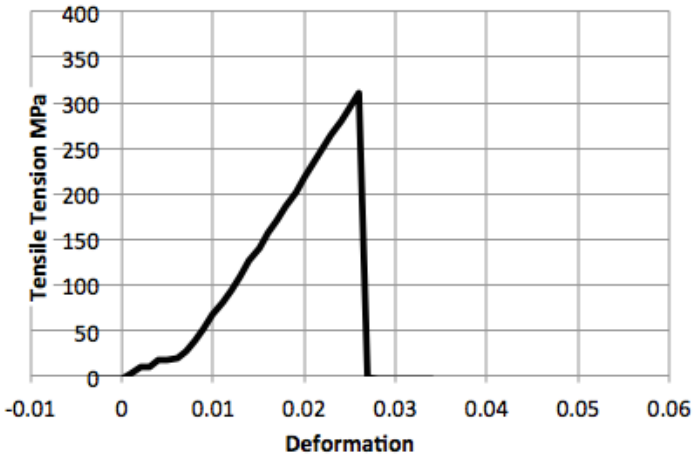

Figure B.6: A stress/deformation chart - sample 7 series 2

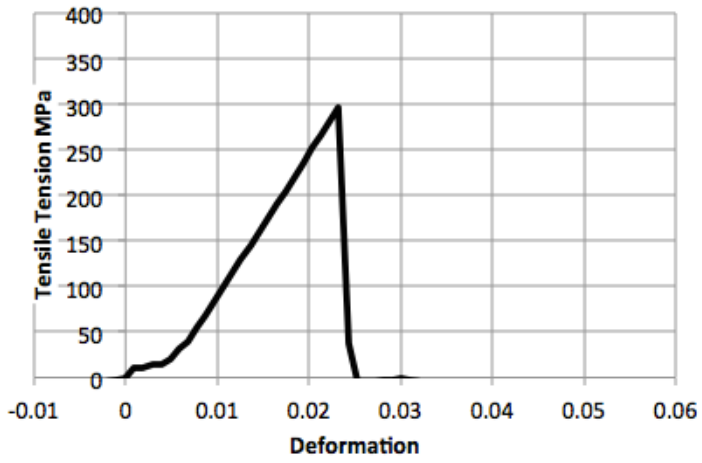

Figure B.7: A stress/deformation chart - sample 12 series 2

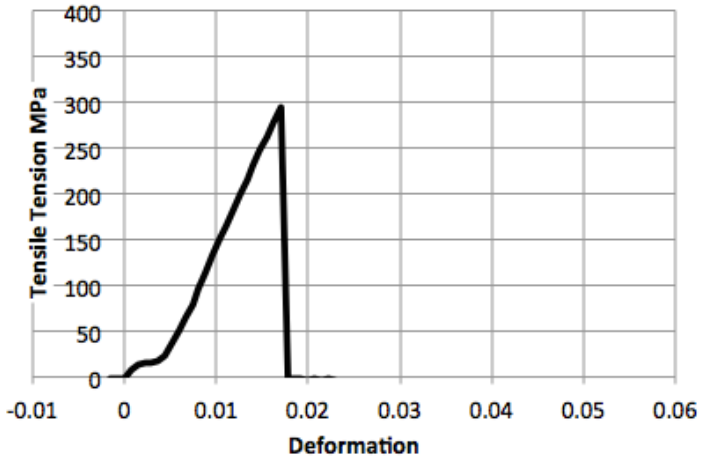

Figure B.8: A stress/deformation chart - sample 14 series 2

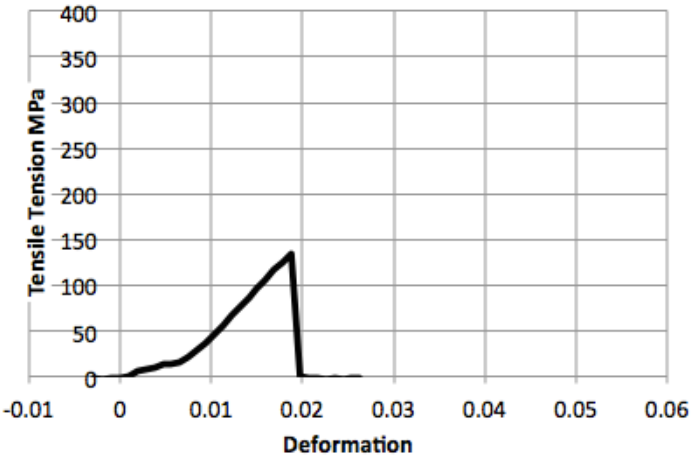

Figure B.9: A stress/deformation chart - sample 1 series 3

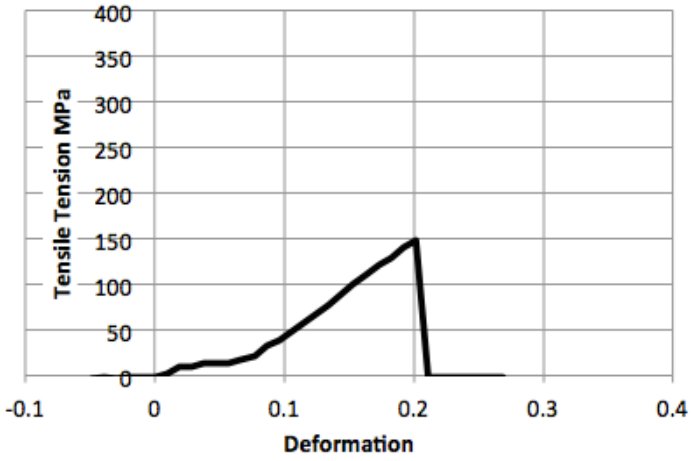

Figure B.10: A stress/deformation chart - sample 5 series 3

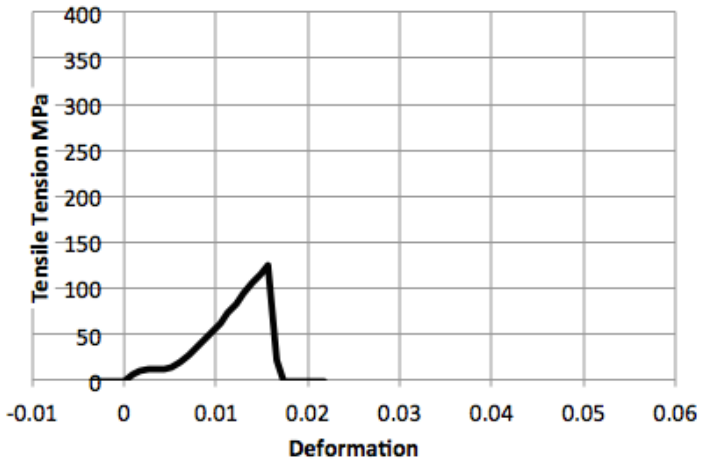

Figure B.11: A stress/deformation chart - sample 12 series 3

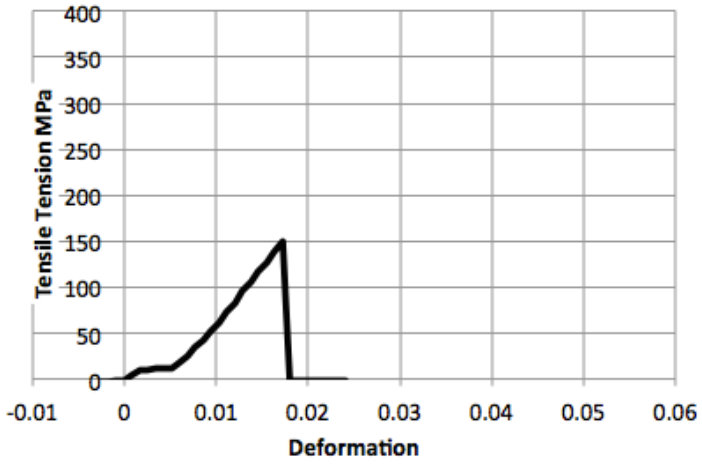

Figure B.12: A stress/deformation chart - sample 15 series 3

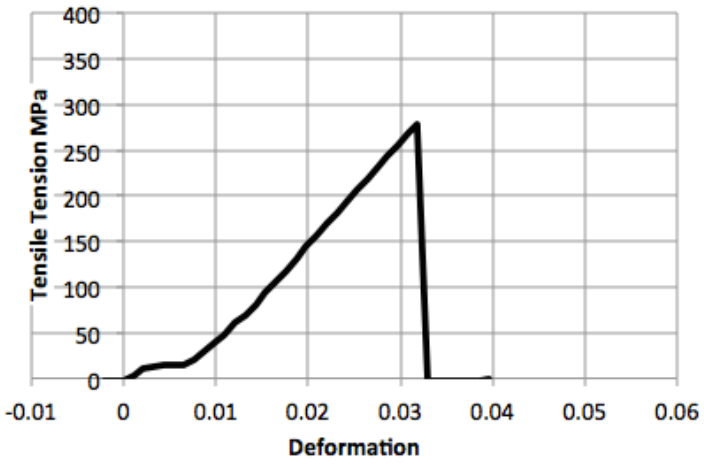

Figure B.13: A stress/deformation chart - sample 4 series 4

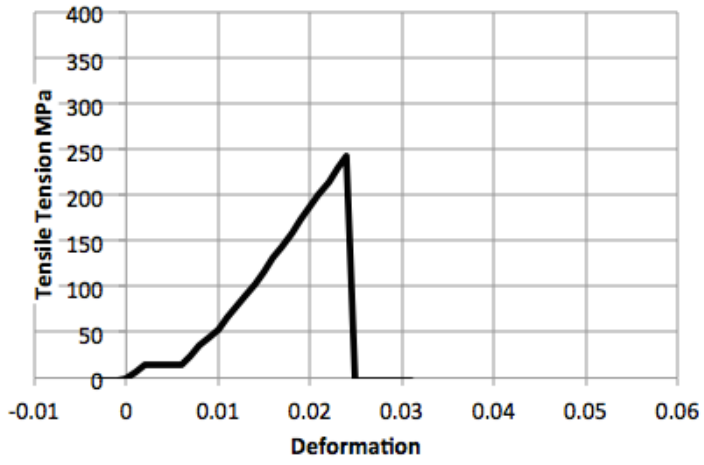

Figure B.14: A stress/deformation chart - sample 6 series 4

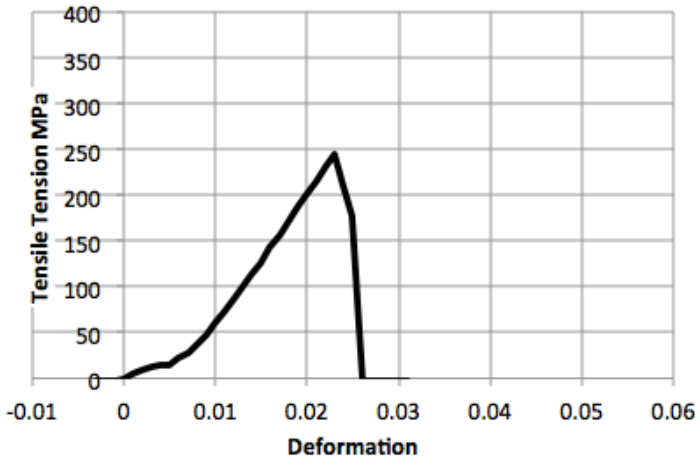

Figure B.15: A stress/deformation chart - sample 13 series 4

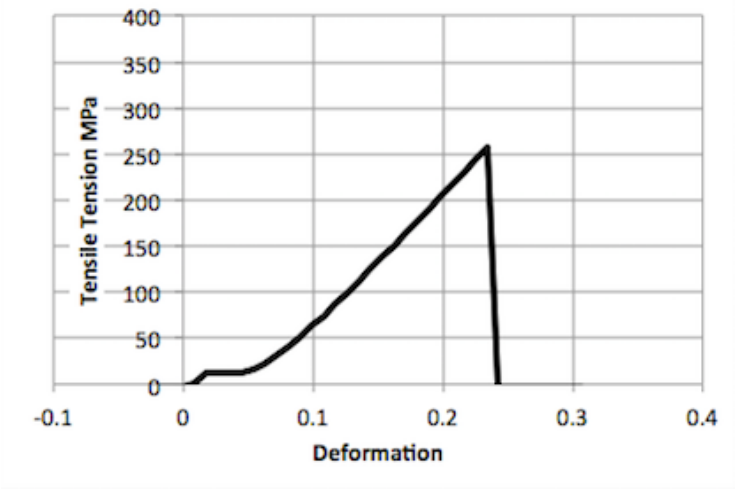

Figure B.16: A stress/deformation chart - sample 15 series 4

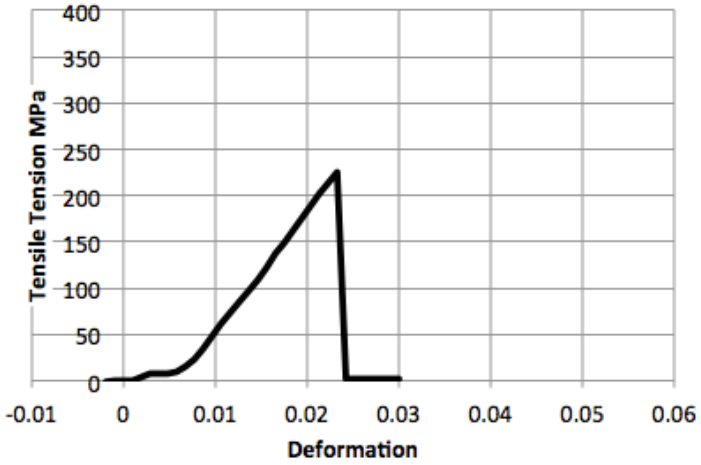

Figure B.17: A stress/deformation chart - sample 4 series 6

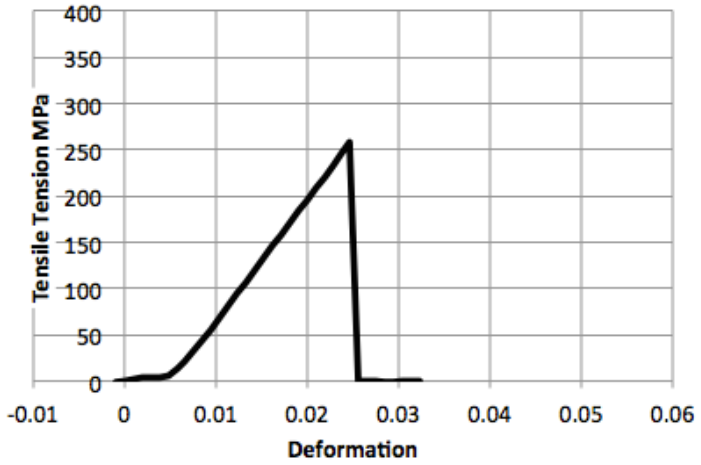

Figure B.18: A stress/deformation chart - sample 10 series 6

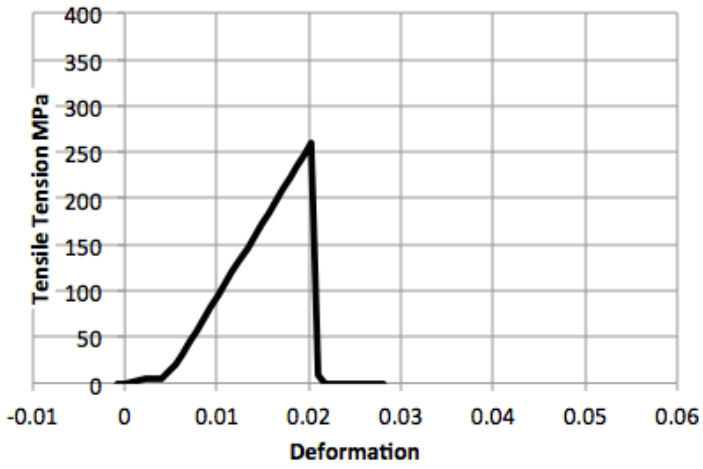

Figure B.19: A stress/deformation chart - sample 12 series 6

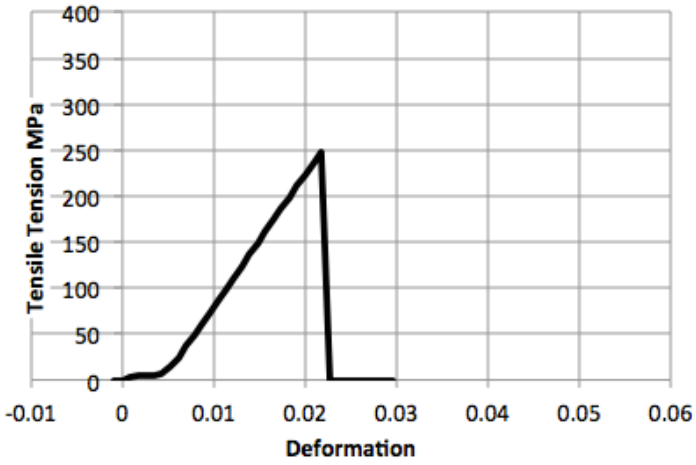

Figure B.20: A stress/deformation chart - sample 13 series 6

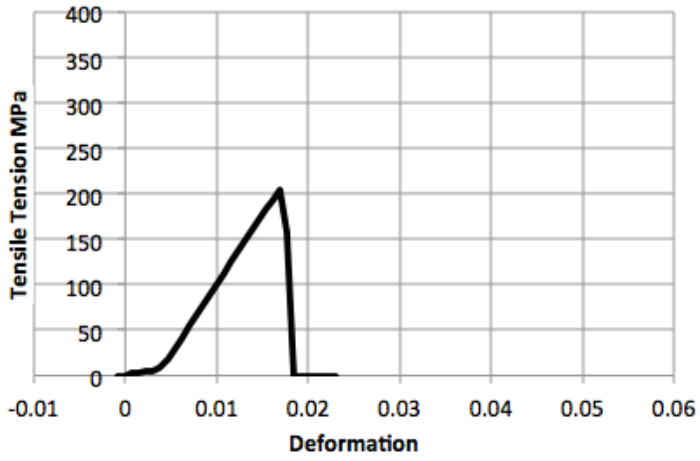

Figure B.21: A stress/deformation chart - sample 6 series 7

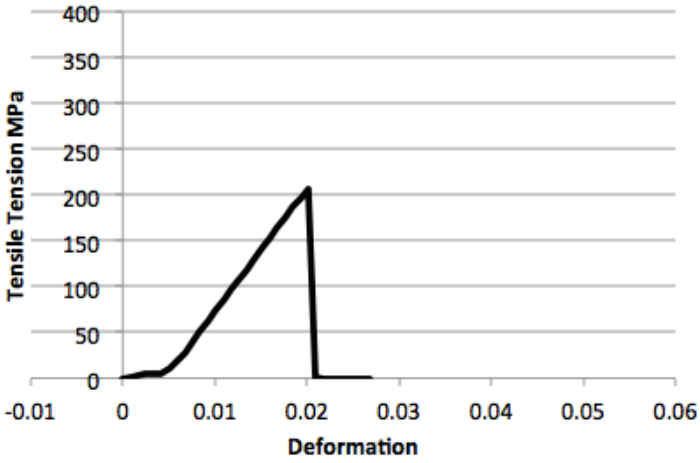

Figure B.22: A stress/deformation chart - sample 7 series 7

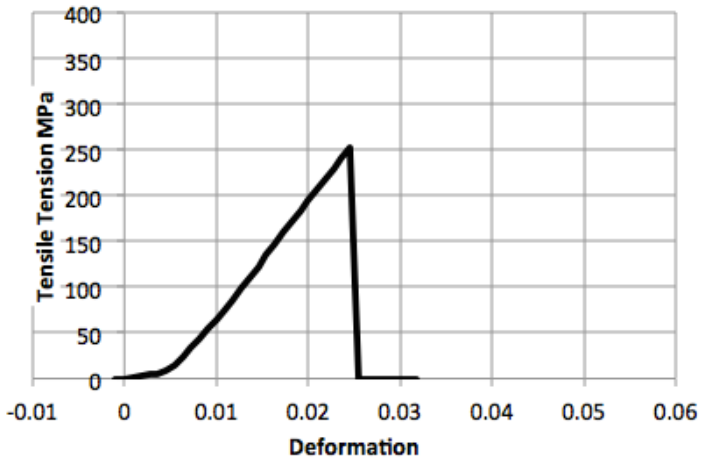

Figure B.23: A stress/deformation chart - sample 10 series 7

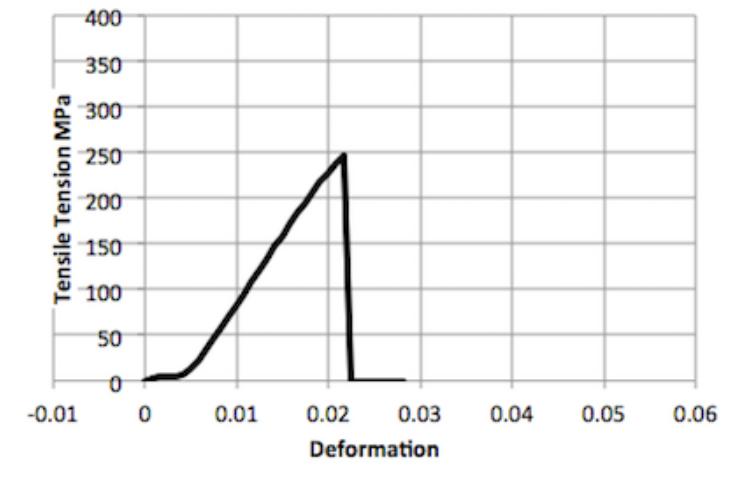

Figure B.24: A stress/deformation chart - sample 13 series 7

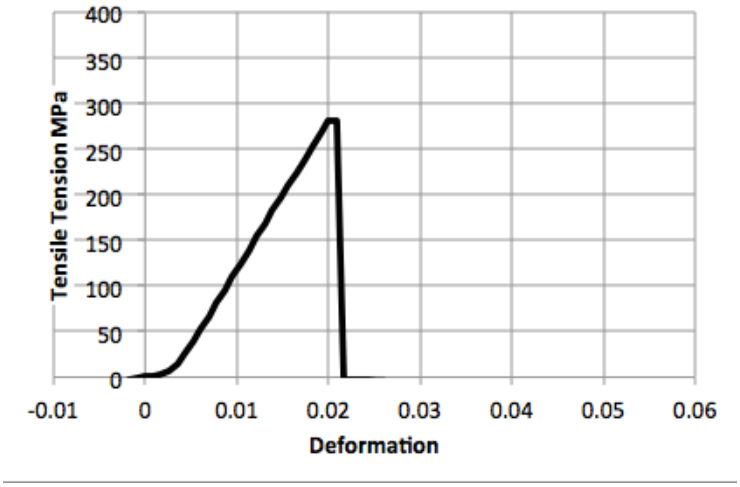

Figure B.25: A stress/deformation chart - sample 1 series 8

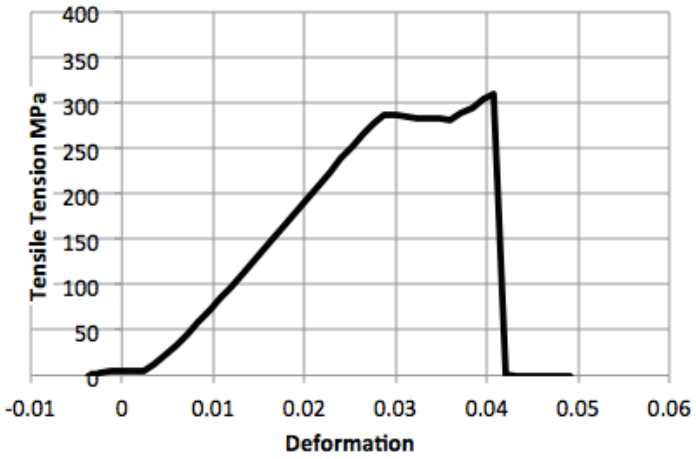

Figure B.26: A stress/deformation chart - sample 11 series 8

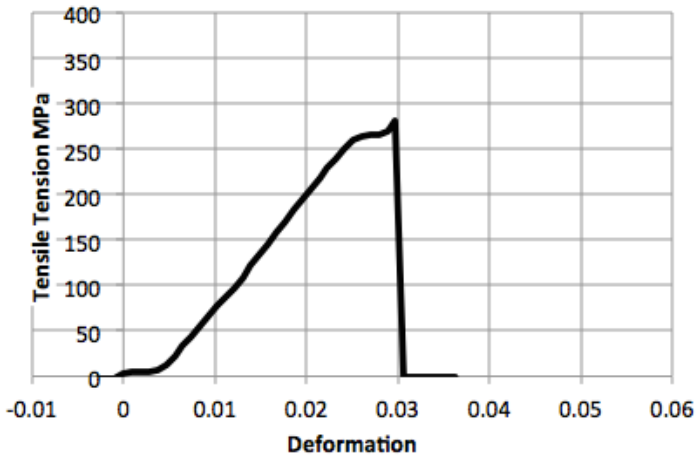

Figure B.27: A stress/deformation chart - sample 12 series 8

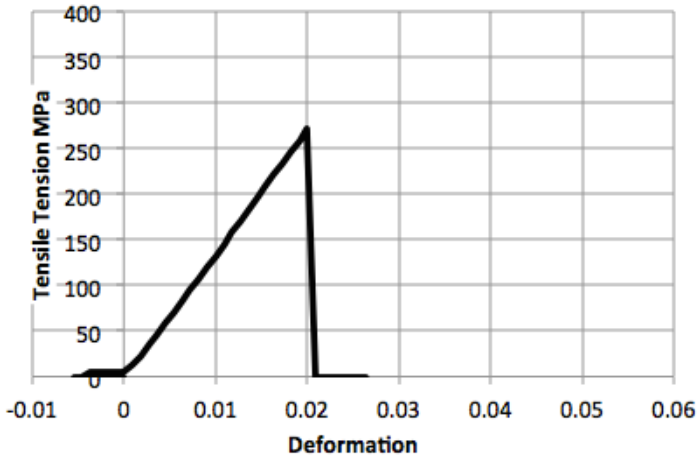

Figure B.28: A stress/deformation chart - sample 1 series 9

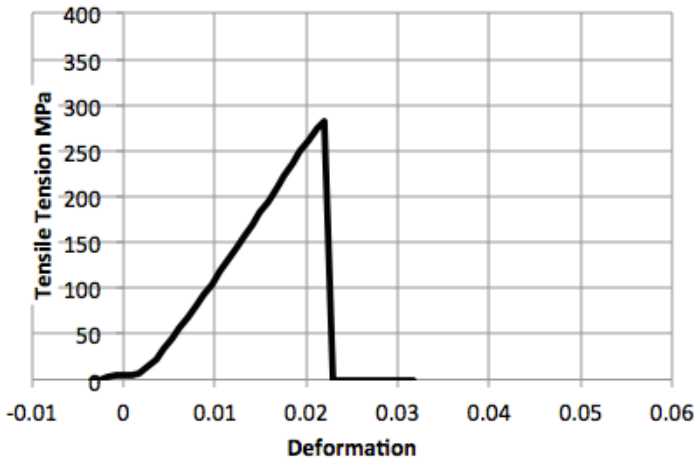

Figure B.29: A stress/deformation chart - sample 6 series 9

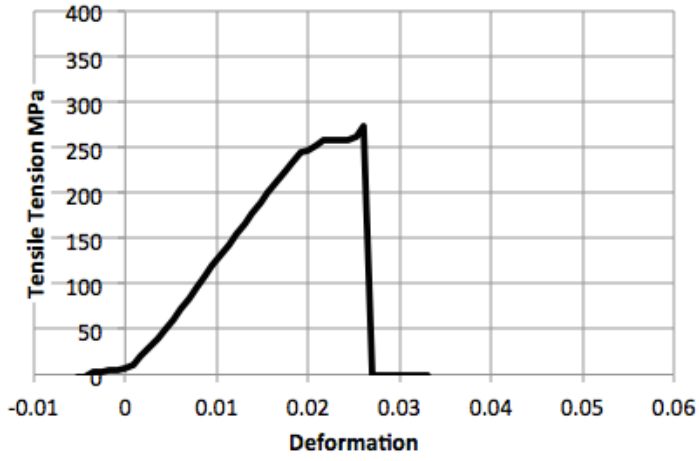

Figure B.30: A stress/deformation chart - sample 9 series 9

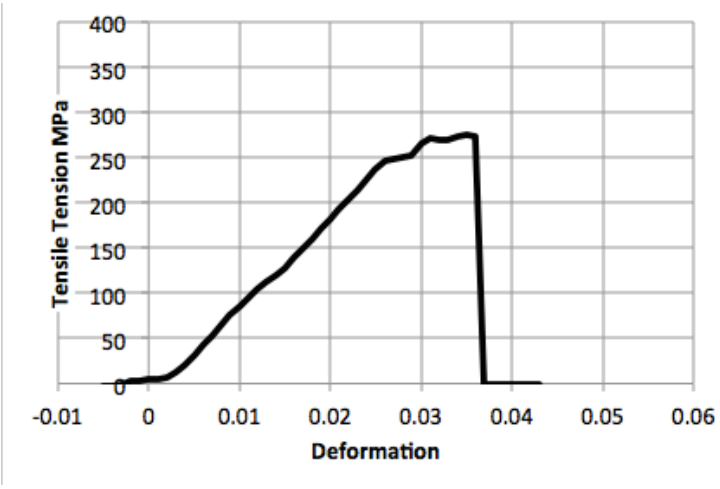

Figure B.31: A stress/deformation chart - sample 14 series 9

Appendix C

FTIR data

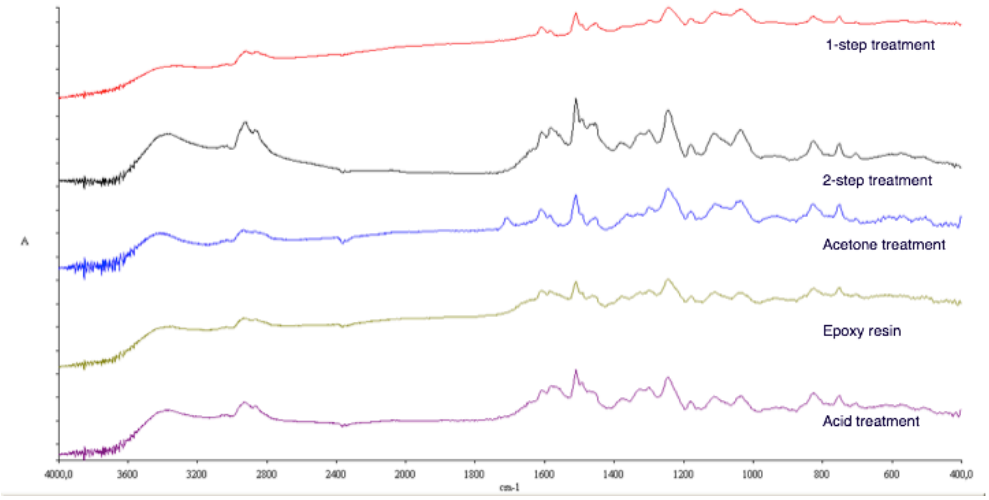

Figure C.1: FTIR image showing the difference of peaks in all samples

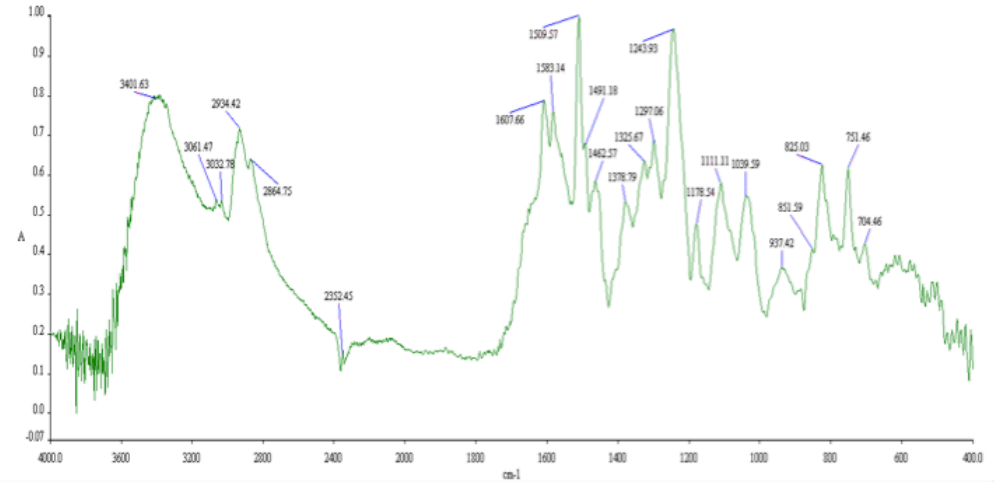

Figure C.2: FTIR image showing the peaks in the epoxy sample

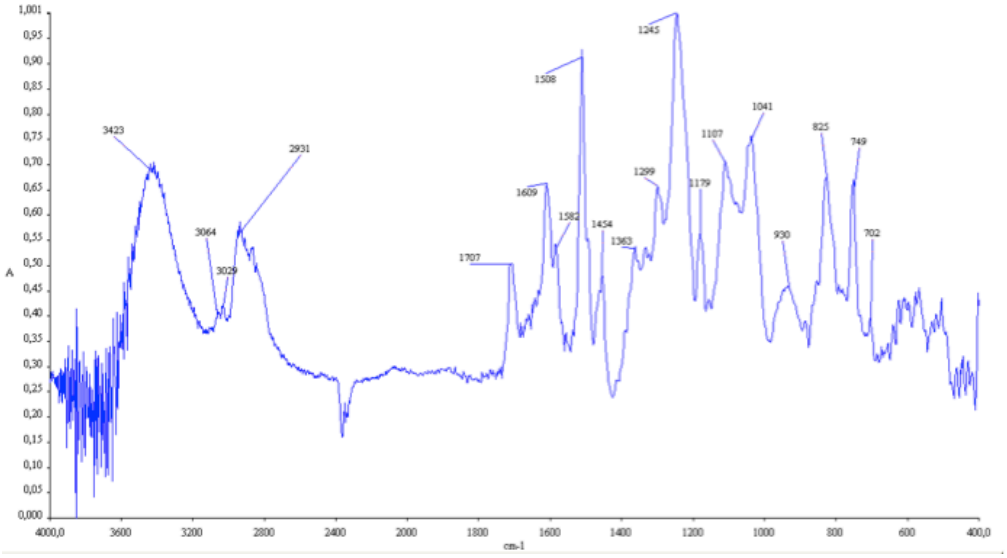

Figure C.3: FTIR image showing the peaks in the acetone treated sample

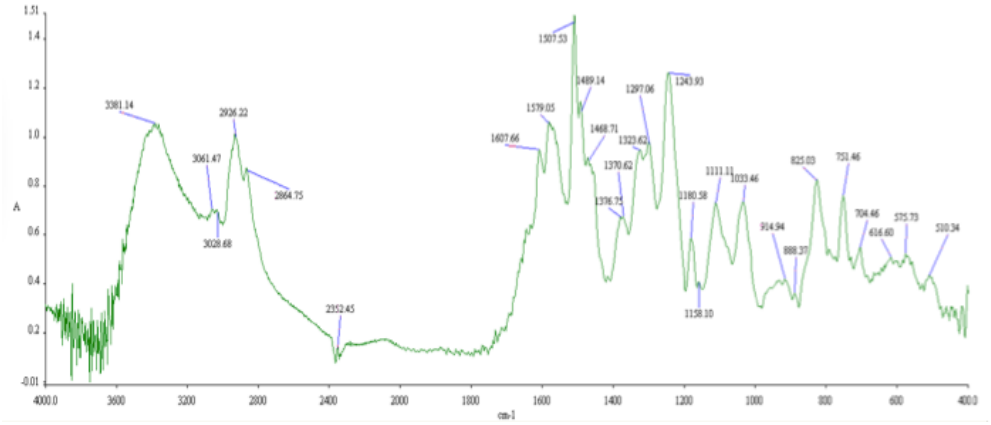

Figure C.4: FTIR image showing the peaks in the acid treated sample

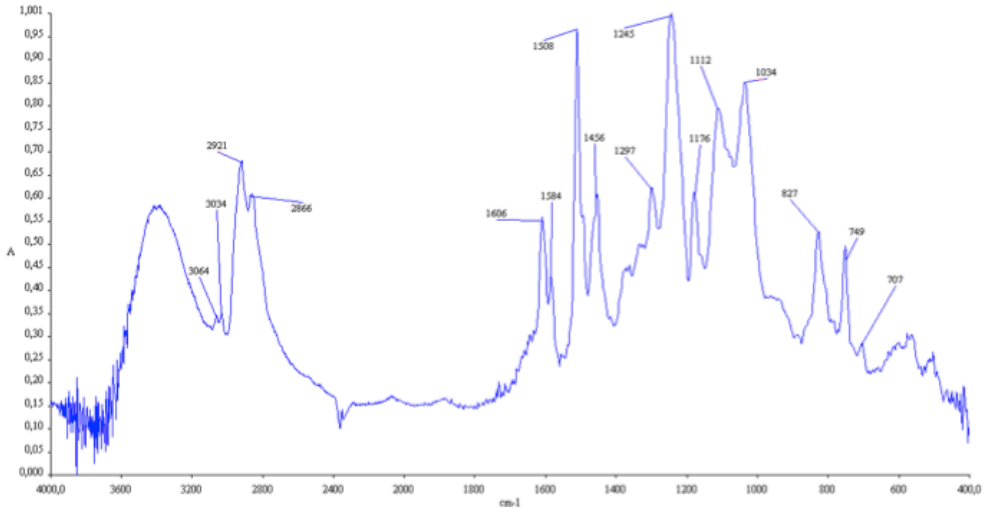

Figure C.5: FTIR image showing the peaks in the 1-step functionalized sample

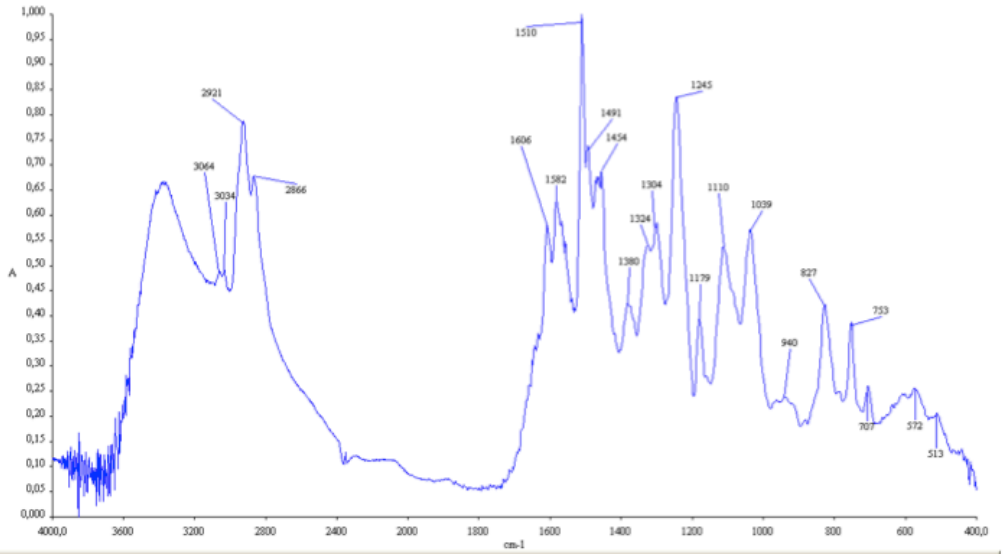

Figure C.6: FTIR image showing the peaks in the 2-steps functionalized sample

List of Figures

List of Tables

Curriculum Vitae

Tselikos Georgios was born in Athens, in 1990. He entered the department of Production Engineering & Management at Technical University of Crete, Chania, in 2008 and graduated in 2014. His graduate research project was ''Hybrid composites consisting of thermosetting matrix, nano-particles and macro-fibers'' sponsored by the ''Incubator of Ideas'' program, under the co-supervision of Prof. G. Stavroulakis and A. D. Gotsis. During his academic years he had the privilege to be selected for a research scholarship, sponsored by DAAD, to visit the iPAT lab at Technical University of Braunschweig and conduct independent research under the supervision of a PhD candidate. Regarding his future plans, the faculty of Aerospace Engineering of TU of Delft, in the Aerospace Structures and Materials department, admitted him for an in MSc in Aerospace Engineering, the period Fall 2014. After that he plans on continuing his education and research goals by applying for an PhD, in the same field of study.